Bandstructure and Electron Dynamics in Semimetallic and Semiconducting Systems

L.M. Claessen

Bandstructure and Electron Dynamics in Semimetallic and Semiconducting Systems

Bandstructure and Electron Dynamics in Semimetallic and Semiconducting Systems

Proefschrift

ter verkrijging van de graad van
doctor in de wiskunde en natuurwetenschappen
aan de Katholieke Universiteit te Nijmegen
op gezag van de rector magnificus Prof.Dr. B.M.F. van Iersel
volgens besluit van het College van Decanen
in het openbaar te verdedigen
op donderdag 10 december 1987
des namiddags te 1.30 uur precies

door
Leendert Michiel Claessen
geboren te Eindhoven

1987

Druk: Krips Repro, Meppel

Promotor : Prof.Dr. P. Wyder

Co-referent : Dr. A.G.M. Jansen

Eigenlijk iedereen die ik goed ken heeft wel op zijn/haar wijze een bijdrage geleverd aan de tot stand koming van dit proefschrift, daarom begin ik graag dit boekje met het bedanken van alle mensen in mijn naaste omgeving. Mijn vrienden en kennissen buiten de fysica, zowel in Nederland als in Frankrijk, zou ik willen bedanken voor het getoonde begrip, (en ook vaak onbegrip) voor mijn aanwezigheid op het lab op de meest onmogelijke tijden.

Hoewel het me onmogelijk is iedereen persoonlijk te noemen hier, al was het alleen maar uit financiele overwegingen met betrekking tot de drukkers van dit boekje, wil ik toch enkelen met name bedanken, (de belangrijkste voor mij staan eigenlijk al op een van de vorige bladzijden).

Vooreerst in Nijmegen vooral Riki als leidster van het thuisfront, alsmede de technici Jan, Jan, en Cees voor de onmisbare hulp tijdens de eerste fasen van mijn onderzoekingen naar de geheimen van de vaste stof. Verder iedereen op de afdeling Exp. Natk. IV, met name Herman, voor de hartelijkheid waarmee ik steeds ontvangen werd als ik weer eens duizend kilometer naar het noorden gereisd was om Nijmegen te bezoeken, alwaar het dan bleek dat ik nog steeds als iemand van de lokale groep gezien werd.

Hier in het verre zuiden, in de internationale "melting pot" genaamd Hochfeld-Magnetlabor, wil ik in het bijzonder Jan-Cees bedanken die een zeer grote stempel gedrukt heeft op het laatste deel van dit proefschrift, en die mij op meer dan gewoon collegiale wijze heeft ingewijd in de wereld van de halfgeleider fysica en de dunne laagjes. Om maar niet te spreken van de vele gesprekken over van alles en nog wat als we het weer even zat waren, of ik het weer eens niet zag zitten. Verder nog mijn oprechte bewondering voor Geert, voor het verdragen van zeer lange meetnachten met mij in Nijmegen, en het delen van een buro in Grenoble.

Herr Schneider-Muntau und seine Magnetbaugruppe danke ich für die vielen Teslas, et je rémercie M. Picoche, pour tenir les alimentations en forme. Auch George Maret möchte ich danken, weil er immer wieder ein bisschen Magnetzeit für mich gefunden hat, auch wenn es da wesentlich kein Zeit mehr gab. Die Techniker Albin und Werner danke ich für die Lösung allerhand Probleme. Further, I like to thank Massimo Altarelli for some claryfing down to earth explanations on difficult bandstructure calculations.

In England, thank you Martyn for showing me the relativity involved in what we are doing, or are trying to do.

En last but not least Rene voor het altijd daar zijn als ik hem nodig had om weer op het juiste pad te geraken, en mijn vader en moeder voor de onmisbare morele steun. Zonder hun hulp was dit alles alles nooit mogelijk geweest.

CONTENTS

PART I

CHAPTER 2 **Plasma resonances in thin Bi films**

PART II

CHAPTER 2 High field magnetic resonances in $Cd_{1-x}Mn_xTe$

PART III

CHAPTER 2 Impact excitation and bottleneck effects in the time-resolved far-infrared photoresponse of high purity InP

CHAPTER 2 Pressure dependence of band offsets in an InAs-GaSb superlattice

CHAPTER 3 investigations of the band line-up in a semimetallic InAs-GaSb superlattice under hydrostatic pressure

II. INTRODUCTION

IV. ANALYSIS OF THE EXPERIMENTAL RESULTS

D. Influence of the Fermi level, and of extrinsic charges

CHAPTER 4 **Theoretical and experimental band line-ups in semiconductors**

"The deeper you go, the more you see"

Dr. Perri Johnson,
in Hamilton Bohannon's;
Let's Start II Dance Again,
FR 12012-A, (1981).

PART I

INVESTIGATIONS ON THE FAR-INFRARED PROPERTIES OF THIN BISMUTH FILMS

CHAPTER 1

General introduction

In the following an experiment will be described concerning the optical responses of thin conducting films due to the collective behaviour of the electron plasma involved. The semi-metal bismuth has been chosen for this investigation because of its intermediate free electron density, on one hand high enough to yield a strong optical response, while on the other hand low enough to insure the validity of classical electrodynamics and semi-free electron behaviour. Moreover the free-electron plasma frequency in this material is conveniently situated in the far-infrared region of the spectrum. The aim of this work is to give a better general understanding of the electrodynamics of thin conducting films as far as optical activity is concerned. Therefore everything will be explained using simple Maxwellian (Fresnel) equations. Besides this strict description of the experiment, much attention will be given to heuristic (handwaving) approaches of the problem in order to see through the physics involved. In the last part of this work a comparison with other experiments on plasma-resonances in thin metal films will be presented showing the real nature of some observed resonances which are often mistaken for electron plasma density oscillations. Furthermore some attention will be given to the presence of ionized-impurity scattering and of two-phonon excitation in the bismuth films.

The essential results of this experiment have been published in a more concise form by L.M. Claessen, A.G.M. Jansen, and P. Wyder in the Physical Review B **33**, 7947 (1986).

CHAPTER 2

Plasma resonances in thin Bi films

ABSTRACT

The optical absorption and transmission of thin Bi films (50-830nm) illuminated with normally incident far-infrared radiation (25-225cm^{-1}) have been measured at low temperatures (T=1.5K). Around the theoretical screened electron plasma frequency (160-170cm^{-1}) a broad absorption band has been observed which disappeared for films thinner than 200 nm. This phenomenon will be visualized in terms of an energy loss mechanism of a lateral electron oscillation due to radiation damping. An electrodynamical analysis of a thin conducting film including the virtual mode theory reveals that a Drude-approximation for the conduction electrons is not sufficient to explain the experimental results in detail. The deviations from this model are discussed in terms of two-phonon processes and electron-ionized-impurity scattering.

I. INTRODUCTION

The plasma frequency of the conduction electrons is defined as the frequency[1] ω for which the dielectric function $\epsilon(\omega)$ equals zero. In semi-conductors and semi-metals this frequency is situated below the visible frequency region owing to a very small electron density. These plasmons can therefore be investigated in a spectral region for which local relations and the Drude-approximation prevail[2,3].

In the semi-metal Bi the plasma frequency[4] is situated in the far-infrared at about 160cm^{-1}. As the optical phonon frequencies are often in the same spectral region as the free electron contributions in semi-conductors, discerning between different absorption mechanisms can be difficult. In Bi however, the optical phonons are infrared inactive[5,6] owing to the crystal symmetry which leaves the free electron absorption as the most important mechanism.

Using a transversal light source as a probe for the free electron excitations it is in general not possible to excite plasmons (i.e. longitudinal excitations) in the electron gas in a direct way. Only by intervention of a rough surface[7,8] or of ionized impurities[9,10] (surface) plasmons can be excited.

In this paper an experiment is described in which thin Bi films (50-830nm) have been illuminated with far-infrared radiation in the spectral region covering the electron plasma frequency. The absorption and transmission have been measured as a function of frequency and film thickness. In films having a thickness in excess of 200nm a broad absorption band is observed around the plasma frequency. In thinner films such an absorption is not present. This resonance is analysed in terms of a transversal excitation of the electron gas in so-called virtual modes. The thickness dependence in the observed resonance can be explained using an energy flow model in which the lateral electron oscillations suffer from radiation damping due to an outgoing electromagnetic plane wave. This effect which has the tendency to damp the oscillation is strongest in thin films, hence introducing a critical film thickness below which the resonance cannot persist. Further an electrodynamical analysis will be presented to explain the optical resonances in detail.

Only a simple Drude-model will be used and elaborated extensively to allow theoretical comparison between Bi and other conductors. These general calculations will show that, besides the film thickness, the most important parameter will be the optical dielectric constant of the lattice ϵ_∞ coming from the polarization of the valence electrons which contribution is extremely large in Bi. A comparison with materials having small ϵ_∞ will be presented.

Deviations from the Drude-approximation as compared with the experimental results will be explained using a two-phonon absorption mechanism in a simplified model. Finally it will be shown that there is some evidence that the deviations can be partly ascribed to an electron-ionized-impurity scattering process which induces longitudinal plasmons in the solid.

II. EXPERIMENT

A. Experimental set-up

For the optical measurements in the far-infrared a Grubb-Parsons Michelson interferometer[14] was used. Equipped with a 12.5μm mylar beam-splitter the spectral range was covered from 25 to 225 cm^{-1}. The high frequency cut-off was due to a black poly-ethylene window at room temperature combined with a cold quartz filter at T=3K. Phase-sensitive detection was achieved by modulating the position of one of the interferometer mirrors at a frequency of 3 Hz.

The substrate with the deposited Bi film was mounted at the end of an oversized waveguide with the film facing the radiation perpendicularly. The system was capable of a simultaneous measurement of the absorption, transmission and the background of the incoming radiation. As detectors bolometers were used made of small chips of Allen-Bradley carbon resistors.

The whole system was under vacuum and immersed in a pumped ^{4}He bath kept at T=1.6K. The reference-bolometer used for the background measurements was mounted above the film but completely shielded from any reflected radiation. Isolated from any direct radiation, the absorption bolometer was thermally connected with the substrate and film via one of the electrical contacts attached to the film. This configuration allows the absorption to be measured in a very direct way by the heating-up of the film. All radiation passing through the film was collected by a Winston-cone and absorbed by the transmission-bolometer. To provide appropriate sensitivity the bolometers and sample were cooled by an additional ^{3}He system. In operation the bolometers could be kept at T=0.9-1.3K and the film, only cooled via the absorption-bolometer, at T=1.5K. Absorption and transmission signals were divided by the background signal and reduced to signals of approximately the same relative strength.

B. Sample fabrication

As a substrate single-crystal quartz plates cleaved perpendicularly to the z-axis were used. This substrate material showed apart from a narrow absorption line at $\simeq$134cm^{-1} no significant absorption for frequencies up to 230cm^{-1} consistent with other experiments[15]. It is therefore allowed to approximate the substrate by a non-absorbing medium having a real refractive index n=2.15. To dispose of Fabry-Perot interferences in the substrate the thickness was made wedgeshaped going from 0.2 to 0.3mm over a diameter of 15mm.

Prior to the deposition of the Bi film four Au-contacts were deposited at symmetrical points on the periphery of the substrate to enable a DC square-resistance measurement in a van der Pauw[16] geometry. The Bi films were deposited by vacuum-evaporation of 99.999% pure Bi on a quartz substrate. The vacuum chamber was equipped with a gasdischarge device to provide in situ substrate cleaning prior to the evaporation. Using an oil-diffusion pump pressures down to 3.10^{-4}Pa could be reached. All films were deposited using a 2-step evaporation process[17] in which first a very thin (30nm) Bi layer is deposited and annealed to enhance epitaxial growth in the second deposition step. The deposition rate was 0.3nmsec^{-1}. The film thickness was controlled during the evaporation by a quartz crystal monitoring device and afterwards checked using an optical interference method. Thicknesses were accurate within 5-10 %. Films were made and investigated in the thickness range from 50 to 830nm.

The film structure was investigated by scanning electron microscopy (SEM) and X-ray diffraction. The latter showed a very strong crystal orientation of the trigonal crystal axis perpendicular to the film surface. The SEM work showed the films to be composed of grains having lateral dimensions 1.5 to 4 times the film thickness. The films had a considerable surface roughness and some protruding crystals at a false orientation. These results are compatible with other experiments[18].

C. Bi properties

In spite of the fact that Bi is a semi-metal with a complex band structure and Fermi-surface[19], it's electrical properties can be described using rather few parameters as long as the experiments do not involve magnetic fields. Being a semi-metal conduction occurs through electrons and holes, but the electrons account for most of the conductivity owing to their very low effective mass ($m^* \simeq .01 m_e$) which is almost isotropic in spite of a very anisotropic mass tensor[20,21]. The electron density at low temperatures[22,23] amounts to $n=3.10^{23}m^{-3}$ for not too thin films. The contribution from the bound charges to the optical properties is represented by ϵ_{∞}, the optical dielectric constant of the lattice which is mainly due to the polarization of the valence electrons[1,27]. At far-infrared frequencies it is essentially frequency independent. In Bi it's numerical value ranges from 60 to 100 dependent on the crystal orientation[4,21,28].

D. DC-results

Using the van der Pauw geometry the DC square-resistance was measured at T=1.5K and ranged from ca. 200 to 5Ω for increasing film thickness from 50 to 830nm. After converting to the DC conductivity (σ_0) the electron scattering time τ was estimated from the Lorentz-Sommerfeld relation[2] [see Eq.(4)]. The scattering time ranged between 4.10^{-14} and 3.10^{-13} sec for increasing thickness of the investigated films. This is of the same order as found in other experiments[9]. From the Fermi energy[24] (E_F=28meV) and the effective mass ($m^*=.01m_e$) the Fermi-velocity can be calculated, which yields in combination with the scattering time τ a value for the electron mean-free-path ℓ. For all films ℓ was of the order of the film thickness.

E. FIR-results

In Figs.1 and 2 the experimental results are plotted for respectively the absorption and the transmission spectra of the Bi films as a function of the film thickness. Due to the absence of a sample having a known absorption and transmission of the same order of magnitude as the Bi films no accurate absolute scales could be obtained. Some residual small scale structures at the spectral ends are due to the normalization process which involves dividing by signals of very low intensity. To keep the picture surveyable all spectra have been shifted upwards an amount as indicated by the numbers in front of each curve.

Fig.1 clearly shows that for films thinner than 200nm the absorption is rather frequency independent, and that for increasing film thickness a very broad absorption band develops at 160cm^{-1}. The transmission (Fig.2) is also

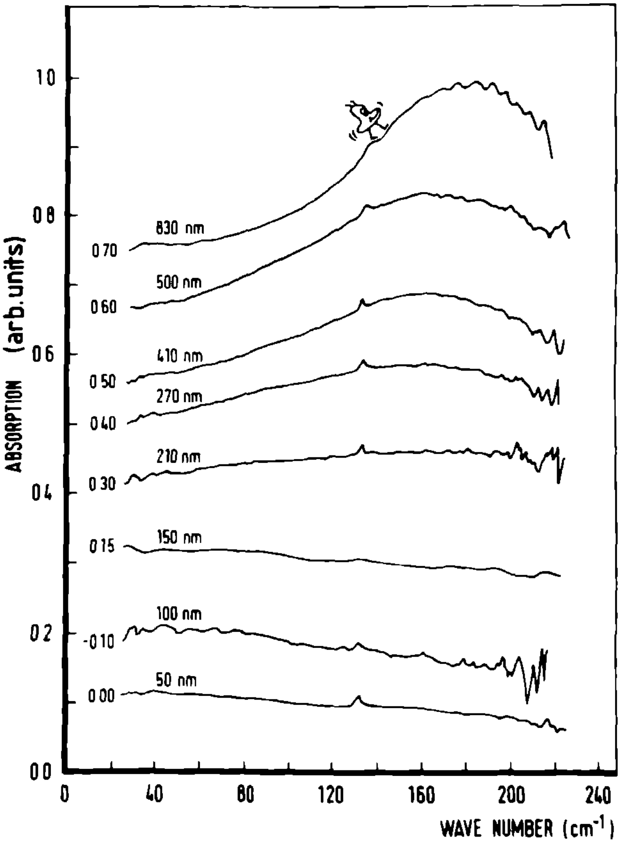

Fig.1. The experimental far-infrared absorption of the Bi films at T=1.5K. The film thickness is given in nm. The numbers in front of each spectrum indicate the real zero absorption on the ordinate scale. The small resonance at 134 cm^{-1} is due to a strong absorption line in the substrate.

featureless for thin films and develops a shoulder at about 160cm^{-1} with increasing film thickness. These results will be discussed in the next sections.

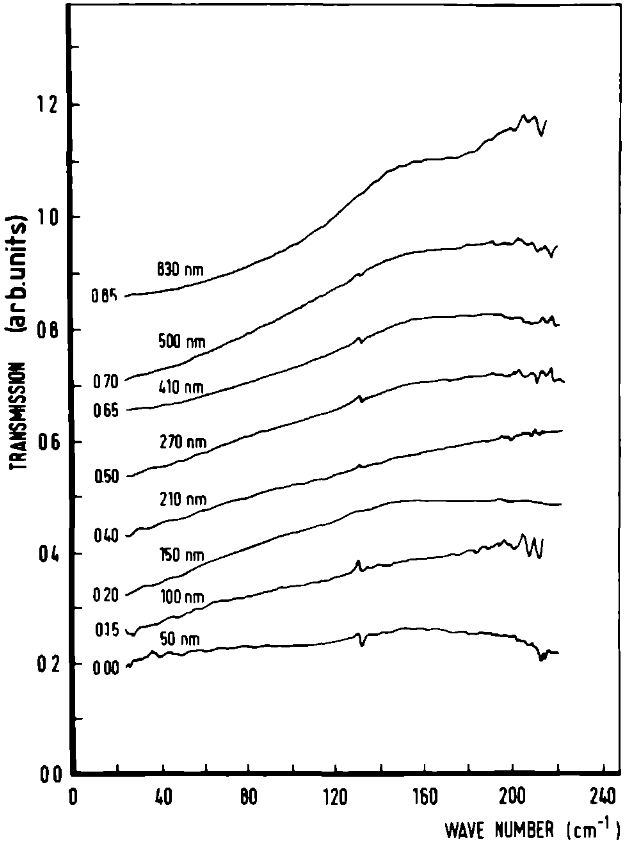

Fig.2. The experimental far-infrared transmission of the Bi films at T=1.5K. For this figure the same comments as given in Fig.1 are applicable.

III. ELECTRODYNAMICAL ANALYSIS

A. Introduction

At optical frequencies the distinction between bound and free charges, which is very definite in DC-cases, becomes less explicit. The usual method of describing the optical properties of a conducting solid is therefore to combine the dielectric permittivity and the free electron contribution in a single effective dielectric function $\epsilon(\omega)$ defined[25] as

$$\epsilon(\omega)=\epsilon_\infty+\frac{i\sigma(\omega)}{\omega\epsilon_0} \tag{1}$$

in which ϵ_∞ is the dielectric contribution from the bound charges and $\sigma(\omega)$ the dynamical conductivity from the free conduction electrons. ϵ_∞ is usually a constant up to frequencies far above the FIR. Likewise an effective displacement current **D** is defined through $\mathbf{D}=\epsilon_0\epsilon(\omega)\mathbf{E}$ and as such incorporates the free electron current **J**. For a non-magnetic medium without external charges the Maxwell equations become

$$\nabla\cdot\mathbf{D}=0 \tag{2a}$$

$$\nabla\mathrm{x}\mathbf{E}=-\frac{\partial\mathbf{B}}{\partial t} \tag{2b}$$

$$\nabla\mathrm{x}\mathbf{B}=\mu_0\frac{\partial\mathbf{D}}{\partial t} \tag{2c}$$

$$\nabla\cdot\mathbf{B}=0 \tag{2d}$$

In the absence of surface charges the correct boundary conditions[25,26] are now the continuity of the tangential **E** and **B** and of the normal displacement current **D**.

As a first step the dynamical conductivity will be used in the Drude-approximation

$$\sigma(\omega)=\frac{\sigma_0}{1-i\omega\tau} \tag{3}$$

with τ the electronic relaxation time, and σ_0 given by the Lorentz-Sommerfeld relation for the DC-conductivity

$$\sigma_0=\frac{ne^2\tau}{m^*} \tag{4}$$

with n the electron density and m* the effective electronic mass. Including the free electron plasma frequency

$$\omega_p^2=\frac{ne^2}{m^*\epsilon_0} \tag{5}$$

$\epsilon(\omega)$ becomes

$$\epsilon(\omega)=\epsilon_{\infty}-\frac{\omega_p^2}{\omega^2+i\omega\omega_\tau} \tag{6}$$

with $\omega_\tau=1/\tau$ the collision frequency. In this approximation ϵ_∞ represents the frequency independent polarization of the valence electrons. Usually Eq.(6) is rewritten as

$$\epsilon(\omega) = \epsilon_\infty\left[1-\frac{\omega_{p^*}^2}{\omega^2+i\omega\omega_\tau}\right] \tag{7}$$

with the screened plasma frequency $\omega_{p^*}=\frac{\omega_p}{\sqrt{\epsilon_\infty}}$.

B. Virtual modes

Consider a film in the $(\hat{x},\hat{y})$-plane having a thickness ranging from -a to +a in the $\hat{z}$-direction and characterized by a dielectric function as given by Eq.(1). Of most interest are solutions of the Maxwell equations having only a periodical lateral co-ordinate dependence[11-13] of the form

$$E=E(z)e^{i(k_x x-\omega t)} \qquad B=B(z)e^{i(k_x x-\omega t)} \tag{8}$$

A straightforward solution of Eq.(2) yields in the case of p-polarization ($E_y=0$) for the $\hat{x},\hat{z}$ components of **E**

$$E_x^{\pm}=e^{i\kappa z}\pm e^{-i\kappa z} \qquad E_z^{\pm}=-\frac{k_x}{\kappa}(e^{i\kappa z}\mp e^{-i\kappa z}) \tag{9}$$

with $\kappa^2=\epsilon(\omega)k^2-k_x^2$, $k=\omega/c$ and the ± signs denote even and odd solutions for E_x with respect to the midplane z=0. In the case of s-polarization ($E_x,E_z=0$) the solution will be

$$E_y^{\pm}=e^{i\kappa z}\pm e^{-i\kappa z} \tag{10}$$

In vacuum Eqs.(9), and (10) are valid provided κ is replaced by κ_0 with $\kappa_0^2=k^2-k_x^2$.

Depending on the parameters κ and κ_0 there exist two different types of solutions for the electric fields.

a) *Non-radiative solutions.*

For $k_x^2 > k^2$, κ_0 will be totally imaginary. In this situation the only physical solution for the fields outside the film is an exponentially decaying field with increasing distance from the film. If $k_x^2 >> k^2$, κ will be imaginary too which means that the fields inside the film are proportional to cosh($i\kappa z$) or sinh($i\kappa z$). For thick films ($|\kappa a| >> 1$) the solutions are now localized at the film surface. These solutions represent the so-called surface plasmons[7,29].

Because of the relation $k_x^2 >> k^2$ surface plasmons are situated in the (ω-k)-diagram in the non-radiative region below the line ω=ck, i.e. having phase-velocities below the speed of light. Therefore in an optical experiment surface plasmons can usually not be excited directly. However, surface roughness can induce coupling between non-radiative excitations and light[7,8].

b) *Radiative solutions.*

If $k_x^2 < k^2$ the solutions are in the radiative region of the (ω-k)-diagram and

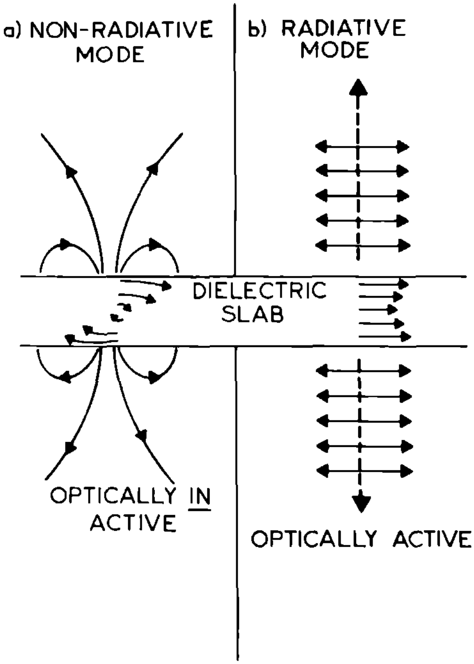

Fig.3. A schematic presentation of the electric field pattern in and outside a thin dielectric slab: a) non-radiative (surface) modes, b) radiative (bulk) modes.

can couple to transversal light. This can be understood by realizing that in this situation κ_0 will be real and the only physical solution for the fields outside the film is an outgoing plane wave that can couple to incident light. This outgoing wave radiates away energy under an angle Θ with the normal of the film given by $\sin\Theta=|k_x/k|$. Because of the energy loss these modes suffer from radiation damping they present no stationary solutions of the Maxwell equations. Hence they are often referred to as virtual modes.

The physical distinction between radiative and non-radiative solutions has been sketched in fig.3, in which a) presents an optically inactive (surface) mode, and b) a (lateral) radiative mode. Using the already mentioned boundary conditions between the film and the vacuum the following virtual mode equations can be derived for the even mode

$$\epsilon(\omega)=-i\ \frac{\kappa}{\kappa_0}\mathrm{cotg}\kappa a \tag{11a}$$

and for the odd mode

$$\epsilon(\omega)=\ i\ \frac{\kappa}{\kappa_0}\mathrm{tg}\kappa a \tag{11b}$$

where 'a' equals half the film thickness. In the case of non-radiative solutions Eq.(11) gives the surface plasmon dispersion relation[7,29]. The radiative solutions of Eq.(11) give the complex virtual mode frequency of which the real part ω_1 represents the resonance frequency and the imaginary part ω_2 the energy loss in time which induces a broadening of the resonance frequency. Kliewer[12,13] et al. have given various solutions of the virtual mode equations for very thick films, and have shown that for a well defined resonance (i.e.$|\omega_2/\omega_1|<1$) the virtual mode absorption of a film will have a Lorentzian lineshape at ω_1 with a width ω_2.

We have calculated the virtual mode frequencies in Bi films for several values of the electronic relaxation time τ by inserting Eq.(6) in Eq.(11) and making the approximation for thin films ($|\kappa a|<1$) and perpendicular incidence (limit $k_x\to 0$).

The results are presented in Fig.4 in which the virtual mode frequency is normalized on the screened plasma frequency ω_{p*} and the film thickness has been made dimensionless. Using the relevant experimental parameters according to section II.C ω_{p*} equals approximately 164cm^{-1}, and unity on the thickness scale in Fig.4 represents a Bi film of ca. 100nm thickness. The solution presented in Fig.4 is due to the even mode, as the odd mode has no physically significant solutions for the investigated Bi films. From Fig.4 we can expect to see a very broad resonance at the screened plasma frequency for films with a thickness in excess of 150nm which is compatible with the experimental results from Fig.1. Fig.4 also reveals that damping due to elec-

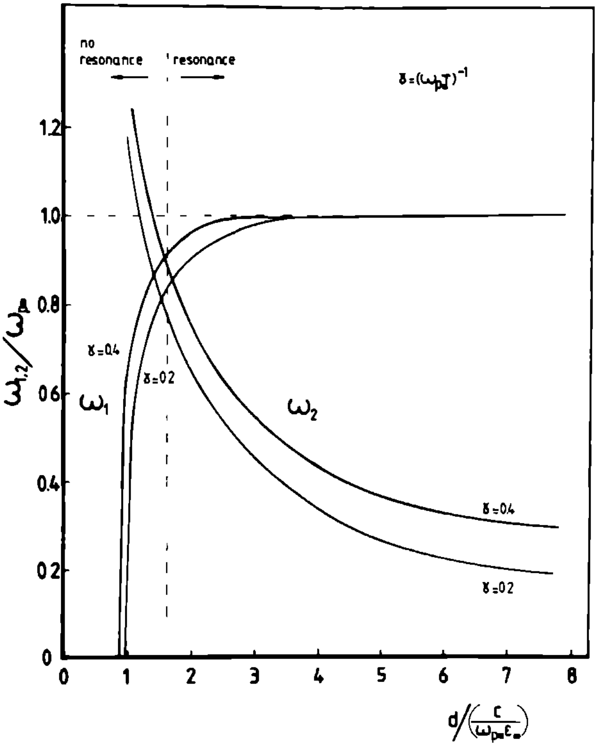

Fig.4. The complex virtual-mode frequency in a thin film as a function of a dimensionless film thickness. The frequencies are normalized on the theoretical screened plasma frequency ω_{p*} and calculated for 2 values of the electronic relaxation time τ represented by the parameter γ. The vertical dashed line marks the critical film thickness below which the resonance disappears by virtue of a too large imaginary frequency. Applied to Bi, unity on the abcis represents a film thickness of ca. 100nm.

tron scattering is only of minor importance as far as the resonance frequency is concerned.

C. Energy loss aspect

In the previous section it has been shown that optically active lateral oscillations can only be present around the plasma frequency in films exceeding a critical film thickness. Qualitatively this can be visualized using the concept of energy content and energy loss.

The thin film oscillation consists mainly of a nearly homogeneous lateral electric field which varies harmonically in time. This field can be conceived as an electromagnetic plane wave which has a time-averaged energy content W=Re[**E**·**D**]. The electromagnetic energy W(d) per unit area stored in a film having a thickness d will therefore be

$$W(d)=\epsilon_0 \mathrm{Re}[\epsilon(\omega)]E_x^2 d \tag{12}$$

This equation shows that only in the case of vanishing $\mathrm{Re}[\epsilon(\omega)]$ a strong electric field resonance can be present at a low energy content. This is a way to see why a virtual mode oscillates preferably only near the plasma frequency.

Following the boundary conditions, E_x will be continuous across the film-vacuum interface and hence will present the amplitude of the outgoing plane wave. The energy transport out of the film per unit area P_r will be accordingly

$$P_r=\epsilon_0 c E_x^2 \tag{13}$$

In the absence of electron scattering energy conservation yields the following expression for the virtual mode energy W(d)

$$\frac{d}{dt}W(d)=-P_r \tag{14}$$

This expression reveals that an oscillation initialized at a certain moment will decay exponentially with a decay time τ_r given by

$$\tau_r= \frac{\mathrm{Re}[\epsilon(\omega)]d}{c} \tag{15}$$

where $\epsilon(\omega)$ is given by Eq.(7). According to Fourier theory such a decay time will cause a frequency spread given by $\Delta\omega\tau_r\simeq 1$. Therefore, for an oscillation close to the plasma frequency the following relation can be derived from Eq.(15)

$$\frac{\Delta\omega}{\omega_{p*}} \simeq \frac{d^*}{d} \tag{16}$$

where d represents a critical film thickness given by

$$d^*= \frac{c}{\omega_{p*}\,\epsilon_\infty} \tag{17}$$

In this derivation the assumption has been made that around the plasma frequency $\mathrm{Re}[\epsilon(\omega)]$ will be of order of ϵ_∞, which makes d just a rough estimate. Eq.(16) reveals immediately that for a well defined resonance the film thickness should be in excess of d (which is close to 100nm in Bi). The expression given in Eq.(16) equals the imaginary part of the virtual mode frequency as can be calculated from Eq.(11a) assuming zero electron scattering, which is a justification for the energy loss concept. d as given in Eq.(17) is also used as a scaling factor on the abcis of Fig.4.

D. Optical response

To obtain the actual shape of the optical absorption and transmission spectra, the virtual modes must be coupled explicitly to an incoming, a reflected, and a transmitted wave[12]. The general way to perform such a calculation is to express the fields inside the film in the fields on both sides of the film using the Maxwell equations giving expressions for the power transmission (T) and reflection (R). The absorption (A) is defined by virtue of energy conservation as A=1-T-R.

As the output of the Michelson interferometer has a beam-divergence of 14 degrees it's necessary to investigate the influence of non-normally incident light on the absorption and transmission spectra. Especially p-polarized light at oblique incidence can cause strong additional optical resonances owing to a non-vanishing component of the electric field perpendicular to the film surface[25,30]. Expressions including this angle dependence are, for a slab without a substrate, given by[12]

$$T=\frac{1}{4}|P_1-P_2|^2 \qquad R=\frac{1}{4}|P_1+P_2|^2 \tag{18}$$

with $P_{1,2}=\dfrac{1+iu_{1,2}}{1-iu_{1,2}}$.

For p-polarized light incident under an angle Θ, $u_{1,2}$ will be given by

$$u_1=\frac{\kappa}{\kappa_0\epsilon(\omega)}\mathrm{tg}\kappa a \qquad u_2=-\frac{\kappa}{\kappa_0\epsilon(\omega)}\mathrm{cotg}\kappa a \tag{19}$$

with κ and κ_0 defined as in Eq.(9), 2a equals the film thickness, and $|k_x/k|$ equals $\sin\Theta$.

For s-polarization we obtain

$$u_1=\frac{\kappa_0}{\kappa}\mathrm{tg}\kappa a \qquad u_2=-\frac{\kappa_0}{\kappa}\mathrm{cotg}\kappa a \tag{20}$$

Substituting all relevant experimental parameters in Eqs.(18) to (20) a calculation reveals that for the investigated Bi films no significant differences should exist between the optical responses for zero-angle incident light and for oblique p- or s-polarized light up to angles in excess of 30 degrees. Therefore, to add to the simplicity of the calculations, all experimental data have been fitted using a model for only normally incident light. In section III.G the angle dependence will be discussed in more detail.

In most theoretical models concerning the optical responses of a thin film supported on a substrate the influence of this substrate is neglected. However, even a perfectly non-absorbing substrate can have due to it's large refractive index a non-negligible influence on the detailed frequency dependence and magnitude of the reflection, absorption, and transmission. This originates in the impedance matching[31] which exists between the film, the substrate, and the vacuum. Only when for instance just a strong narrow resonance peak has to be investigated the substrate can be neglected. Because of this influence we have employed the expressions derived by de Kort[31] et al. for the optical properties of a film supported on a substrate. Following the notation in their paper, T and R are given by[32]

$$T=\left|\frac{\alpha}{\beta}\right|^2 \qquad A=\left|\frac{\gamma}{\beta}\right|^2 \tag{21}$$

with

$$\alpha = i\omega c(F_1^+-F_1^-)\,(F_2^+-F_2^-) \tag{22a}$$

$$\begin{aligned}\beta = {} & (F_1^++F_1^-)\,(\omega^2F_2^+F_2^--c^2) + (F_2^++F_2^-)\,(\omega^2F_1^+F_1^--c^2) + \\ & + i\omega c(F_1^++F_1^-)\,(F_2^++F_2^-) + 2i\omega c(F_1^+F_1^-+F_2^+F_2^-)\end{aligned} \tag{22b}$$

$$\gamma = (F_2^++F_2^-)\,(\omega^2F_1^+F_1^-+c^2) + (F_1^++F_1^-)\,(\omega^2F_2^+F_2^-+c^2) + 2i\omega c(F_1^+F_1^--F_2^+F_2^-) \tag{22c}$$

and with

$$F_i^+= -\frac{1}{k\sqrt{\epsilon_i}}\mathrm{cotg}\left(ka_i\sqrt{\epsilon_i}\right) \qquad F_i^-= \frac{1}{k\sqrt{\epsilon_i}}\mathrm{tg}\left(ka_i\sqrt{\epsilon_i}\right) \tag{23}$$

In these equations the index i=1 refers to the medium facing the radiation, which is the Bi film in our experiment. The index i=2 refers consequently to the substrate.

In the calculations the following substitutions are made in Eqs.(21),(22), and (23): ϵ_1 according to Eq.(7) with the Bi-parameters from section II.C, the scattering time τ as calculated from the DC square resistance values, and the

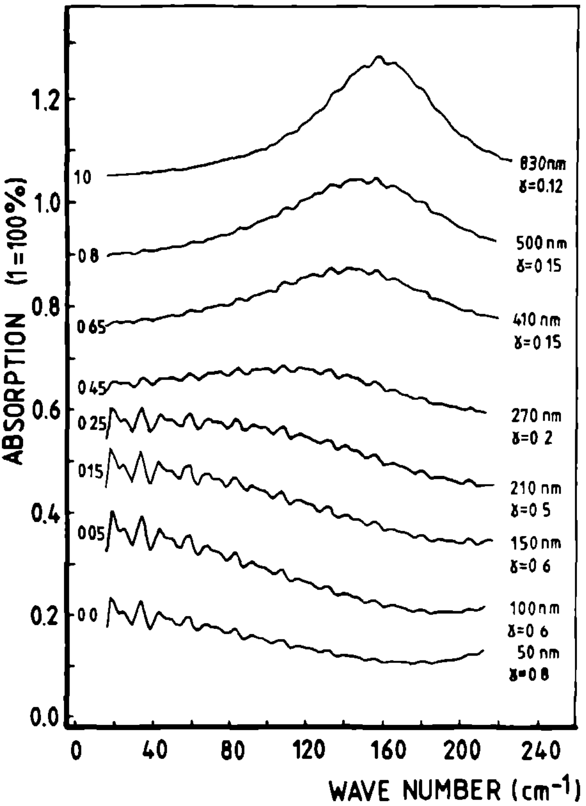

Fig.5. The theoretical far-infrared absorption of thin Bi films on a wedge-shaped quartz substrate calculated in the Drude-approximation. The film thickness is given in nm and the numbers in front of each spectrum indicate the real zero on the ordinate. The electronic relaxation rate is presented by $\gamma=\frac{1}{\omega_{p*}\tau}$. The parameters used for the calculation are: $\frac{m^*}{m_e}=0.01$, $\epsilon_\infty=100$, $n=3x10^{23}m^{-3}$, $\omega_{p*}=164cm^{-1}$, $n_{quartz}=2.15$.

film thickness $2a_1$. The refractive index of the substrate n is substituted in $\epsilon_2=n^2$ and the substrate thickness is $2a_2$. The results for the absorption and the transmission of this model calculation in the Drude-approximation are presented in Figs.5 and 6 in which the scattering time τ is presented by the parameter $\gamma=1/(\omega_{p*}\tau)$. To include the wedgeshape of the substrate the computer program integrates over the substrate thickness in discrete steps which leaves some residual small-scale structures in the theoretical spectra.

To investigate the influence of the substrate inserting $\epsilon_2=1$ in Eqs.(21), (22), and (23) revealed that the main effect of the substrate on the absorption is a considerable smoothing and broadening effect on the resonance, especially at the high-frequency side. The overall absorption was also strongly reduced by the presence of the substrate. Similar non-negligible effects were found concerning the transmission.

E. Comparison between Drude-model and experiment

Fig.5 reveals in the absorption a frequency and thickness dependence which differs considerably from the experimental absorption. Firstly the shift of the resonance towards lower frequencies for thin films which could be expected on ground of the virtual mode frequencies is not seen experimentally. Secondly the theoretical resonance broadening is narrow as compared with Fig.1.

Fig.6 reveals a striking difference between the experimental and the theoretical transmission. The predicted maximum in the transmission around ω_{p*} is observed as a shoulder in the experiment. This particularly strong deviation is the most important evidence that the Drude-approximation is not sufficient to describe the far-infrared properties of thin Bi films in detail. In the next sections several mechanisms will be discussed to explain the apparent discrepancy between the experiment and the Drude-theory.

F. Deviations from the Drude-model

a) *Non-local effects.*

Figs.5 and 6 clearly reveal that the Drude-model fails to account for the detailed shape of the absorption and transmission spectra. From the expressions for $\epsilon(\omega)$ it's easy to show that the skindepth δ will be of order of 5-20μm in the frequency region of interest, which is in excess of the electron mean-free-path and of the film thickness. Hence electrodynamics are not yet in the anomalous regime[2,3] and local relations between fields and currents can be used.

b) *two-phonon processes.*

To investigate the influence of optical phonon resonances the dielectric function of the Bi films was used in the following model

$$\epsilon(\omega)=\epsilon_{\infty}+\chi_{ph}+\chi_{fc} \qquad (24)$$

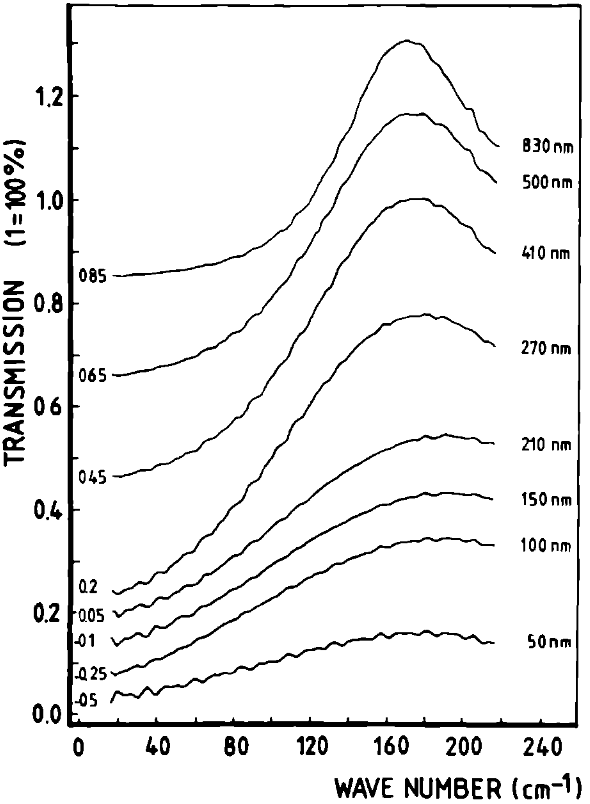

Fig.6. The theoretical far-infrared transmission of the Bi films on a wedge-shaped quartz substrate calculated in the Drude-approximation. For this figure the same comments as given in Fig.5 are applicable.

in which χ_{fc} represents the free-electron contribution according to Eq.(6), and χ_{ph} the susceptibility caused by the optical phonons. In the classical approximation χ_{ph} is given by

$$\epsilon_\infty + \chi_{ph} = \epsilon_\infty \frac{\omega_L^2 - \omega^2 - i\omega\Gamma}{\omega_T^2 - \omega^2 - i\omega\Gamma} \tag{25}$$

in which ω_L is the longitudinal optical (LO) phonon frequency, ω_T the transversal optical (TO) phonon frequency, and Γ represents the damping.

The phonon contribution according to Eq.(25) is presented in Fig.7, which is extended to higher frequencies than those of experimental relevance.

By inserting Eq.(25) in Eqs.(21), (22), and (23) a calculation of the absorption and the transmission yields the results as shown in Figs.8 and 9. In these calculations we have used the following parameters to match the theory with the experiment: ϵ_{∞}=90±5, ω_T=205±5cm^{-1}, ω_L=220±10cm^{-1}, and Γ=150±50cm^{-1}. In Fig.7 the phonon contribution is presented for these parameters. From Figs.8 and 9 it can be seen that experiment and theory conform fairly well, except for an unexplained bulge in the high-frequency transmission of the thickest film.

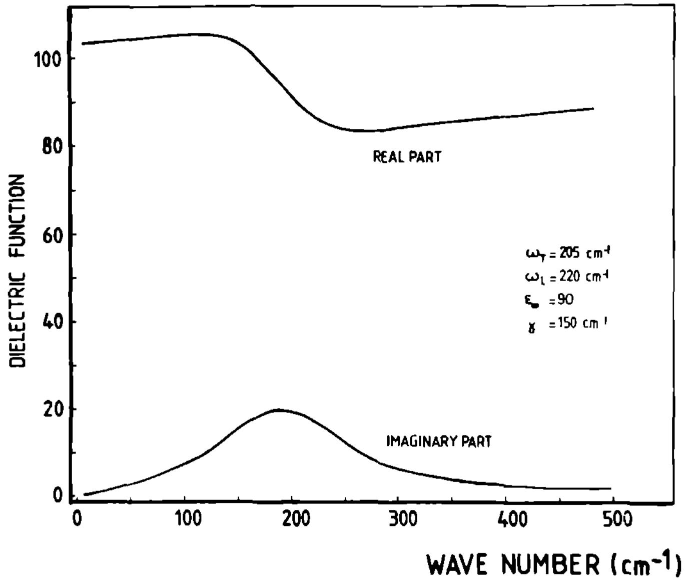

Fig.7. The contribution from the lattice to the dielectric function corresponding to Eq.(24). The presented parameters yield a good theoretical description of the experimental absorption and transmission.

As Bi has a rhombohedral[33] crystal structure with 2 atoms in each unit cell the first order fundamental lattice absorption is forbidden because the optical (zone-centered) phonons produce no electric dipole-field[5,6] and hence are infrared-inactive. Using Raman scattering[33,34] the optical phonon frequencies near the zone-center are established as 75cm^{-1} (TO) and 100cm^{-1} (LO). MacFarlane[35] has obtained the wavevector dependent optical phonon branches along the trigonal crystal-axis from neutron diffraction. The frequencies range from 75 to 102cm^{-1} (TO-branch) and from 100 to 108cm^{-1} (LO-branch). Therefore the phonon contribution suggested by Fig.7 is

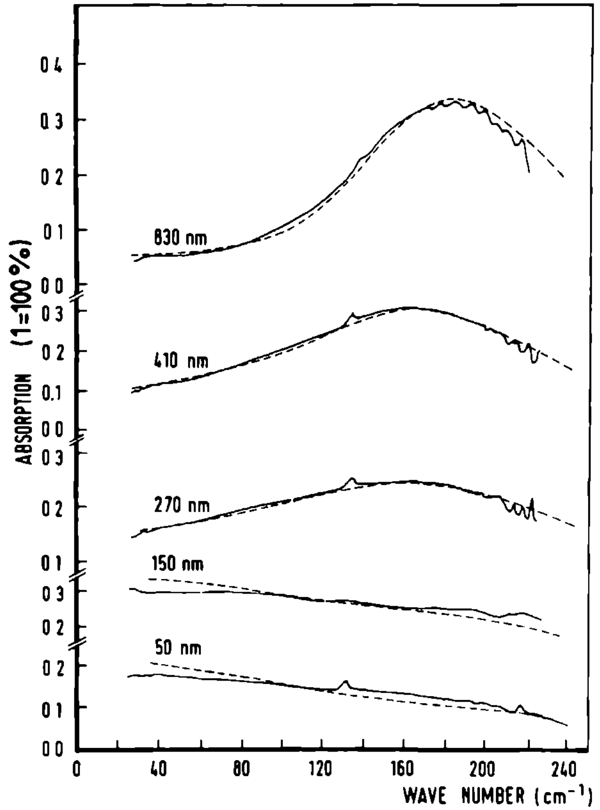

Fig.8. The experimental absorption of the Bi films compared with the theoretical model (dashed line) including the phonon contribution as given by Eqs.(24) and (25). The parameters used for the calculation are as presented in Fig.7. The calculation includes the wedge-shaped substrate and has been smoothed to dispose of some residual Fabry-Perot interferences.

expected to arise from a summation band i.e. a two-phonon process. As the wavevectors of the two phonons can cancel each others momentum no restriction to zone-centered phonons has to be made, thus allowing for a frequency spread[36] in the two-phonon absorption band. Lax and Burnstein[37] suggest that this two-phonon absorption process involves second order terms in the electric moment produced by charge deformations. One vibrational mode of the lattice induces charges on the atoms and simultaneously another mode causes a vibration of the induced charges which produces an electric dipole moment that can couple with the radiation field. Following this theory only short-wave-length phonons can contribute very effectively to this mechanism, and accordingly two-phonon absorption will mainly arise from a pair of zone-boundary phonons. Considering the experimentally found phonon frequencies near the zone-boundary[35] in Bi, two-phonon absorption is therefore expected to be strongest in the region between 200 and 220cm^{-1}.

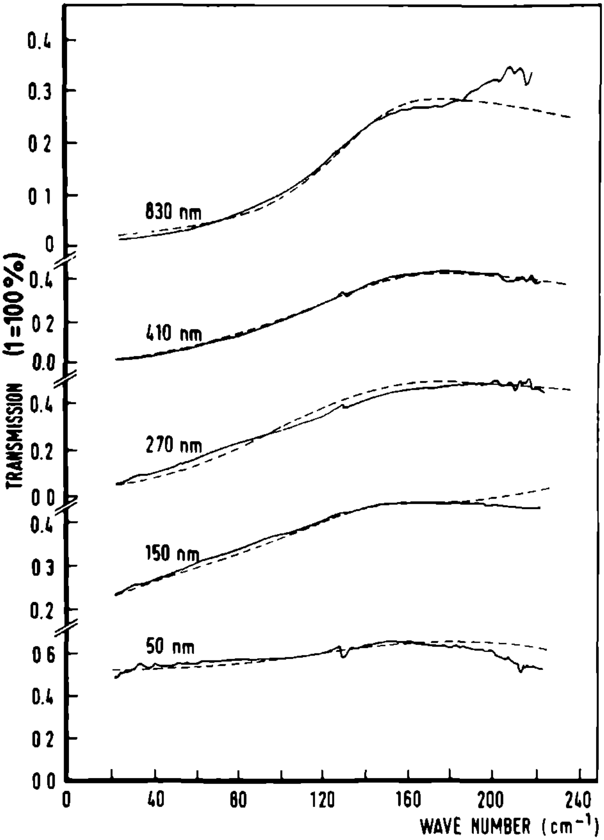

Fig.9. The experimental transmission of the Bi films compared with the theoretical model (dashed line) including the phonon contribution. For this figure the same comments as given in Fig.8. are applicable.

A detailed calculation performed by Cowley[38] indicates that the two-phonon contribution is weak but shows in a smoothed form a distinct resemblance to the plot presented in Fig.7. This similarity between one- and two-phonon contributions to the dielectric function is not unexpected as in two-phonon processes the dielectric susceptibility $\chi_{2ph}(\omega)$ originates in principle in combinations of all pairs of phonons having frequencies ω_1 and ω_2 with $\omega_1+\omega_2=\omega$. Approximately $\chi_{2ph}(\omega)$ should resemble as such a self convolution of $\chi_{ph}(\omega)$ according to

$$\chi_{2ph}(\omega)\propto \int\chi_{ph}(\omega_1)\chi_{ph}(\omega-\omega_1)d\omega_1 \tag{26}$$

The result of such a self convolution is roughly a strong smoothing and a doubling of the arguments of the involved function. Therefore it is reasonable to approximate the two-phonon contribution by a single-phonon process (as depicted in Fig.7), including a strong damping and doubled resonance frequencies.

c) *Electron-impurity scattering.*

Figure 10 presents the dielectric function used to obtain the theoretical absorption and transmission spectra depicted in Figs.8 and 9, and gives a comparison with the Drude-model. To keep the picture surveyable not all films involved in the experiment have been included. A rather similar deviation from the Drude-model as observed in the plots has been reported by Gerlach[9] et al. derived from reflection measurements on bulk Bi between 50 and 500cm^{-1}. This phenomenon is ascribed to the scattering of conduction electrons by ionized impurities which causes the collision time τ to become frequency dependent. In this report we'll give an overview of the main points of this theory and make a comparison with our experimental results.

In the Drude-approximation the dynamical resistivity $\rho(\omega)$ has the form

$$\rho(\omega)= \frac{\omega_\tau}{\epsilon_0\omega_p^2} - \frac{i\omega}{\epsilon_0\omega_p^2} \tag{27}$$

in which ω_p is the unscreened plasma frequency. The real part of $\rho(\omega)$ represents the scattering effects and is frequency independent. A more realistic scattering theory results in

$$\rho(\omega)=\hat{\rho}(\omega)- \frac{i\omega}{\epsilon_0\omega_p^2} \tag{28}$$

in which $\hat{\rho}(\omega)$ will be necessarily complex[10] and represents the frequency dependent scattering mechanisms. Therefore any observed frequency depen-

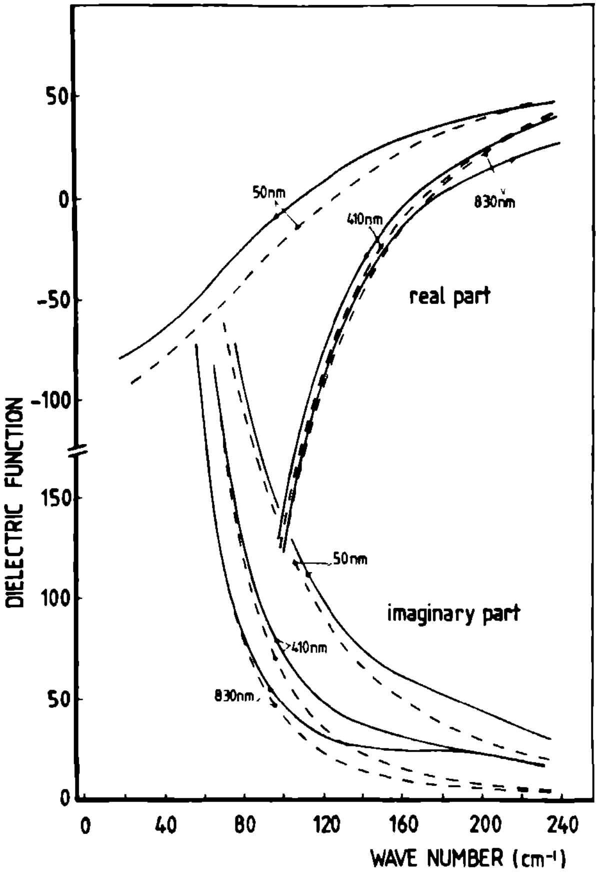

Fig.10. The dielectric function of Bi films of various film thickness. The solid line presents the dielectric function including the two-phonon contribution. The Drude-model dielectric function is given by a dashed line.

dence in the real part of the dynamical resistivity $\rho(\omega)$ unambiguously indicates a deviation from the Drude-model.

According to an extensive theoretical treatment for which we refer to Gerlach[10], the influence of electron-ionized-impurity scattering on Re$\hat{\rho}(\omega)$ is only appreciable for $\omega > \omega_{p^*}$. The effect consists mainly of a strong peak in the real resistivity rising a factor 5 to 10 in magnitude over the Drude-resistivity in the region from ω_{p^*} to ca. $4\omega_{p^*}$ followed by a powerlaw decrease which continues up to very high frequencies. These results are compatible with their experimental findings. The electron-ionized-impurity scattering can be visualized as follows[9,10,39]. In principle real plasmons (i.e. longitudinal charge density fluctuations having $\nabla \cdot E \neq 0$) cannot be induced by transversal light ($\nabla \cdot E = 0$). The spherical field of a screened ionized impurity can however break the transversal symmetry and thus allows for a longitudinal component in the total electric field. Above the screened plasma frequency real plasmons can now be excited. For $\omega < \omega_{p^*}$ the screening cloud of electrons around the impurity follows the frequency of the electromagnetic wave and the electrons oscillate along the ionized impurity. For $\omega > \omega_{p^*}$ real plasmons

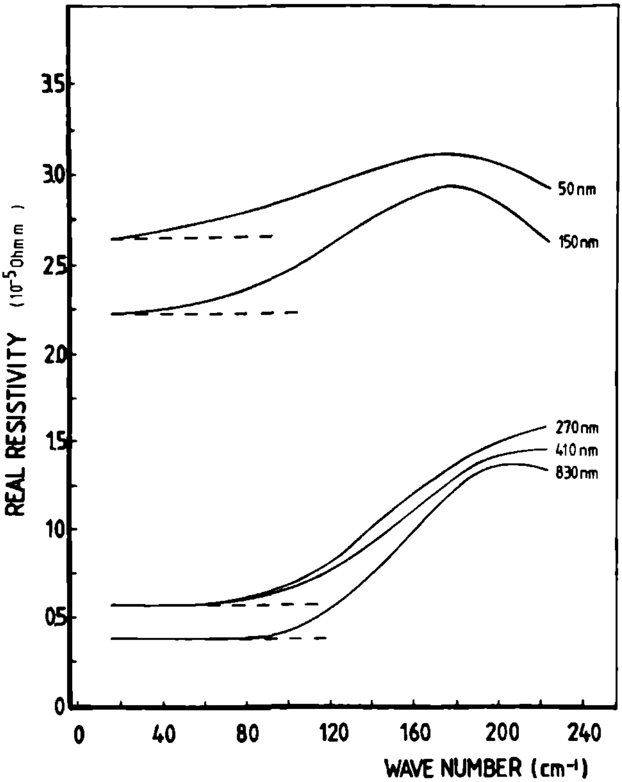

Fig.11. The real resistivity of the Bi films (solid line) as derived from the dielectric function of figure 10. The Drude-contribution which is frequency independent is indicated by a dashed line.

are excited which oscillate at a frequency close to ω_{p^*}. Through these plasmons energy is dissipated from the incident radiation which manifests itself in a strong increase of the absorption, and hence of ω_τ. Due to plasmon decay in single particle excitations (Landau damping[1,40]) plasmons can only exist in a small frequency region above ω_{p^*}. Therefore for high frequencies of the incident light the plasmons will have no phase correlation with the rapidly oscillating electromagnetic field and absorption (and ω_τ) will be strongly reduced.

To check on this phenomenon we have determined the real part of the dynamical resistivity and the optical conductivity of the investigated films using the dielectric function presented in Fig.10. The results for the dynamical resistivity $\rho(\omega)$ and the dynamical conductivity $\sigma(\omega)$ are presented in Figs.11 and 12 and compared with the Drude-model. The principal features predicted by the theory of impurity scattering are clearly visible. The effect is however not as pronounced as expected. The most important discrepancy between the real resistivity as depicted in Fig.11 and the impurity-scattering theory is that the predicted increase becomes appreciable already at frequencies considerably below the plasma frequency ω_{p^*}.

Plasmons are formed[1] near the zeros of $\epsilon(\omega)$. Given by this condition, the complex frequency of the onset of plasmons becomes in the long wavelength limit $\omega_1+i\omega_2$ with

$$\omega_1=\sqrt{\omega_{p^*}^2 - \tfrac{1}{4}\omega_T^2} \tag{29a}$$

$$\omega_2=\tfrac{1}{2}\,\omega_T \tag{29b}$$

Thus a shift towards lower frequencies as well as a broadening and smoothing of the plasmon peak can be expected for damped electron systems. From the experimentally measured scattering rates ω_T (going from 2.5×10^{13} to $3.3\times10^{12}\,\mathrm{sec}^{-1}$ for increasing film thickness) and the observed plasma frequency ω_{p^*} (160-170cm^{-1}) it must be concluded that damping of the electronic system cannot account for the observed shift towards lower frequencies of the position where the real resistivity increases. This discrepancy between the experiment and the impurity-scattering theory remains yet unexplained.

In conclusion, on behalf of this experiment no exclusion can be given whether the observed deviations from the Drude-model are descendent from two-phonon contributions or from electron-ionized-impurity scattering, although the latter possibility seems less likely in view of the experimental results.

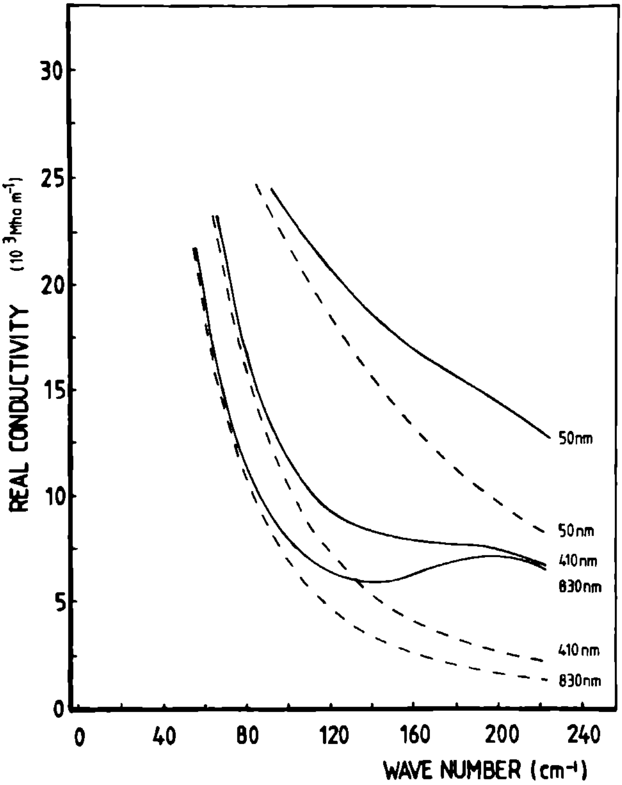

Fig.12. The real (optical) conductivity of the Bi films (solid line) as derived from the dielectric function of figure 10. The Drude-conductivity is given by a dashed line.

G. Importance of the lattice contribution

The calculations of the optical properties of the Bi films in the Drude-approximation reveal that a strong maximum should be seen in both the absorption and the transmission at the screened plasma frequency ω_p*. According to these calculations the absorption and transmission spectra are almost independent on the angle of incidence and on the nature of the polarization. This differs from the generally obtained results for the optical responses of e.g the alkali-metals both theoretically and experimentally[25,30,41]. In these treatments a narrow plasma peak and dip are found in respectively the absorption and the transmission only when using p-polarized radiation at non-normal incidence. These differences in the optical properties are mainly caused by the magnitude of the valence electron screening, i.e. the numerical value of ϵ_{∞}. In Bi, owing to very small bandgaps[1,27,35], ϵ_{∞} is very large whereas in most metals it is of order of unity.

Using Eq.(7) for $\epsilon(\omega)$ and including a considerably large collision frequency ω_{τ} it is easy to show that for real frequencies the condition $|\epsilon(\omega)|<<1$ can only be satisfied for a sufficiently small ϵ_{∞}. As for the radiative solutions of the fields in the thin film the most important parameter κ in Eq.(9) is given by

$$\kappa^2=k^2(\epsilon(\omega)-\sin^2\Theta) \tag{30}$$

it will be obvious that for Bi the angle dependence can be neglected. Qualitatively this can be understood by considering that the real refractive index of Bi is very large and hence all incoming radiation is strongly refracted towards the normal of the film. Substituting Eq.(30) in Eq.(9) shows that for Bi films the normal electric field component will be negligible.

For metals having $\epsilon_{\infty}\sim1$ the condition $|\epsilon(\omega)|<1$ is easily satisfied around the real plasma frequency. Hence by virtue of Eqs.(9) and (30) a large electric field normal to the film can be present at the plasma frequency only, which causes a strong absorption of the incident p-polarized radiation. This kind of absorption from p-polarized light is sometimes[41] mistaken for a real longitudinal plasmon excitation owing to a suspected longitudinal electric field component which is however not present ($\nabla\cdot E=0$). Another explanation[30] is the presence of a standing wave resonance that induces surface charges. Such a resonance is a simplified form of the more elaborated standing density waves as discussed by Melnyk[26] after the so-called Tonks-Dattner plasma-capacitor modes that are real longitudinal excitations. These modes have not been detected in our experiment. To illustrate the effect of ϵ_{∞} on the optical responses we have made a model calculation for a hypothetical Bi film having no screening of the valence electrons, i.e. ϵ_{∞} equals unity. As such Eq.(7) gives the dielectric function of a free-electron gas. The result for a theoretical plasma frequency of $164\mathrm{cm}^{-1}$ is presented in Fig.13 for a film having a thickness of 800nm. The strong angle and polarization dependence reappears just as predicted. For normally incident light no absorption resonances are present. This can be explained by inserting the relevant parameters in the virtual mode expressions [Eq.(11)]. The resulting virtual mode frequency is situated in Fig.4 in the region having $\omega_2>>\omega_1$ and hence no defined resonance will be present.

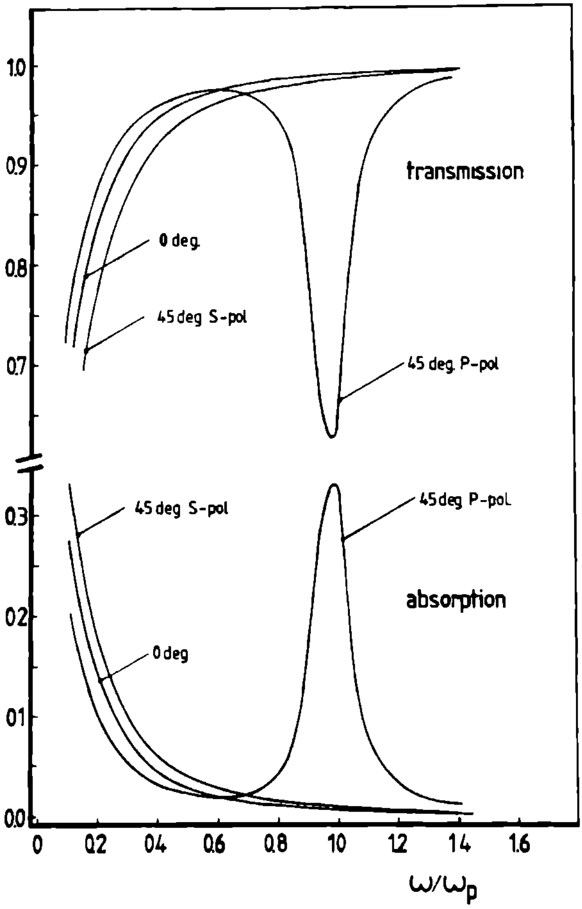

Fig.13. The theoretical absorption and transmission of a hypothetical Bi film of 800nm thickness having no valence-electron screening ($\epsilon_{\infty}=1$), and a plasma frequency of 164cm^{-1}. The calculation is performed for perpendicular incidence and for 45^0 s- and p-polarization. The electronic scattering time τ is given by $\omega\tau=10$.

IV. CONCLUSION

In conclusion we have shown that around the plasma frequency a broad thickness dependent optical resonance is present in thin Bi films illuminated with far-infrared radiation. This resonance is purely transversal and can be partly explained by a screened free-electron gas in the Drude-approximation. The extremely large value of the optical dielectric constant of the Bi-lattice turns out to be a significant parameter in the determination of this optical resonance.

Deviations from the Drude-model can be explained either by two-phonon processes or by electron-impurity scattering. On grounds of this experiment it is still uncertain which of these two processes is the major one.

From an experimental point of view it has been shown that for Bi non-normal incidence is not important and that despite of the fairly rough film structure and a complex anisotropic crystal structure the films can be nicely approximated with a flat homogeneous isotropic film having bulk properties.

Acknowledgements

The authors wish to thank Dr. A.P. van Gelder and Dr. H. Sigg for the valuable discussions on the electrodynamics of thin films. Drs. W.J Kaal receives our appreciation for preliminary work on the experimental set-up. We are greatly indebted to prof. P. Grosse from the Technical University of Aachen for drawing attention to the electron-ionized-impurity scattering mechanism.

References

1. D. Pines, Elementary excitations in solids, (W.A.Benjamin, New York, 1964).
2. H.E. Bennet, and J.E. Bennet, in proceedings of the international colloquium on the optical properties and electronic structure of metals and alloys 1965 (Paris), Edited by F. Abèles, (North Holland, Amsterdam, 1966) p.175-188.
3. G.E.H. Reuter, and E.H. Sondheimer, Proc.Roy,Soc.London **A195**, 336 (1948).
4. W.S. Boyle, and A.D. Brailsford, Phys.Rev.**120**, 1943 (1960).
5. R. Zallen, Phys.Rev.**173**, 824 (1968).
6. R.N. Zitter, and P.C. Watson, Phys.Rev.B **10**, 607 (1974).
7. R.H. Ritchie, Surface Science **34**, 1 (1973).
8. G. Rasigni, J.P. Palmari, and M. Rasigni, Phys.Rev.B **12**, 1121 (1975).
9. E. Gerlach, P. Grosse, M. Rautenberg, and W. Senske, Phys.Stat.Sol.(b). **75**, 533 (1976).
10. E. Gerlach, and P. Grosse, in Festkörperprobleme XVII, Adv.in Sol.State Physics, Edited by J. Treusch, (Dortmund, 1977) p.157-193.
11. K.L. Kliewer, and R. Fuchs, Phys.Rev.**150**, 573 (1966).
12. R. Fuchs, K.L. Kliewer, and J. Pardee, Phys.Rev.150, 589 (1966).
13. K.L. Kliewer, and R. Fuchs, Phys.Rev.**153**, 498 (1967).
14. G.W. Chantry, M.M. Evans, J. Chamberlain, and H.A. Gebbie, Infrared Phys.**9**, 85 (1969).
15. E.V. Loewestein, D.R. Smith, and R.L. Morgan, Appl.Opt.12, 398 (1973).
16. L.J. van der Pauw, Philips Tech.Rev.**20**, 221 (1958/59).
17. K. Abdelmoula, B. Parolo, C. Pariset, and D. Rinard, Thin Solid Films **62**, 273 (1979).
18. A. Barna, P.B. Barna, R. Fedorowich, G. Radnoczi, and H. Sugawara, Thin Solid Films **36**, 75 (1976).
19. M.S. Dresselhaus, in The physics of semimetals and narrow-gap semiconductors-1970 (Dallas), Proceedings of the conference, Edited by D.L. Carter, and R.T. Bate, (1970) p.3.
20. R.N. Zitter, Phys.Rev. **127**, 1471 (1962).
21. A.A. Cottey, J.Phys.C: Solid State Physics **8**, 4135 (1975).
22. Yu.F. Komnik, E.I. Bukhshtab, Yu.F. Nikitin, and V.V. Andrievskii, Sov. Phys. JETP.**33**, 364 (1971).
23. J.M. Noothoven van Goor, Donors and acceptors in Bi, Philips Res.Repts.Suppl.**4**, 1 (1971)
24. R.L. Blewitt, and A.J. Sievers, J. of Low Temp.Phys.13, 617 (1973).
25. A.R. Melnyk, and M.J. Harrison, Phys.Rev.B **2**, 835 (1970).

26. A.R. Melnyk, in Polaritons-1972 (Taormini), Proceedings of the first Taormini research conference on the structure of matter, Edited by E. Burnstein, and F. de Martini (Pergamon, 1972) p.221-228.
27. R. Schuchhardt, R. Rudolph, R. Keiper, and H. Krüger, Phys.Stat.Sol.(b). **97**, 257 (1980).
28. C. Nanney, Phys.Rev.**129**, 109 (1963).
29. W. Steinman, Phys.Stat.Sol. **28**, 437 (1968).
30. A.J. McAllister, and E.A. Stern, Phys.Rev.**132**, 1599 (1963).
31. C.G.C.M. de Kort, J.H.M. Stoelinga, and P. Wyder, Physica **101B**, 1-21 (1980)
32. In reference 31 several expressions not affecting the results should be corrected as follows:
eq.2.13 expression for E^t; $cE_2^-/i\omega F_2^-$ must be preceded by a minus sign.
eq.2.14 expression for α; $F_1^+ + F_1^-$ should read $F_1^+ - F_1^-$.
eq.2.17 F_1^+ and F_1^- should be interchanged.
eq.2.19 F_2^- and F_2^+ should be interchanged.
33. R.N. Zitter, in The physics of semimetals and narrow-gap semiconductors, see this paper reference 19, p.289-295.
34. W.B. Grant, H. Schulz, S. Hüfner, and J. Pelzl, Phys.Stat.Sol.(b). **60**, 331 (1973).
35. R.E. MacFarlane, in The physics of semimetals and narrow-gap semiconductors, see this paper reference 19, p.289.
36. W.G. Spitzer, in Semiconductors and Semimetals vol.3 Edited by R.K. Willardson, and A.C. Beer, (Ac.Press, New York, 1967) p.17.
37. M. Lax, and E. Burnstein, Phys.Rev.**97**, 39 (1955).
38. R.A. Cowley, Adv.Phys.**12**, 421 (1963).
39. P. Grosse, in Recent developments in condensed matter physics vol.1, Edited by J.T. Devreese, (Plenum Publ.Corp., 1981) p.783.
40. O. Madelung, Introduction to Solid-State Theory sec.2.1, (Springer-Verlag, New York, 1978).
41. H. Mayer, and L.M. Blanaru, Z.Phys.**249**, 424 (1972).

PART II

MAGNETIC RESONANCES IN DILUTE SEMIMAGNETIC SEMICONDUCTORS AT FAR-INFRARED ENERGIES

CHAPTER 1

General introduction

The following part of this thesis deals with electron paramagnetic resonances (EPR) in dilute semimagnetic semiconductors (DMS). These DMS are often made of II-VI semiconductors in which part of the cations has been replaced by Mn^{2+} ions. Due to a partially filled $3d^5$ shell, Mn^{2+} ions posses a S=5/2 total electron spin which is six-fold degenerated. Applying a magnetic field lifts this degeneracy and optical transitions obeying the selection rule $\Delta S_z=1$ can be induced between the now separated energy levels. A common method to study the magnetic excitations in DMS is to measure the sample transmission of fixed frequency microwave or far-infrared radiation as a function of the magnetic field in the Faraday configuration. This method will be used in the experiments described in this thesis.

A widely used DMS for EPR studies is the wide gap II-VI semiconductor $Cd_{1-x}Mn_xTe$ in which x presents the fraction of manganese atoms. Usually x ranges from 0 to .7. The upper limit to this manganese concentration is due to the fact that pure CdTe has another crystal lattice (zincblende fcc) than pure MnTe (hexagonal). Therefore, in order to study the properties of the manganese atoms in their undisturbed fcc host lattice, the manganese concentration x has to be smaller than $x \simeq .7$.

As a function of concentration x, the magnetic properties of $Cd_{1-x}Mn_xTe$ exhibit some different phases. For very low concentrations $x<.01$ there exists no interaction between the Mn^{2+} ions and one observes in principle paramagnetic resonances of individual ions giving rise to very narrow resonance lines. For increasing concentrations the Mn^{2+} ions start to feel each other through dipole-dipole interaction. Because of a random manganese ion distribution in the lattice the experienced internal dipole field will not be the same for all ions, hence giving rise to a significant broadening of the observed resonance energies. Line-shape analysises of the resonances in this concentration regime can be used to study the strength of the dipole-dipole interaction. If the concentration of manganese atoms exceeds $x \simeq .03$, nearest neighbour (NN) interaction becomes important. The NN will be proportional to $-2J_1S_{z1}S_{z2}$ in which J_1 is the Heisenberg ferromagnetic exchange parameter, and which energy equals roughly 10 Kelvin. (Because of the antiferromagnetic nature of the interaction an extra minus sign is included.) The exchange interaction tends to reduce the effect of the dipole-dipole interaction, and therefore the resonance energies sharpen again with concentration. This effect is called exchange narrowing. For concentrations $x>.19$ every Mn^{2+} atom will have at least one nearest neighbour of its own kind (percolation limit) which gives the onset for the existence of spin-glass and antiferromagnetic phases in the sample. For even more increasing concentrations the observed excitations will become more and more collective and can be conceived as a chain of interacting Mn^{2+} spins due to NN interaction. Such a chain can be described by a magnon, and presents the onset of antiferromagnetic resonances (AFMR) in the sample, although experiments concerning for example specific heat measurements predict a transition to the antiferromagnetic phase at much higher manganese concentrations ($x \simeq .6$).

The purpose of the experiment described in the following paper is mainly to investigate the presence of AFMR and magnon modes in samples below the often mentioned critical concentration $x_c = .6$. As a second aim the EPR of the single Mn^{2+} ions will be followed as a function of concentration and magnetic field up to very high field strengths. Concerning the latter experiment, the EPR linewidth increases strongly at medium concentrations due to the already mentioned dipole-dipole interaction. The linewidth easily surpasses a few teslas for $x > .01$. Hence, experiments in high magnetic fields as previously not available are necessary, in combination with far-infrared radiation in order to observe properly the resonances in samples having a medium or large manganese content. As a bycoming advantage, for concentrations of order of $x \simeq .1$ the exchange narrowing can be reduced by a competition between the internal exchange fields and the externally applied magnetic field, allowing us to determine the strength of these internal fields.

Concerning the onset of AFMR at concentrations $x > .1$ as previously discussed, we have been able to follow and identify the magnon excitations in the sample as a function of both energy and manganese concentration. It is shown for the first time that the magnon modes start at zero magnetic field with a finite resonance energy, and increase with field according to a g-factor equal to 2. Previously obtained resonances,using either Raman or neutron scattering techniques, usually without a magnetic field, have now been identified as coming from the same magnon mode.

The following sections contain a slightly modified version of a paper concerning the experiment mentioned above which has recently been submitted to the Physical Review B. This work has been done together with Dr. A.Wittlin from the Institute of Physics, Warsaw, Poland.

CHAPTER 2

High field magnetic resonances in $Cd_{1-x}Mn_xTe$.

ABSTRACT

We have studied magnetic resonances in $Cd_{1-x}Mn_xTe$ as a function of the manganese concentration x at high magnetic fields up to 22T, by means of far-infrared magnetospectroscopy at T=4.2K. For concentrations $x \geq .3$ an antiferromagnetic-like resonance (AFMR) is observed which extrapolates to a finite zero-magnetic field excitation energy. This zero-field energy increases with concentration x and agrees for x=.65 with energies observed earlier in inelastic neutron scattering and Raman scattering experiments. The AFMR g-factor is found to equal 2 for all concentrations x. Therefore the observed AFMR is expected to rise rather from a single than from a double magnon excitation. For concentrations $x \leq .1$ the electron paramagnetic resonance (EPR) of the Mn^{2+} ions is observed up to the highest magnetic fields. For x=.1 a significant line-broadening is found with increasing magnetic field, which is attributed to the competition between external magnetic fields and the exchange-field induced line-narrowing.

I. INTRODUCTION

Magnetic properties of the semimagnetic semiconductor $Cd_{1-x}Mn_xTe$ at low temperatures have recently been the subject of several experimental and theoretical investigations[1-8], due to the fact that this system is very suited for the study of short-range magnetic interactions in dilute materials. As the manganese concentration x increases, the crystal undergoes a spin-glass (SG) transition at x=.17, and above $x \simeq .6$ a transition to an antiferromagnetic (AF) phase[9]. However, neither the details of the magnetic phase diagram, the magnetic structures in the ordered phase, nor the precise critical concentrations x_c for the onsets of the different magnetic excitations[10-12] are fully understood. For instance, the magnetic susceptibility and specific heat investigations[9] of $Cd_{1-x}Mn_xTe$ at low temperatures have indicated a short-range magnetic ordering already below the critical concentration $x \simeq .6$, which was later confirmed by neutron scattering experiments[13]. In a subsequent series of Raman scattering investigations[1,14,15] antiferromagnetic-like excitations interpreted as magnon modes have been observed also at concentrations well below x=.6. These resonances were attributed to the formation of small antiferromagnetic domains in the sample. Two different interpretations of these magnon modes have been proposed, namely one-magnon excitation at the Brillouin zone center[1], or two-magnon processes at the zone boundary[14]. Later obtained results of inelastic neutron scattering are more in agreement with the single magnon model proposed by Ramdas[1], however its validity is still under dispute[11,16].

To understand more fully these excitations we present in this paper the results of magnetotransmission experiments performed on $Cd_{1-x}Mn_xTe$ samples having a wide range of manganese concentrations. The experiments were carried out in magnetic fields up to 22T in the far-infrared (FIR) range of the spectrum. Because the applied excitation frequencies are over an order of magnitude higher than in conventional EPR experiments, we can now observe the magnetic resonances at low temperatures over the whole range of manganese concentrations.

A pronounced feature of the EPR spectra in $Cd_{1-x}Mn_xTe$, as well as in other semimagnetic semiconductors[17], is a significant increase of the resonance linewidth upon decrease of the temperature or increase of the manganese concentration. Therefore, typical EPR experiments at low magnetic fields have been limited until now to either low concentrations or high temperatures. This experimental drawback becomes increasingly worse at concentrations in excess of $x \simeq .2$ due to resonance shifts to lower energies as has been observed recently[18]. Therefore the use of very high magnetic fields and consequently high excitation energies, as applied in our experiment, are necessary to investigate properly the low temperature resonances for higher manganese concentrations x.

For large x the resonance energies covered in our experiment correspond to previously observed energies of collective excitations in the ordered phase (AFMR), whereas for small $x(<.1)$ single Mn^{2+} EPR modes can be observed up to the highest magnetic fields. Furthermore at these high fields at low concentrations practically all Mn^{2+} spins will be lined up because the value of the external magnetic field will approach the value of the internal exchange fields, hence allowing a study of magnetic resonances near complete magnetic saturation.

II. EXPERIMENT

The single crystals of $Cd_{1-x}Mn_xTe$ with $.002 \leq x \leq .65$ were grown by a modified Bridgeman Technique at the Institute of Physics in Warsaw. All samples were cleaved along the (110) plane and polished in the form of discs having diameters from 6 to 10 mm and thicknesses from 1-5 mm.

Magnetotransmission measurements were made in the Faraday configuration at T=4.2K. At fixed laser frequencies the transmission was measured as a function of the magnetic field. The FIR radiation was generated by an optically pumped FIR molecular gas laser. A standard lightpipe system was used to collect the radiation on the sample. as a detector a LHe-cooled detector made of an Allen Bradley carbon resistor was used. A polyhelix-Bitter solenoid provided DC magnetic fields up to 22T. For some samples measurements at very low excitation energies (ν<200 GHz) have been done using a backward wave oscillator.

III. RESULTS AND DISCUSSION

A. High concentrations

Fig.1 shows the transmission for six $Cd_{1-x}Mn_xTe$ samples with x between .002 and .65 as a function of magnetic field. The frequency of the incident radiation was 561 GHz. The transmission values were scaled at B=0T to permit relative comparison between different spectra. Note that with increasing manganese concentration the resonance shifts to lower fields and the linewidth increases as observed before[18,19]. However, the low field measurements were unable to distinguish whether the observed shift to lower fields with concentration was caused either by changes in the g-factor[19] or by the presence of internal fields[20]. Therefore, in fig.2 the positions of the resonance energies are plotted versus magnetic field for several concentrations.

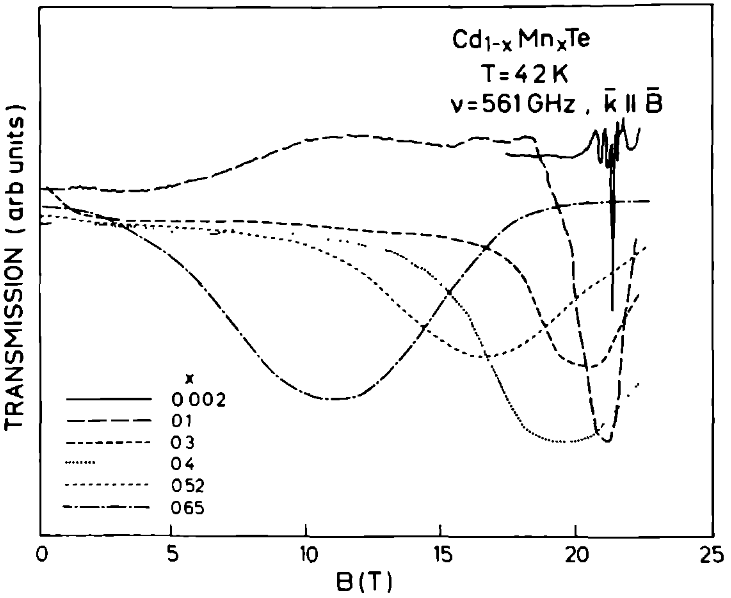

Fig.1. The transmission of 561 GHz radiation as a function of magnetic field for all $Cd_{1-x}Mn_xTe$ samples, $.002 \leq x \leq .65$. The transmission values are relatively scaled to allow easy comparison of the resonance positions.

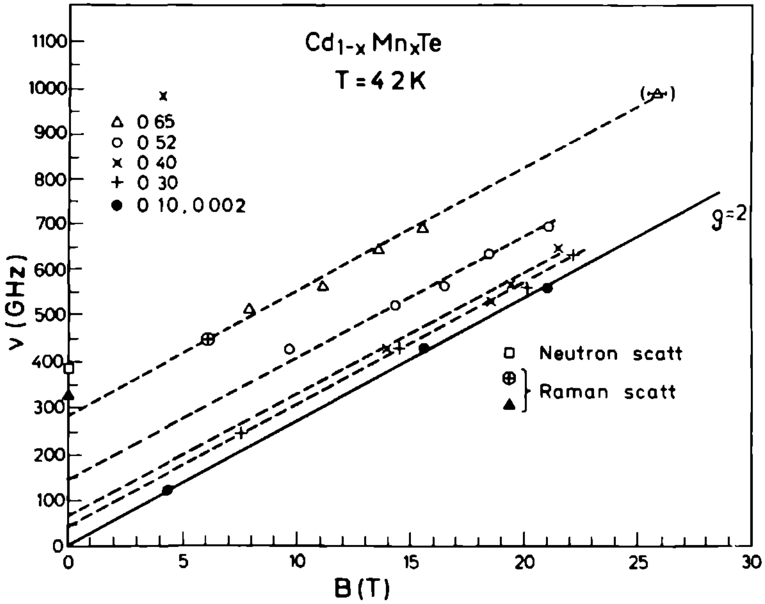

Fig.2. The resonance frequency versus magnetic field for several manganese concentrations. The position of the high field resonance at 989 GHz for x=.65 presents an extrapolated value, because only a part of the resonance could be observed below B=22T. The solid line marks a g=2 EPR transition. The dashed lines present least square fits to the experimental results. For comparison the obtained magnetic excitation energies from neutron scattering, (□); refs.13 and 16, and of Raman scattering, (⊕); ref.1, and (△); ref.14 are also indicated.

The solid line marks a g=2 EPR transition, and it is clearly shown that all dashed lines, which present least square fits to the measurements, have practically the same slope as the g=2 resonance. This figure also shows that for $x \geq .3$ a linear extrapolation of the resonance frequency to zero magnetic field yields a finite resonance energy which can be attributed to an antiferromagnetic resonance mode (AFMR).

Although the extrapolation from fairly high fields to zero magnetic fields may introduce certain errors, it is still interesting to compare these results with those of other low, or zero field studies of the magnetic excitations in Mn-rich $Cd_{1-x}Mn_xTe$. For this reason we have included in fig.2 also some results of inelastic neutron scattering[16] (NS), and Raman scattering[1,14] (RS) experiments. Corresponding points in the figure mark the positions of the resonances observed by these techniques. Especially the agreement with the RS data at B=6T is very good and convincing. The deviations for the zero field RS and NS data is possibly due to slight differences in chemical composition of the used samples. Moreover those measurements have been done at either lower (1.8K) or higher (10K) temperatures which introduces some changes in the resonance energies.

To display better the zero-field resonances, their energies are plotted in Fig.3 as a function of the manganese concentration x together with the Raman[1,14] and neutron scattering[16] results. This figure suggests that the low temperature far-infrared resonance as observed in our experiment for x≥.3 is an AFMR at finite magnetic fields.

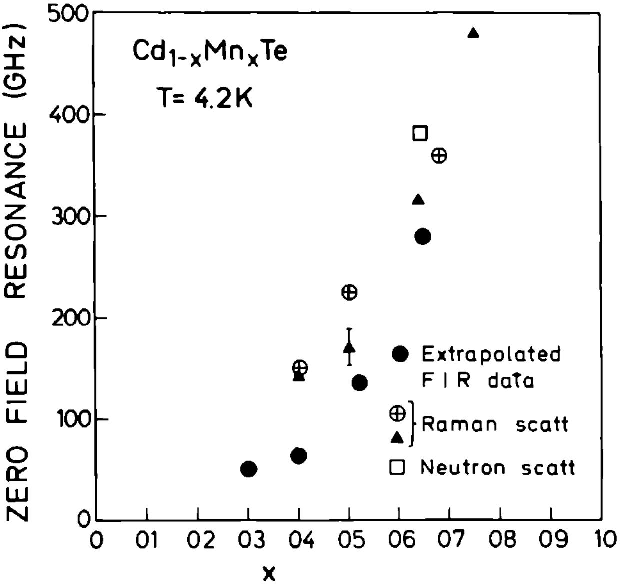

Fig.3. The zero-field resonance frequency as a function of the manganese concentration x. (⊕); Raman results from ref.1, (Δ); Raman results from ref.14, and (□); neutron scattering results from ref.16. (●) represent linear extrapolated points of FIR data from fig.2.

Moreover, for x=.65 the resonance frequency complies well with the magnon excitation observed in neutron scattering experiments. With decreasing concentration x this resonance energy decreases and finally disappears near x≃.25, in reasonable agreement with the theoretical value of the percolation limit x_c=.19 for an fcc lattice. Such behaviour of AFMR is thought to be typical for resonances in dilute antiferromagnets[21], as above the percolation limit x_c small antiferromagnetic chains can be formed. Furthermore this agrees well with the Raman results[1] which have shown the persistence of a magnon mode up to quite low x values.

Now we would like to address the problem of the origin of the magnetic Raman excitation as observed by Ramdas[1], and Grynberg et al[14]. Figs.2 and 3 strongly indicate that the excitation energies as observed in these experiments correspond to the resonances seen in the magnetotransmission spectra, and as such are likely to have the same physical origin. Ramdas[1] describes the magnetic Raman peak as a single quantum (magnon) excitation in the antiferromagnetic ordered phase of $Cd_{1-x}Mn_xTe$. On the other hand Grynberg[14] analyses the results as a two-magnon effect, excluding single magnon excitation on grounds of a symmetry argument and the absence of higher energy magnetic excitations. However, as pointed out by Sievers[22], in a two-magnon process one magnon is emitted from each of the the normally degenerated spin-wave branches at the magnetic Brillouin Zone boundary. An external magnetic field splits these branches, of one magnon the energy is decreased, and of the other one the energy is increased with the same amount, henceforth yielding a two-magnon excitation energy independent on the magnetic field. As Fig.2 clearly shows the resonance frequency of the excitation to have a dependence on magnetic field corresponding to a g-factor equal to 2, we must unambiguously conclude that the observed AFMR is essentially due to a single magnon excitation, and *not* to a two-magnon process.

B. Low concentrations

Below x≃.1 the EPR resonance position, as seen in fig.1 is very well described by g=2 without a finite zero-field resonance energy, indicating the absence of antiferromagnetic ordering. The resonance positions versus magnetic field have become rather independent of the concentration. Therefore in principle we observe now the resonance energy of single Mn^{2+} spins, but having a linewidth affected by both dipole-dipole, and exchange interaction. The first mechanism tends to broaden the linewidth for concentrations x>.1, whereas the latter due to nearest neighbour interaction, for x>.3, will narrow the observed resonance (exchange narrowing). Because of this exchange narrowing, usual EPR measurements at low magnetic fields yield a linewidth for x=.1 of approximately 400 G. As shown in fig.1 however, the linewidth of the x=.1 resonance is much larger. This can be due to the very strong applied magnetic field which is of the same order of magnitude as the internal fields, hence reducing the importance of the exchange interaction. Measured linewidths at a few magnetic field values for x=.1 are given in fig.4, and

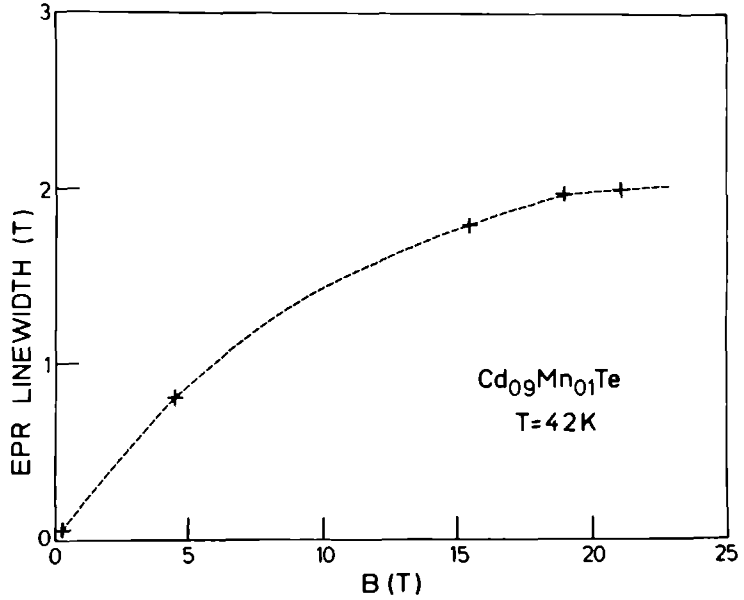

Fig.4. The linewidth of the EPR signal of the x=.1 sample as a function of the magnetic field at T=4.2K. The dotted line serves only as a guide to the eye.

show an increase with magnetic field which tends to saturate above B≃18T, thus supporting the idea of the external magnetic field approaching the strength of the internal exchange fields.

As a last analysis to demonstrate the separate spin character of the high field resonance at x=.1, fig.5 shows a fit to the line shape using a simple Bloch 2-level spin model for non-interacting localized spins taking into account the effects of electromagnetic wave propagation in a parallel slab[23]. The lineshape was fitted with a .75 Lorenzian, .25 Gaussian shape function. The static sample magnetization was used as a fitting parameter and found to be equal to 7±1 emu/g at B=21 T, in agreement with results of high field magnetization measurements which gave 6.1 emu/g at the same field[24].

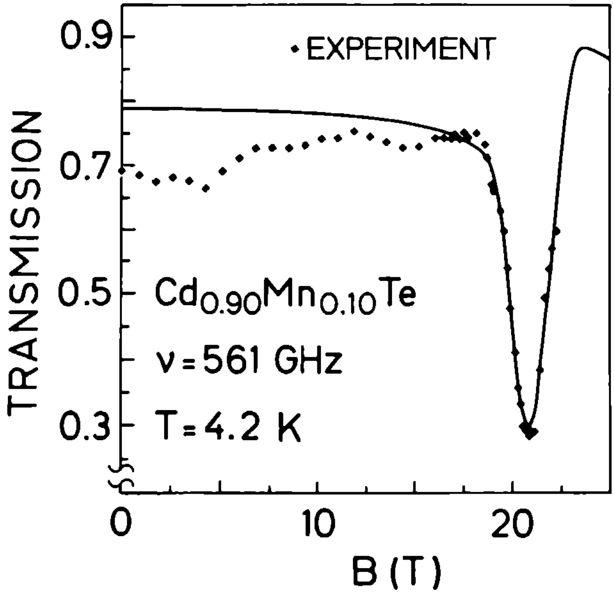

Fig.5. The transmission of 561 GHz radiation as a function of the magnetic field for the x=.1 sample, together with a theoretical fit using a model for separated independent spins as described in the text.

IV. CONCLUSION

In summary, we have measured magnetic resonances at high magnetic fields in $Cd_{1-x}Mn_xTe$ for a broad range of manganese concentrations x. At low concentrations a line-broadened paramagnetic resonance is observed having a g-factor equal to 2. At concentrations $x \geq .3$ an antiferromagnetic resonance is observed which complies very well with previously observed magnon modes using Raman and neutron scattering techniques. On grounds of the observed magnetic field dependence of this excitation the resonance is ascribed to a single magnon mode having a g-factor equal to 2, and not to a two=magnon mode as recently has been suggested.

Acknowledgements.

The authors are grateful to Professor S. von Molnar for a critical reading of the manuscript, and to Dr. A. Mycielski for a generous gift of samples. A.W. acknowledges financial support from the Max-Planck-Gesellschaft.

References

1. A.K. Ramdas, J.Appl.Phys.53, 7649 (1982).
2. J.K. Furdyna, J.Appl.Phys.53, 7637 (1982).
3. R.E. Kremer and J.K. Furdyna, Phys.Rev.B31,1 (1985).
4. P. Wolf, Proc.Int.Conf."The application of high magnetic fields in semiconductor physics", Würzburg 1986.
5. K.C. Hass, B.E. Larson, H. Ehrenreich and A.E. Carlsson, J.of Magnetism and Magnetic Materials 54-57, 1283 (1986).
6. T.M. Giebultowicz, J.J. Rhyne, W.Y. Ching, D.L. Huber and R.R. Galazka, J.of Magnetism and Magnetic Materials 54-57, 1149 (1986).
7. B.E. Larson, K.C. Hass and R.L. Aggerwal, Phys.Rev. B33, 1789 (1986).
8. Su-Huai Wei and A. Zunger, Phys.Rev.Lett.56, 2391 (1986).
9. R.R. Galazka, S. Nagata and P.M. Keesom, Phys.Rev.B22, 3344 (1980).
10. M.A. Novak, O.G. Symko, D.J. Zheng and S. Oseroff, Phys.Rev.B33, 6391 (1986).
11. U. Steigenberger, B. Lebech and R.R. Galazka, J.of Magnetism and Magnetic Materials 54-57, 1285 (1986).
12. A. Petrou, D.L. Peterson, S. Venugopalan, R.R. Galazka, A.K. Ramdas and S. Rodriguez, Phys.Rev.Lett.48, 1036 (1982).
13. T. Giebultowicz, M. Kepa, B. Buras, K. Clausen and R.R. Galazka, Solid State Commun.40, 499 (1981).
14. M. Grynberg, M. Picquart, J.Phys.C: Solid State Phys.14, 4667 (1981).
15. M. Piquart and M. Grynberg, J.Appl.Phys.53, 8166 (1982).
16. T. Giebultowicz, B. Lebech, B. Buras, W. Minor, M. Kepa and R.R. Galazka, J.Appl.Phys.55, 2305 (1984).
17. A. Wittlin, R. Triboulet and R.R. Galazka, J.Crystal Growth 72, 380 (1985).
18. R.E. Kremer and J.K. Furdyna, Phys.Rev.B32, 5591 (1985).
19. S.B. Oseroff, Phys.Rev.B25, 6584 (1982).
20. D.J. Webb, S.M. Bhagat and J.K. Furdyna, J.Appl.Phys.55, 2310 (1984).
21. M.C.K. Wiltshire, J.Phys.C: Solid State Phys.,10, L37 (1977).
22. A.J. Sievers, in "Elementary excitations in solids", Ed. by A.A. Maradudin and G.F. Nardelli, Plenum Press, N.Y. London 1969.
23. D.P. Mullin and J.K. Furdyna, J.Appl.Phys.51, 2799 (1980).
24. D. Heiman, E.D. Isaacs, P. Beda and S. Foner, Phys.Rev.B35, 3307 (1987).

PART III

TIME-RESOLVED FAR-INFRARED SPECTROSCOPY OF SHALLOW DONOR RECOMBINATION MECHANISMS IN VERY PURE InP.

CHAPTER 1

General introduction

At low temperatures, conduction in (slightly) n-doped semiconductors occurs mainly through the presence of electrons in the conduction band coming from ionised shallow donor impurities. These are atoms in the semiconductor host lattice of which the electrons in the outer atomic shell are weakly bound. The donor atom can give up one electron to the conduction band, leaving behind effectively a single fixed positive charge. Therefore the presence of this donor in the lattice is more or less equivalent to the presence of a hydrogen atom in the vacuum. The binding energy of the additional electron to the impurity atom can as such be rather accurately described by a hydrogen-like model, in which all energy levels are as in a free proton-electron pair only with the dielectric permitivitty ϵ_0 replaced by $\epsilon_0\epsilon_s$, in which ϵ_s is the static dielectric constant of the host material, and with the free-electron mass replaced with the effective electron mass at the bottom of the host materials conduction band. Dependent on the semiconductor this yields for III-V semiconductors an effective Rydberg energy of the order of 5 to 10 meV. Therefore these shallow impurities are energetically seen situated several meV below the conduction band and can be easily ionised, which populates the conduction band with electrons. As in hydrogen atoms the groundstate is called the 1s level and the most important excited states are the 2s/2p levels which are degenerate at zero magnetic field. The process of ionisation occurs mainly in three different fashions:

1) Thermal excitation from the 1s or the 2s/2p states to the conduction band.

2) Optical excitation from the 1s state directly to the conduction band or to excited states from which further thermal excitation into the conduction band occurs. The latter processes are called photo-thermal ionisation or photo-thermal conductivity.

3) Impact ionisation from the ground state or an excited state into the conduction band through collisions of accelerated electrons (due to an applied electric field) with the impurities.

From these processes (thermal)-photoconduction presents a very important mechanism. On one side using simple electronics, a far-infrared detector can be built as the detectors conductivity is directly proportional to the intensity of the incident radiation. On the other side the photoconductive processes can be used to characterise the impurity contents of the sample as will be discussed shortly.

Applying a magnetic field to these systems lifts the degeneracy of the hydrogen-like energy levels. Using fields of a few teslas, the 2p level splits in $2p_0$, $2p_-$ and $2p_+$. The $1s \rightarrow 2p_+$ transition rate becomes very strong, dominating the spectral response of the system to incident radiation. In such a way it is possible to construct a sensitive narrow-band tunable far-infrared detector. Due to central cell corrections from the ground state with respect to the hydrogen-like model, transition energies are slightly impurity dependent. Therefore investigation of the $1s \rightarrow 2p_+$ transitions in rather pure samples can reveal the chemical nature of the impurities in the semiconductor.

On grounds of the application of photoconducting systems as far-infrared detectors it is highly interesting to look at the dynamical responses of these shallow donor systems in order to find out how fast such a detector can be. In this context little is known about the timescales involved in exciting electrons from the ground state into higher states or into the conduction band, which are processes that govern the response time of the detector (i.e. the onset of photoconduction). After excitation to the conduction band, decay times to bound states determine the time resolution of such a detector. In this study the decay times are studied as a function of incident radiation intensity, magnetic field, and applied bias voltage on the detector. The presence of excited states which act as bottleneck reservoirs for electrons as well as the sometimes dominant role of impact re-excitation will be thoroughly discussed. The following chapter contains a slightly modified version of an article by J.M. Chamberlain, A.A. Reeder, L.M. Claessen, G.L.J.A. Rikken, and P. Wyder in the Physical Review **B35**, 2391 (1987).

CHAPTER 2

Impact excitation and bottleneck effects in the time-resolved far-infrared photoresponse of high purity InP

ABSTRACT

The time-resolved photoresponse of high purity ($\mu_{77K} \simeq 10$ m^{2}V^{-1}s^{-1}) n-type indium phosphide has been investigated at $\lambda = 118.8$ μm using a pulsed far-infrared laser. An effective conduction-band lifetime of 60 ns is found which increases slightly in a magnetic field. For sample DC bias voltages exceeding a few volts per centimetre long tails develop in the photoresponse which last more than 10 μs. The behaviour of these tails is examined for various incident laser powers, magnetic fields and sample bias voltages. It is shown that a four level model involving impact excitation from impurity states is necessary to describe the photoconductive response. A critical requirement of the model is that the lifetimes of participating "bottleneck" states are 2 μs and 10 μs. On the basis of known transition probabilities these bottlenecks are therefore tentatively assigned to the $2p_-$ and 2s states.

I. INTRODUCTION

Time-resolved studies of far-infrared photoconduction are a comparatively direct means of examining the dynamical properties of the non-equilibrium distribution following disturbance by pulsed laser excitation. The equilibrium far infra-red (FIR) photoconductivity of InP has been studied for over a decade[1] and has been used as a sensitive assay technique for shallow donor contaminants[2,3] and to investigate solid state analogues of the H- system[3,4]. Despite this significant interest in equilibrium effects, very little attention has been paid to dynamical measurements in this system.

High power CW FIR lasers have been used to saturate the $1s \rightarrow 2p\pm$ transitions and the cyclotron resonance[5-7] in GaAs; impurity-state and Landau-level lifetimes have been inferred from these measurements assuming appropriate two-level or three-level models. It is a conclusion of such measurements for GaAs that very long effective lifetimes of up to 500 ns, can be found for the $2p_-$ state which acts effectively as a "bottleneck" in the recombination process.

Although no saturation-absorption measurements have been described for InP, Ohyama[8] has reported extremely long ($\simeq 5$ μs) lifetimes for conduction band electrons in InP using FIR pulses synchronised with an external electric field and/or flashlamp. The possible existence of such long lifetimes in InP, and the likely consequences for the kinetics of the shallow donor photoconduction process, motivated an examination[9] of pulsed FIR photoconductivity cin very high purity InP. The present article presents additional experimental information and provides a mechanism to explain the long "tails" which could be seen in the photoresponse. A model involving multiple re-excitations into the conduction band is developed which implies the presence of two "bottleneck" states. Numerical simulations of the photoresponse based on this model are presented and compared with the experimental data.

Section II describes the electrical properties of the samples and the experimental arrangement. The results are presented in Section III and the discussion of these data falls into two parts. Section IV A analyses the behaviour of the short-term (<1 μs) photosignal in comparison with the behaviour of GaAs, and provides an explanation of characteristic "overshoot" effects of the photoresponse with respect to the laser stimulus. Section IV B fully describes the model which is used to explain the long term (>1 μs) photoconductivity. It is shown that the results obtained by this model depend critically on the values of the transition rates involved, which are consistent with reported values in the literature.

II. EXPERIMENT

Samples of very high purity indium phosphide[10] were provided with four ohmic contacts: the electrical characteristics of these samples are given in Table 1.

TABLE 1. *Characteristics for different samples.*

Sample	n 10^{14}cm^{-3} (at 300K)	n 10^{14}cm^{-3} (at 77K)	μ m^{2}V^{-1}s^{-1} (at 300K)	μ m^{2}V^{-1}s^{-1} (at 77K)	Thickness (μm)
No.1	2.0	2.3	.484	11.4	8
No.2	1.6	1.6	.47	12.9	13
No.3	1.1	1.1	.48	12.3	10

The specimens were mounted in a 4.2 K immersion cryostat in a magnetic field with light pipe access. An electrically pulsed Q-switched (EQ switched) CO_2 laser described elsewhere[11] in detail was used to pump a FIR waveguide laser with CH_3OH as the active medium. In figure 1 the laser system is presented. The CO_2 laser is used in the pulsed mode in which the gasdischarge is pulsed with a duration of roughly 100μsec. A CdTe electrooptical crystal in the laser path is used to rotate the angle of polarisation of the laserlight which in combination with a $\lambda/4$ plate makes the Q-factor of the laser cavity tunable. Laseraction can therefore only occur when a high voltage is applied during ≃100nsec to the CdTe crystal, in such a way producing laserpulses of 50 to 100nsec. This system was capable of producing FIR pulses of variable length (75-500 ns) with a repetition rate of 300 Hz, and having a very good reproducibility. The maximum FIR power at the sample was 500 mW, which corresponds to an intensity ≃5 W cm^{-2}. In most of the present experiments the specimen bias arrangements were configured in a constant current mode although the constant voltage mode was also used on occasions.

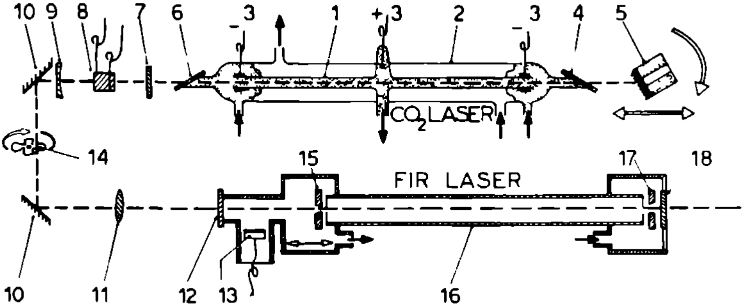

1	discharge tube	10	Au mirror
2	water cooling jacket	11	ZnSe focussing lense
3	HV electrodes	12	AR ZnSe window
4	ZnSe Brewster window	13	microphone
5	adjustable diffraction grating	14	chopper
6	Ge Brewster window	15	adjustable incoupling mirror
7	$\lambda/4$ plate	16	waveguide
8	CdTe EO crystal	17	outcoupling mirror
9	outcoupling mirror	18	quartz window

Fig.1. The EQ-switched far-infrared laser system.

Figure 2 shows the general experimental system: the a.c. photoresponse of the sample is examined with a boxcar after preliminary amplification by a wideband preamp. The boxcar is triggered by the laser EQ switch, and a

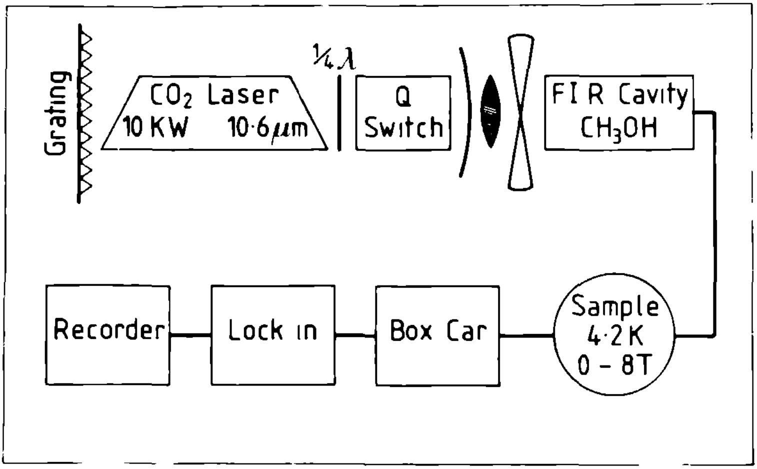

Fig.2. The general experimental arrangement.

lock-in is finally used to provide synchronous amplification. The photoresponse of a sample of n-GaAs (N_D - N_A =$2x10^{15}cm^{-3}$) was used to monitor the FIR laser output. Maan[12] has shown that this sample is capable of following the laser pulse.

The response characteristics of the measurement system were thoroughly investigated with dummy samples to ensure there were no artifacts in the experimental response. Particular attention was paid to the minimisation of stray EM pulses from the laser, and to the possibility of "geometrical" or electronic artifacts in the time resolved response.

III. RESULTS

The photoconductive response as a function of time for a typical InP sample (No.3) is shown in figure 3.

The sample dc bias is in this case well below the threshold value for impact ionisation or excitation effects. For the narrowest laser stimuli the decay is adequately represented by a single exponential with characteristic time τ. Examination of the photoresponse as a function of incident laser power indicates that τ is independent of laser intensity. The application of a magnetic field of 3.75 T (i.e.the resonant field for the 1s-$2p_+$ transition when λ=118.8 μm) produces a small, albeit significant, increase in τ for the same sample under identical bias and illumination conditions. Average values of τ for B = 0 and B = 3.75 T are 125 ns and 150 ns respectively. Effective con-

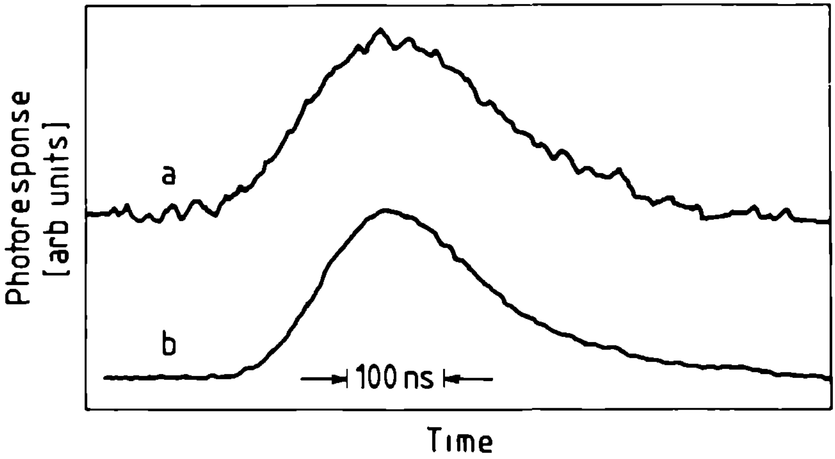

Fig.3. Photoconductive response of sample No.3 below V_T at 4.2K. a) 3.75T, b) 0T.

duction band lifetimes are obtained from these values in Section IV A. The magnetic field has no effect, within the limits (≃20 ns) of experimental observation, on the rise profile of the pulse.

The development of the InP photo-signal as a function of time is shown in figure 4 for increasing pulse widths and constant peak power. The breakdown in the simple exponential decay shape is evident for the widest photoresponses observed. The figure also indicates, for a particular InP response curve, the profile of the FIR laser stimulus. A characteristic "overshoot" between the maxima of stimulus and response is noted. Care was taken to ensure that this was not an artifact of the experimental geometry or signal-retrieval systems. The overshoot was found to increase approximately linearly with the integrated energy of the input pulse as shown in figure 5.

The comparatively simple photoresponse signal was observed to develop additional structure when the sample bias was raised above a characteristic threshold value V_T corresponding to a sample electric field of the order of 1 V cm^{-1}. Figures 6 and 7 show the development of these "tails" for B = 0 and 3.75 T.

The noise pattern in the tail is strongly suggestive of a random multiplication process. In some cases, dependent on compensation ratio and bias, the signal height of the tail was found to exceed that of the initial photoresponse. The existence of a prominent tail was noted at magnetic fields between 0 and 6 T: the shape of the tail is not resonant with the $1s \rightarrow 2p_+$

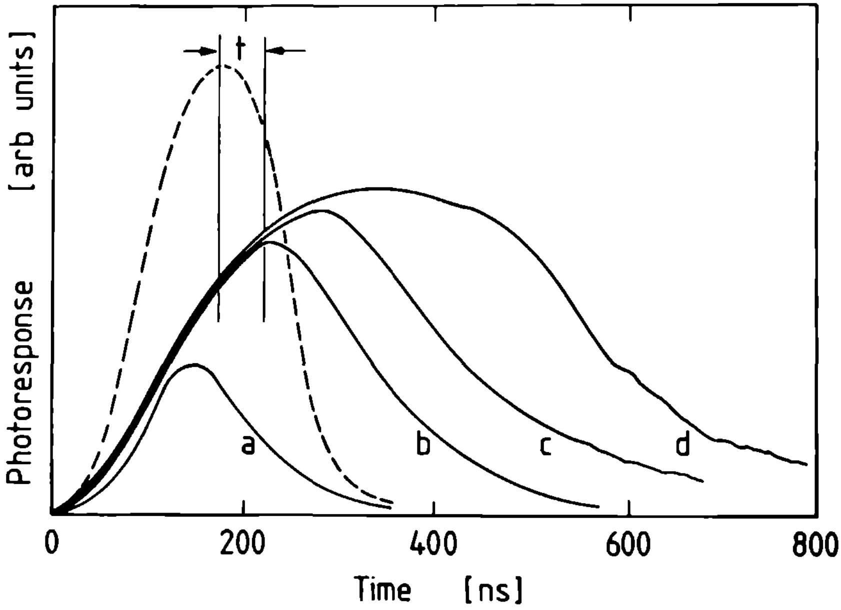

Fig.4. Development of short-term photoresponse of sample No.3 at 4.2K for increasing input pulse width. The stimulus pulse for one particular response (b) is shown as a dotted line, and the overshoot t is indicated.

signal. V_T was found to increase approximately linearly with magnetic field, and this strongly suggests the participation of impurity states in the tail mechanism. Similar observations of the tail were also made at 2 K. The photoresponse tails were seen in all the samples used with varying patterns and types of electrical contacts.

The dependence of the photoresponse on magnetic field at different times after excitation was investigated. Figure 8 indicates the difference in spectral information carried in the initial pulse and the tail: it is apparent that only a small amount of information is carried in the tail, whereas the short term response displays more strongly the $1s \rightarrow 2p_+$ transition.

The effects on both the initial and tail photoresponses when the incident laser power was varied were examined for the B=0 and B=3.75 T cases. Figure 9 shows this variation for samples No.3 and 1 at 3.75 T. It is evident that the initial photoresponse is beginning to saturate for laser powers > 5% of maximum. The tail, however, displays markedly different properties. In a magnetic field the tail photoresponse remains constant over some two to

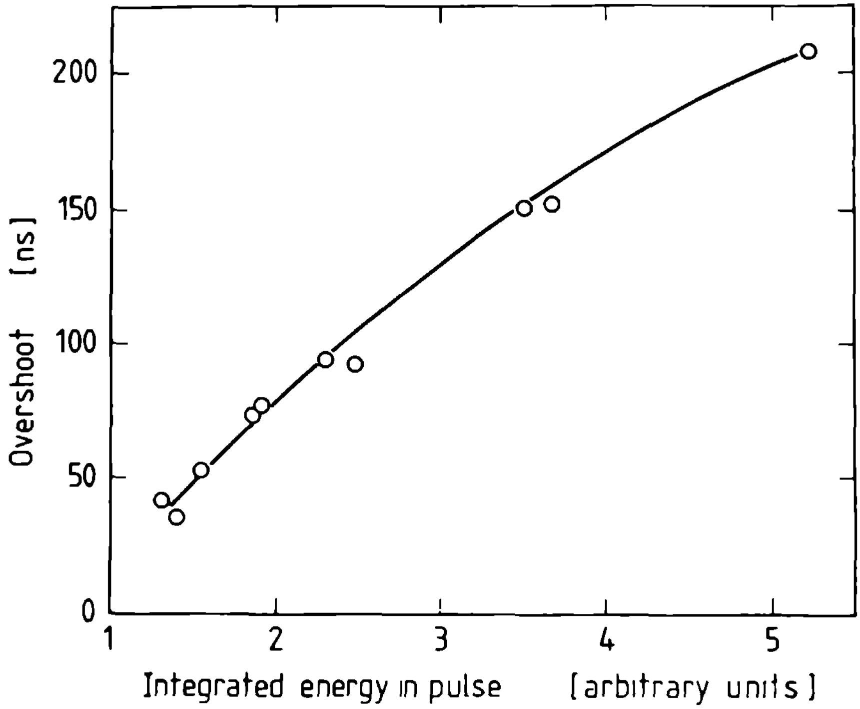

Fig.5. Graph of overshoot versus integrated input pulse energy for sample No.3 at T=4.2K.

three orders of magnitude change in incident laser intensity, whereas at zero field it decreases superlinearly.

The tail is believed to originate (next section) from a multiplication and "recycling" process which is random in nature, the efficiency of which would seem to be dependent on sample compensation ratios. It was, in some samples, difficult to establish the tail photoresponse in zero applied magnetic field.

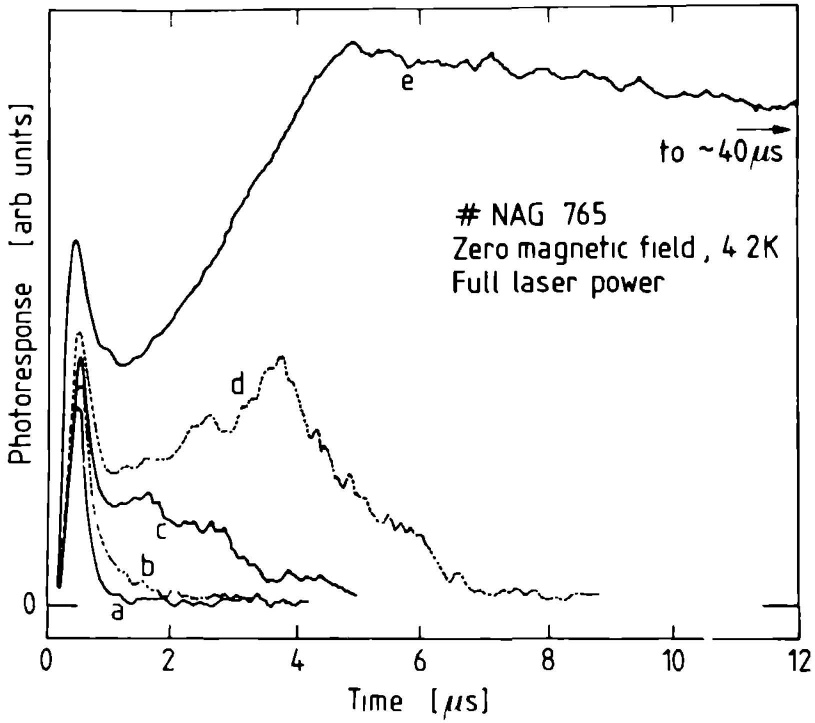

Fig.6. Characteristic tail patterns at 4.2 K, for sample No.3 at B = 0 T. The conditions of sample bias are a) 1.2 V cm^{-1}, b) 1.4 V cm^{-1}, c) 1.6 V cm^{-1}, d) 1.8 V cm^{-1}, e) 4 V cm^{-1}.

IV. DISCUSSION

A. Mechanism for the initial photoresponse ($t < 1$ μs)

The conventional processes of optical excitation and photoconduction are considered to be responsible for the initial photoresponse observed in figure 3. The photoexcitation process occurs in a characteristic time τ_{1c}, given by $\tau_{1c}=(\sigma_{1s}F)^{-1}$, where F is the photon flux and σ_{1s} the photoionisation cross section. With values[6] of F and σ_{1s} ($\simeq 10^{-14} cm^2$) appropriate to these conditions, τ_{1c} is much less than 1 ns. Using simple order of magnitude arguments and the known sample impurity concentration, it may be shown that a significant fraction (> 50%) of the donors are ionised by the laser pulse. This is consistent with the observation (figure 9) that the initial peak in the photoresponse begins to be saturated when $(I/I_0) > 5\%$. Furthermore, the sample

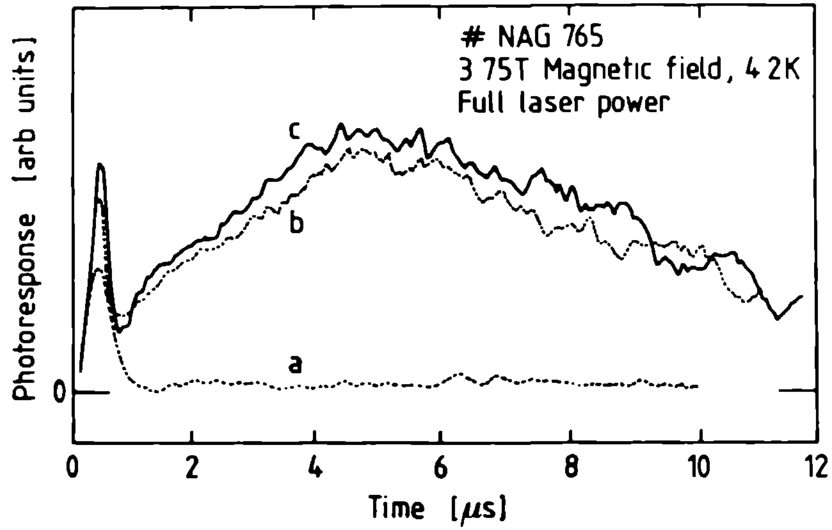

Fig.7. Characteristic tail patterns at 4.2 K for sample No.3 at B = 3.75 T. The conditions of sample bias are a) 4 V cm^{-1}, b) 6.8 V cm^{-1}, c) 10 V cm^{-1}.

resistance (as calculated from the photosignal during saturation) closely matches the minimum obtainable dc resistance due to thermal ionisation of donors, hence supporting the argument that a very large fraction of the donors are ionised. At zero magnetic field, injection into the conduction band is at approximately 2.5 meV. An effective carrier temperature, T_e, is established within $\simeq 10^{-11}$s by carrier-carrier scattering[6,7]. The warm electron gas gains further energy from each optically excited electron and from dc carrier heating, losing energy by acoustic phonon emission. Under present conditions this total heating rate is estimated at 3 μw. The analysis of McManus et al[13] provides an approximate value of $T_e \simeq 5$K, assuming 10^{-9}s as the time for acoustic phonon emission[13,14] under the present conditions. Electrons in the gas eventually decay through excited impurity states: the possibility of thermal re-excitation is not considered to be significant in this case.

To obtain an absolute value from the present measurements for the conduction effective lifetime, τ in InP at zero field under low bias conditions, it is necessary to deconvolve the laser decay profile from the experimental data of figure 3. A reasonable estimate may be made by noting the difference in decay times (50 ns) for the InP sample and GaAs detector, and assuming an effective lifetime of 10 ns in GaAs[6]. The effective lifetime is therefore 60

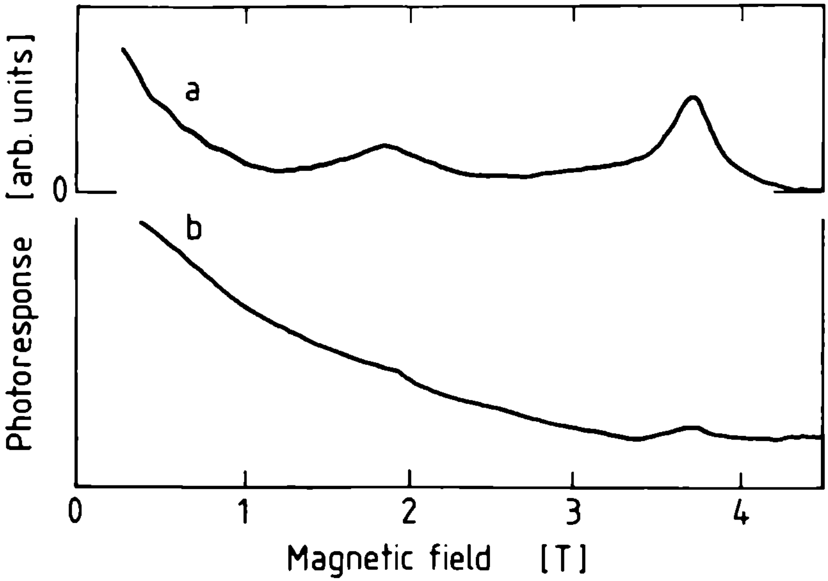

Fig.8. Photoconductive response versus magnetic field for sample No.2 at 4.2 K. a) short term response, b) tail response.

ns, a value supported by more recent experiments which directly measure this lifetime[15]. Consequently τ at the resonant magnetic field will be 85 nsec. The subsequent decay to the ground state occurs predominantly by phonon emission through excited states[16]: this process will be discussed more fully in the next section.

The characteristic "overshoot" in the photoresponse with respect to the stimulus (figure 5) has been investigated as a function of the integrated energy in the laser pulse. The effect is observed in a number of samples: a suggested explanation is that the overshoot represents an effective time (t) during which the electron mobility rises as the number of acoustic phonons (emitted by the rapidly cooling electron population) diminishes.The acoustic phonon population is created within a few nanoseconds of optical excitation and leaves the epilayer during the time t. Using a simple kinetic theory argument the time t_o for ballistic ejection from an epitaxial layer of thickness l is:

$$t_0=\frac{l}{v_s} \quad (1)$$

where v_s is the velocity of sound. This time is increased by a factor (l/λ),

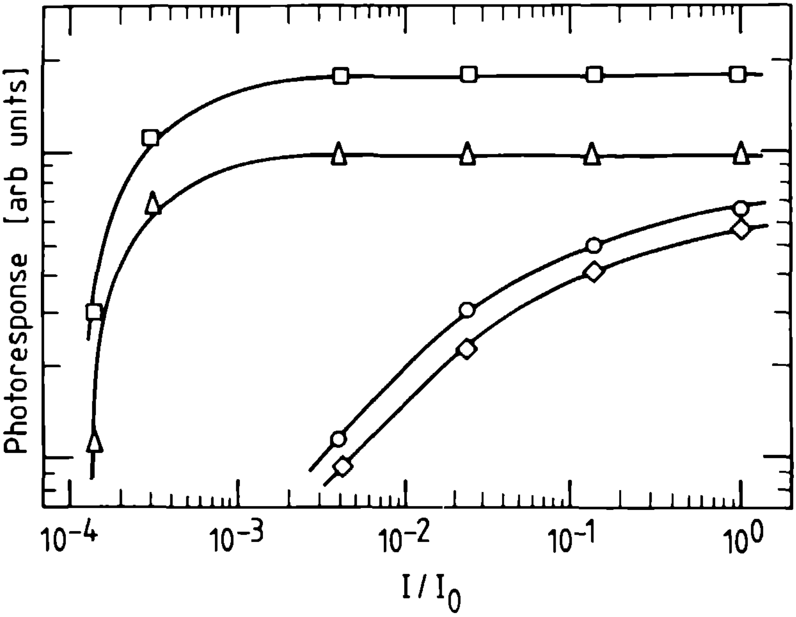

Fig.9. Effects of varying laser power (I/I_0) on tail and short-term response for 2 samples at 4.2 K and B = 3.75 T. □: sample No.1, tail. Δ: sample No.2, tail. ◇: sample No.3 short term. O: sample No.1, short term.

where λ is the phonon mean free path. λ will diminish with increasing phonon population, i.e. at higher laser powers. Thus

$$t=\frac{l^2}{v_s}\lambda \tag{2}$$

Using values of $l=10\ \mu m$, $v_s=10^3 ms^{-1}$, and $\lambda\simeq \frac{1}{2}\mu m$ (deduced from the greatest number density of optically excited carriers) an order of magnitude value of 60 ns is obtained, consistent with the observed overshoot.

A slight increase in the decay-time of the short-term response is noted in the resonant field of 3.75 T. This is probably attributable to decreased transition probability as the conduction band wavefunctions shrink in the magnetic field.

Since the N=0 Landau level lies at a lower energy than the $2p_+$ state, at 3.75 T, the transfer of electrons into the conduction band takes place by either tunnelling or phonon emission. Saturation-absorption measurements for GaAs[6] at the resonant field for the $1s\rightarrow 2p_+$ imply that this process occurs in

$\simeq$20 ns in GaAs, so that a slight increase in signal risetime (with respect to measurements at B=0T) might also be expected in the InP samples. However, although this is not within the resolution of the present experimental arrangement, recent preliminary measurements[15] with a 3 ns resolution system show no such increase in rise-time at the resonant field.

B. Mechanism for the long-term photoresponse ($t>1\mu s$)

The fundamental mechanism thought to be responsible for the "tails" in the photoresponse at $V>V_T$ is impact excitation of neutral donors at a relatively low (1-2 V cm^{-1}) bias field. This process is distinct from "normal" impact ionisation which will occur at somewhat higher bias fields.It was first invoked to explain changes in the magnetoresistance of epitaxial n-GaAs:[17] the changes in excited state populations produced by this mechanism in GaAs have very recently been investigated using far infrared spectroscopy[18]. The process envisages multiple re-excitations from excited states: we extend this idea to consider an avalanche process leading to the observed increases in sample photoresponse which can continue for very long periods (up to $\simeq$40 μs in some cases).

In the only other report known to the present authors of "tails" in the submillimetre photoresponse of a semiconductor, Brown et al[19] ascribe the effect to electrons trapped in a hybrid impurity band. Impurity band conduction is known to decrease substantially in magnetic fields[20], typically by a factor of 15 in fields of 2 T, so that some reduction in tail signal might be expected. Since the tail is seen to be prominent at magnetic fields of up to 6 T, this is unlikely to be the operative mechanism in our case. Furthermore, impurity banding in these samples is unlikely due to their low doping concentration (see Table 1).

The approximately linear increase in V_T as the magnetic field is raised is consistent with an initiating process such as impact excitation from a population of electrons in a 2s state. The mechanism will then proceed in an essentially random fashion, with carrier multiplication into the conduction band from impact-excited electrons in higher-lying excited impurity states. The photosignal rapidly (4-5 μs) attains a maximum value representing a dynamic equilibrium between excitation and trapping processes: some variation in the maximum value of this photosignal is therefore to be expected as the efficiency of the conduction band multiplication process will be dependent on sample compensation ratios.

A simple rate equation formalism was used[9] to account for the temporal characteristics of the tail. The conduction band population was obtained from the numerical solution of three coupled rate equations describing electron populations in the ground state, the conduction band and a suitable "bottleneck" impurity state. The fitting parameters of these equations were consistent with reported lifetimes[6,16] of appropriate "bottleneck" states for zero field and 3.75T measurements. The evidence of figure 8 that there is very little spectral information present in the tail is considered to be generally supportive of the "carousel" mechanism giving rise to the tail, as such spectral information will be lost in the repeated excitation and trapping processes.The "carousel" mechanism invokes a single crude "return" parameter to account for carrier impact excitation into the conduction band. This single parameter requires refinement to adequately represent the complex excitation process alluded to above. For instance, one consequence of this over-simplification is that the simple rate equation simulations[9] cannot satisfactorily account for the incident laser power versus photosignal characteristics (figure 9) or for the marked variation of these characteristics in a magnetic field.

A further attempt was therefore made to model the kinetic processes prevalent at the outset of the impurity breakdown in order to explain the general shapes of the observed tails and, in particular, the remarkable result (see figure 9) that the tail signal in a magnetic field sustained over several orders of magnitude reduction in the stimulating laser power level.

It is proved that the photoresponse in a magnetic field can be most simply explained by invoking a four level model as shown in figure 10. The rate equations pertinent to this model are:

$$\frac{dn}{dt} = -\alpha n(n+N_A) + rnN_3 + S(t)N_1 \tag{3a}$$

$$\frac{dN_1}{dt} = -\beta_{12}nN_1 + \beta_{21}N_2 + \beta_{31}N_3 - \beta_{13}nN_1 - S(t)N_1 \tag{3b}$$

$$\frac{dN_2}{dt} = \beta_{32}N_3 - \beta_{12}nN_1 - \beta_{21}N_2 \tag{3c}$$

$$\frac{dN_3}{dt} = \alpha n(n+N_A) - rnN_3 - \beta_{32}N_3 + \beta_{13}nN_1 - \beta_{31}N_3 \tag{3d}$$

The source term S(t) representing the initial input of electrons into the conduction band by the FIR pulse was taken as a Lorenzian of appropriate half width.Eqs.3 above were solved numerically and computer-generated simulations of the photoresponse of InP were obtained for a variety of parameter choices.

Results of these simulations are shown in figure 11 for zero magnetic field and at 3.75 T. For ease of comparison appropriate experimental tails are also plotted on this figure. The inset to figure 11 presents a graph of the

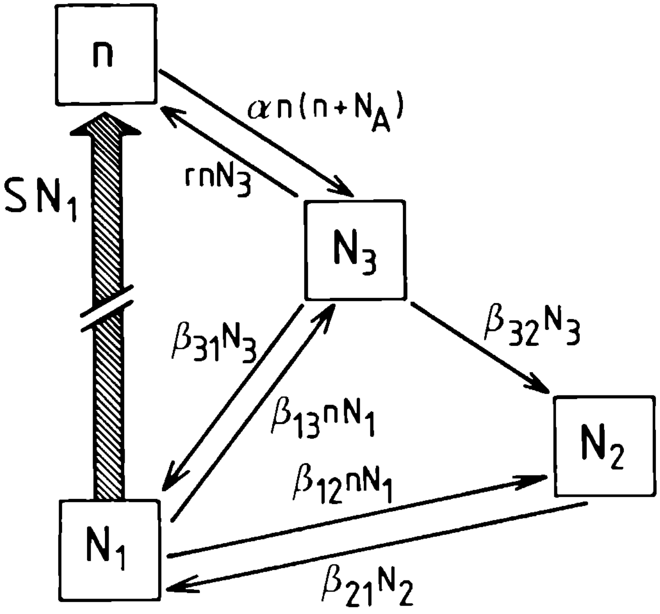

Fig.10. Model of recombination and impact excitation processes. Only those transition rates relevant to the present model are indicated. n is the conduction band population, N_1 the impurity ground-state population and N_2 and N_3 populations of excited states (see text). N_A is the acceptor concentration.

maximum simulated photosignal at 3.75 T as a function of incident laser power for both the short-term and tail components. It is evident from the figure that eqs.3 can satisfactorily account for the presence of a tail at low laser powers even when the short-term photoresponse has virtually disappeared.

A direct mathematical analysis demonstrates the need to assume a fourth "level" to account for the eventual decay of the tail. It may be shown that such a long-term decay will not occur with three "levels". It is assumed that the dominant process for the production of a long-lived tail is the inelastic scattering of electrons from the impurity ground state (population N_1) into an excited state or group of states represented by the population N_3. A subsequent ionisation into the conduction band may then occur which is represented by the rate parameter, r, as in the three-level mode[19]. The present model, however, requires the existence of a second state (or group of states)

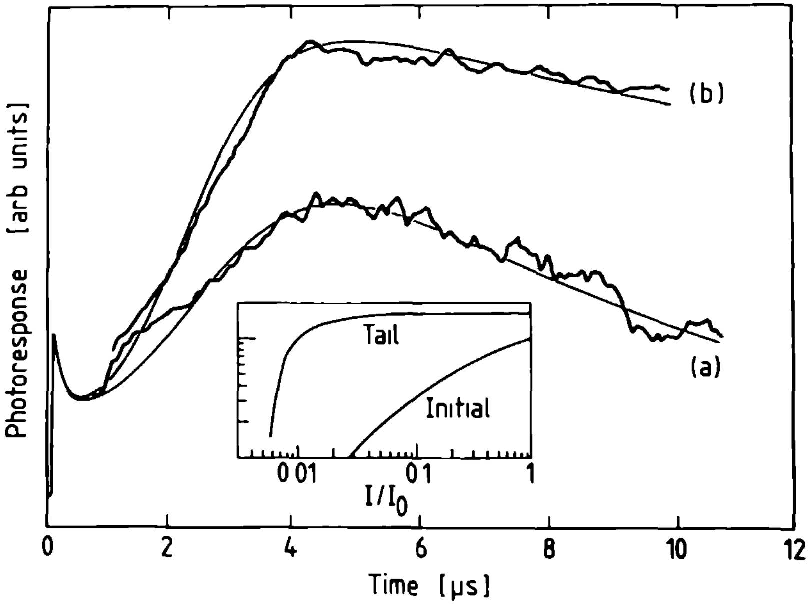

Fig.11. Simulations of photoconductivity. Appropriate experimental data are reproduced for comparison. Curve a) is a simulation for the resonant magnetic field: α=6x10^{-8}cm^{3}s^{-1}, r=6x10^{-8}cm^{3}s^{-1}, β_{32}=2x10^{5}s^{-1}, β_{21}=10^{6}s^{-1}, β_{12}=3x10^{-9}cm^{3}s^{-1}, β_{13}=7.2x10^{-9}cm^{3}s^{-1}, β_{31}=5x10^{5}s^{-1}. The initial N_1=2x10^{14}cm^{-3} and N_a=3x10^{13}cm^{-3}. Curve b) is a simulation for zero field for which β_{32}=0s^{-1}. The inset shows simulated saturated data for tail and initial response at 3.75 T.

at an intermediate energy and for which the electron population is N_2. Slow recombination processes to the ground state are then invoked to explain the eventual decay of the tail over several tens of microseconds. The physical justification for the choice of parameters used in the simulations and the possible nature of the states represented by the populations N_2 and N_3 will now be considered.

The analysis of Ascarelli and Rodriguez[16] concludes that in zero magnetic field the 2s state acts as an effective bottleneck in the phonon assisted recombination process. However, in a magnetic field it is likely that the lower energy 2p$_-$ state can also act as a bottleneck and this is supported by the lifetime measurements of Allan et al.[16] for GaAs. It is therefore reasonable to suggest an assignment of the population N_2 to the 2p$_-$ state and the population N_3 predominantly to the 2s state: the consequences of the degeneracy of these states at zero magnetic field will be examined later. Calculations of the 2p_→1s and 2s→1s lifetimes for InP using the analysis of Ascarelli and Rodriguez[16], and an appropriate deformation potential[21], yield values of 10 μs and 2 μs respectively. The decay parameters β_{21} and β_{31} were chosen using these lifetimes for the simulations of figure 11. The chosen conduction band decay parameter,α , is consistent with the effective lifetime of 60 ns obtained from the short-term response measurements. The critical dependence of the resulting shape of the photoresponse curve on the value of the parameters used in the model will be discussed shortly.

The chosen values of the impact excitation parameters r, β_{13} and β_{12} are in general agreement with those reported by Scholl[22]. It is possible to comment on the relative sizes of some of these parameters by analogy with the reported cross sections for electron impact in atomic hydrogen[23]. Such comparisons indicate that the cross section for 1s→2p_ excitation is at least a factor of three smaller than for either 1s→2s or 1s→$2p_0$ excitations, which is consistent with the relative chosen values for β_{12} and β_{13} and with the tentative assignments of the N_2 and N_3 populations previously discussed. Finally, it is noted that the faithful simulation of the experimentally observed tail requires a minimal impact ionisation of the N_2 state(s): this is implied by simple consideration of angular momentum conservation and wavefunction symmetry[24].

Figure 11 displays a photocurrent simulation in which the parameter β_{32} is set at zero. The striking similarity between this computer-generated plot and the zero magnetic field data implies a zero transfer rate between the N_3 and N_2 populations in zero magnetic field, which is to be expected from the degeneracy of the 2s and 2p_ states and the population assignments previously discussed.

The critical dependence of the simulations on the choice of the relevant parameters will now be considered. The model proposed in figure 10 shows only those transitions which are numerically found to have a substantial influence on the photoconductive response.

Figure 12 shows the effects of varying several parameters for a photoresponse simulation at 3.75 T. Curve a) shows the simulation which most closely resembles the experimental data (see Figures 11 and 7). Curve b) represents a slight decrease in the impact excitation parameters corresponding to lower sample bias conditions. The curves c), d) and e) demonstrate the effects of varying the recombination rates. The criticality of the choice of parameters is evident from the figure. The simulations based on the eqs.3 provide a reasonable description of the tail behaviour with the correct choice of parameters.However, the short term response (<1 μs) is not so well represented by the present model and there are two major reasons for this. The first is that the simulations do not take into account the overshoot effects discussed in section IV A, which are important on this timescale. The second

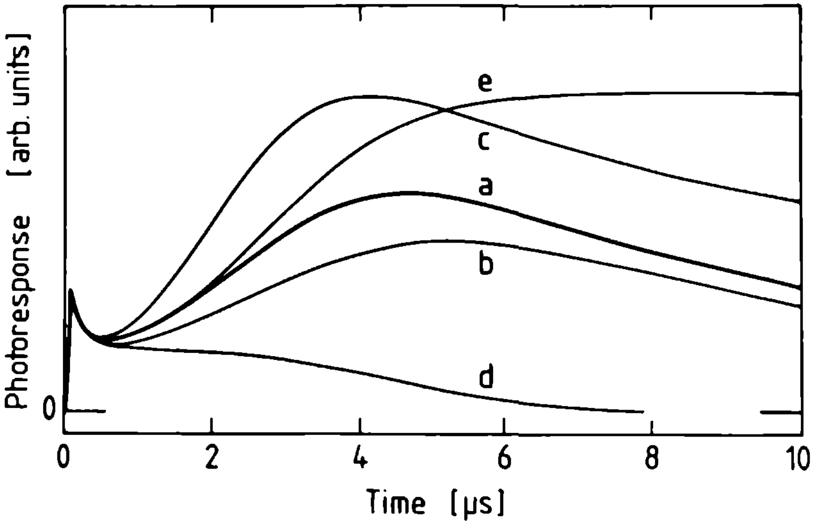

Fig.12. Simulations of the photoconductive response for a variety of model parameters. Curve a) has the same parameter choice as curve a) in fig.10. (i.e. transition times are 2 µs and 10 µs for 2s-1s and $2p_-$-1s respectively). Curve b) as curve a), but all impact excitation parameters reduced by 5%. Curve c) as curve a), but the 2s-1s transition time equals 5 µs. Curve d), 2s-1s transition time 1 µs. Curve e) 2s-1s transition time equals 2 µs and $2p_-$-1s transition time equals 2µs.

is that the model assumes instantaneous capture by the state, whereas in reality a cascade through a sequence of short-lived states will occur.

There was some experimental evidence that tail formation in zero field was more difficult to establish, and had a greater susceptibility to sample variation and laser power, than tail formation at the resonant magnetic field. Although this behaviour is not fully understood it is suspected to be related to the relative magnitudes of the slightly higher bias required in a magnetic field and the random internal electric fields[25] associated with the ionised impurities. It was not possible, however, to apply a comparable high bias at zero field, because of the onset of total breakdown produced by direct impact ionisation of the ground state.

The noisy appearance of the tail, particularly at long (>5 µs) times is perhaps a manifestation of the onset of filamentary conduction processes which have been observed in GaAs[26] and Ge[27].

V. CONCLUSIONS

The photoconductive response of high purity n-InP samples has been studied at 4.2 K using 75-500 ns pulses of 118.8 μm radiation from a CO_2 pumped FIR laser. At low sample bias voltages the photoresponse is a slightly asymmetric pulse represented by a simple exponential decay of characteristic times 125 ns and 150 ns at B=0 and 3.75 T respectively, which correspond to effective lifetimes of 60 and 85 ns. The significance of these times relative to other measurements in GaAs is discussed. The development of this photosignal was monitored as a function of the laser stimulus power, and overshoot effects were observed where the sample photoconductance continued to increase for a period (of order 50 ns) whilst the stimulus power fell. The effect was seen to be approximately proportional to the magnitude of the input power integrated over the laser pulse period. This was interpreted as the characteristic time during which the electron mobility rose whilst acoustic phonons diffused into the substrate.

At sample bias voltages exceeding a threshold of a few volts per centimetre the photosignal was seen to develop a long tail extending to several tens of microseconds. The very long conduction band lifetime deduced by Ohyama[8] for electrons in InP under similar bias conditions is almost certainly a manifestation of the same effect. The threshold voltage for this tail was found to increase approximately linearly with applied magnetic field.The spectroscopic properties of the tail were investigated, together with the variation in tail shape and size with incident laser power. An earlier rate equation model for the process was critically examined, and its shortcomings pointed out. A model involving impact-excitation and slow recombination between the ground impurity state, the conduction band and other states (or groups of states) has been developed, and computer simulations based on this model are presented. The shapes of the initial pulse and the long-lived tail at B=0 and 3.75 T are seen to be faithfully reproduced by this model, together with the saturation behaviour as a function of laser power. The fitting parameters required by the simulations are seen to be consistent with assignments of the N_2 population in the model to the $2p_-$ state and the N_3 population to the 2s state and with reported impact excitation cross sections and phonon decay rates.

Acknowledgements
The experimental work was performed at the University of Nijmegen (Netherlands). We acknowledge the support of FOM (Nederlands), SERC (UK) for a research studentship (AAR) and for travel facilities (JMC). We are indebted to D.Anderson and L.Taylor (RSRE, Malvern, UK) for generous gifts of samples, to G. Hill (SERC III-V Facility, Sheffield) for assistance with sample preparation and A. v. Etteger (Nijmegen) for designing

the laser system. Several useful discussions with J.C. Maan and L. Eaves are also acknowledged.

References

1. J.M. Chamberlain, H.B. Ergun, K.A. Gehring and R.A. Stradling, Solid State Communications **9**, 1563 (1971).
2. C.J. Armistead, P. Knowles, S.P. Najda and R.A. Stradling, Journal of Physics C: Solid State Physics **17**, 6415 (1984).
3. A.A. Reeder, J.M. Chamberlain, R.J. Turner and G. Hill, Solid State Communications **57**, 355 (1986).
4. K.K. Bajaj, J.R. Birch, L. Eaves, R.A. Hoult, R.F. Kirkman, P.E.Simmonds and R.A. Stradling, Journal of Physics C: Solid State Physics **8**, 530 (1970).
5. C.R. Pidgeon, A. Vass, G.R. Allan, W. Prettl and L. Eaves, Phys.Rev. Lett. **50**, 1309 (1983).
6. G.R. Allan, A. Black, C.R. Pidgeon, E. Gornik, W. Seidenbusch and P.Colter, Phys. Rev. B **31**, 3560 (1985).
7. C.R. Pidgeon, G.R. Allan, A. Black, B. McGuckin, M. F. Kimmitt and P.C. Colter, Solid State Communications **53**, 1140 (1985).
8. T. Ohyama, E. Otsuka, S. Yamada, T. Fukui and N. Kobayashi, Jpn. J.Appl.Phys.22, L742 (1983).
9. J.M. Chamberlain, A.A. Reeder, L.M. Claessen, G.L.J.A. Rikken and P. Wyder, Physica **134B**, 426 (1985).
10. L. Taylor and D. Anderson, J. Crystal Growth **64**, 55 (1983).
11. H.J.A. Bluyssen and A.F. van Etteger, IEEE J. Quant. Electronics QE-G16, 1347 (1980).
12. J.C. Maan, Thesis, 1979, University of Nijmegen (unpublished), (1979).
13. J.B. McManus, R. People, R.L. Aggarwal and P.A. Wolff, J. Appl. Phys. **52**, 4748 (1981).
14. Sh.M. Kogan, Sov. Phys. Solid State **4**, 1813 (1963).
15. G.L.J.A. Rikken, J.M. Chamberlain and P. Wyder, to be published.
16. G. Ascarelli and S. Rodriguez, Phys. Rev. **124**, 1321 (1961).
17. J.L. Robert, A. Raymond, R. Aulombard, C. Bousquet and A. Joullie, in Lecture notes on Application of High Magnetic Fields in Semiconductor Physics, edited by G. Landwehr (Wurzburg, 1976), p.533.
18. C. Trager, D.A. Cowan and R.A. Stradling, Physica **134B**, 250-254 (1985).
19. F. Brown, A. Anderson and P.A. Wolff, Int. Journal of Infrared and Millimeter Waves **1**, 277 (1980).
20. B.I. Shkiovskii and E.L. Efros, Electronic Properties of Doped Semiconductors, (Springer, New York, 1984).
21. Landolt-Bornstein: Numerical Data and Functional Relationships in Science and Technology, edited by D. Bimberg, (Springer-Verlag, New York,1982), Vol. 17, p.281.
22. E. Scholl, Journal de Physique Colloque **42**, suppl. 10, C7-57 (1981).

23. N.F. Mott and H.S.W. Massey, Theory of Atomic Collisions, (Oxford University Press, Oxford, 1965).
24. W. Rosner, G. Wunner, H. Herold and H. Roper, Journal of Physics B: Atomic and Molecular Physics 17, 29 (1984).
25. G.E. Stillman, C.M. Wolfe and J.O. Dimmock, in Semiconductors and Semimetals, edited by R.K. Willardson and A.K. Beer (Academic Press, New York, 1977), vol. 12, p.169.
26. K. Aoki, K. Miyamae, T. Kobayashi and K. Yamamoto, Physica 117B and 118B, 570 (1983).
27. J. Mannhart, R.P. Hubener, J. Parisi and J. Peinke, Solid State Communications 58, 323 (1986).

PART IV

A FAR-INFRARED INVESTIGATION ON THE PRESSURE DEPENDENCE OF THE BANDSTRUCTURE IN AN InAs-GaSb SUPERLATTICE

CHAPTER 1

General introduction

During the last decades the study of artificially made semiconductor structures has received a lot of attention. Especially devices made of Si, or III-V materials have been the subject of a very vast research area. However, also the interest in II-VI compounds is increasing very rapidly nowadays. The general idea behind making structures incorporating different semiconductors lies in the field of making new electronic devices such as (infrared)-lasers, detectors and very fast switching elements. In the context of fast electronical components a lot of efforts are being made to construct devices exhibiting negative differential resistance features, which open up possibilities for inherent bi-stability, (Bloch) oscillators and the construction of all kinds of active elements. A well known example is the recently realised double barrier quantum well, designed to show resonant electron tunnelling and negative differential resistance. All these structures have in common the presence of some thin layers of one semiconductor grown in a special configuration on top of another semiconductor. Therefore they can be all mentioned under the name "heterostructures".

Quite recently the research area on these structures has become experimentally accessible due to the near perfection obtained by sophisticated growth techniques such as for instance molecular beam epitaxy (MBE) and metal organic chemical vapour deposition (MOCVD), which allow the growth of very pure epitaxial layers on top of each other with very abrupt boundaries at the interfaces.

In this context, among the most intriguing systems are the so-called superlattices (SL) which consist of many thin layers of generally two different materials grown alternately on top of each other. This creates in the growth direction (i.e. perpendicular to the layers) an additional periodicity superimposed on the original lattice period. The fascinating feature of such a superlattice is that due to the artificially created periodicity the band structure in this direction will be drastically changed by the formation of new mini-brillouin zones which create mini-bands and new mini-gaps in the original energy bands. If the layers are thin enough particles can move (by tunneling) more or less freely in the growth direction through the different layers, and to some extent the periodicity and the layered two-compound structure can be neglected. What rests is a new bulk material having in one direction a strongly modified band structure featuring different energy gaps and different electron effective masses. In this sense a superlattice is essentially different from similarly looking heterostructures consisting of a set of separated non-interacting quantum wells grown on top of each other.

The existence of interfaces between two semiconductors as present in all artificial structures gives rise to new physical properties due to the difference in energy of the energy bands in the two adjacent materials. Charge transfer can occur from a filled band in one material at a higher energy than an empty band in the other material, which causes strong bending of the bands due to the static potential evoked by the charge redistributions. A well known example of band bending is the high mobility 2-dimensional electron gas at the interface of an GaAs-AlGaAs heterojunction. In this system charge is transferred from the heavily doped AlGaAs to the undoped GaAs in which the electrons accumulate at the interface and cause a strong band bending. The conduction band sinks through the Fermilevel established by the two materials and forms as such a nearly triangular potential well in which the electrons are being trapped. In the context of such systems it is of fundamental interest to know the band structure at the interfaces in detail, the most important question being the exact values of the band discontinuities, i.e. the energy differences between two similar bands in the two adjacent semiconductors in contact. This problem is generally known under the name of band line-up or band-offset and will be the *Leitmotiv* of this part of the thesis.

Experimentally the band line-up problem lies in how to measure the discontinuity between two similar bands at an interface within a few hundred meV, a notorious example being the often disputed line-up at the interface of the aforementioned GaAs-AlGaAs heterojunction. Theoretically the problem lies in developing a procedure that calculates band discontinuities in an universal way, compatible with experimental findings.

From experimental point of view many attempts have been made to determine the band line-up of different systems among which for instance luminescence measurements on the energy levels in single and two-stepped quantum wells, voltage capacitance transport measurements on quantum wells and other similar structures, and lately XPS and UPS electron diffraction methods in which the core levels of the individual atoms are being probed at the interface of single heterojunctions. Especially the latter method seems to be very promising although it remains difficult to acquire a resolution within some hundred meV. However, the interface between the two narrow-gap III-V semiconductors InAs and GaSb exhibits a very peculiar band line-up that makes a much more accurate determination of the band offsets possible, provided a suited experimental structure is made of these materials. The peculiarity lies in the broken gap line-up in which the InAs conduction band (CB) is at a lower energy than the GaSb valence band (VB). Due to this overlap between a normally filled GaSb VB and an empty InAs CB, charge transfer will occur leaving behind holes in the GaSb and electrons in the InAs. Optical as well as transport properties of samples containing such an interface will in principle depend on the occurrence of this charge transfer, and as such this overlap has become an important and relatively easy to probe feature. Therefore the InAs-GaSb interface forms a sensitive system to investigate band offsets.

When making a superlattice out of these materials, the superlattice periodicity will modify the band structure in such a way that, for suited layer thicknesses, an electron-like subband (E_1) coming from the InAs CB will be present at a lower energy than a hole-like subband (H_1) coming from the GaSb VB, hence causing charge transfer from H_1 to E_1. Using magneto-optical methods it is possible to measure very accurately (within a few tens of meV) the energy spacing E_1-H_1 between the subbands. From E_1-H_1 it is rather straightforward to determine the only free parameter in the system: the band offset Δ between the InAs CB and the GaSb VB at the interface.

In the following an experiment will be described in which the band offset Δ will be determined in an InAs-GaSb superlattice. Moreover hydrostatic pressure will be applied to the SL in order to deliberately change the energy gaps of both materials in a known way. The resulting pressure dependent band offset Δ is measured and the results are compared with existing theories concerning the calculation of Δ. The merit of this method is to change in one system using an external parameter (pressure) the band structure properties of the two materials in a known way without having to take a whole different sample that can posses unknown deviations from the previous sample. Theories which predict correctly band offsets in this system at zero pressure are adapted for pressure induced changes, and the in such a way obtained theoretical predictions on Δ as a function of pressure are compared with the experimental results. In this manner firstly a band line-up theory has to be able to predict correctly the zero pressure band offset, and secondly it also has to predict the experimentally observed pressure dependence. This makes the InAs-GaSb SL system under pressure a very suited and sensitive instrument to test band line-up theories.

Part IV of this thesis is organised as follows: In chapter 2 a slightly modified version of an article by L.M. Claessen, J.C. Maan, M. Altarelli, P.Wyder, L.L. Chang, and L. Esaki in the Physical Review Letters 57, 2556 (1986) will be presented. This article contains the essence of the experiment and the theoretical reflections in a concise way. Chapter 3 will deal more fully with the properties of superlattices, with magneto-optics, and with the theoretical analysis. In chapter 4 a more general outline of the band line-up problem will be presented and the experimental results will be placed in this context.

CHAPTER 2

Pressure dependence of band offsets in an InAs-GaSb superlattice

ABSTRACT

Using magneto-optical methods we have measured the pressure dependence of the energy difference between the subbands in an InAs-GaSb superlattice associated with the GaSb valence band and the InAs conduction band respectively. The experimental results obtained at hydrostatic pressures up to 12kBar allow a determination of the pressure dependence of the energy separation Δ between the InAs conduction band and the GaSb valence band at the InAs-GaSb interface. Δ is found to decrease at a rate of ≃5 meV/kBar, which is less than expected on grounds of usual assumptions concerning band energy shifts induced by hydrostatic pressure. This result shows that both the conduction- and the valence band offsets are pressure dependent. This experiment constitutes therefore a critical test for different band line-up theories.

I. INTRODUCTION

Usually, the relative positions of the energy bands within a single bulk semiconductor are well known. However, the positions of the band edges in one semiconductor relative to those in another when they are in contact with each other (band line-up at the interface) remains a problem in solid-state physics which is neither experimentally nor theoretically well understood. Yet this problem has become particularly relevant, and at the same time experimentally accessible, through the possibility of the growth of high quality interfaces and heterojunctions by modern growth techniques like MBE.[1,2].

Conceptually the band line-up problem can be divided into two parts:

i. Which energy level must be lined up at the interface in order to determine the band offsets.
ii. Where does the "line-up" level lie with respect to the band edges in each semiconductor.

There exist several band line-up theories, but the accuracy of both experimental and theoretical values is by far not sufficient to distinguish clearly between them. The essential difference between these theories is their choice of the "line-up" level as mentioned in point ii. As hydrostatic pressure has a strong effect on the relative positions of the energy bands in a solid, and therefore in general on the positions of the bands with respect to this common "line-up" energy, it is of considerable interest to investigate the band line-up at a semiconductor interface as a function of pressure and to compare the results with existing band line-up models. For this purpose we present experimental results of the pressure dependence of the line-up of the bands at a InAs-GaSb interface, by the use of magneto-optical methods applied on a superlattice made of these two materials.

II. EXPERIMENT

We have chosen the InAs-GaSb interface because it has been studied experimentally very carefully before[3-6] and because this system provides one of the most severe tests for any band line-up theory. The peculiarity of this system being that the conduction-band (CB) edge of InAs is at a lower energy than the valence-band (VB) edge of GaSb. This fact leads to a strong dependence of the electronic properties of InAs-GaSb heterostructures, e.g. superlattices (periodic alternate thin GaSb and InAs layers), on the exact value of this energy overlap. Several results of optical experiments on this system can be explained with a value of 150 meV for this difference, with an experimental error of 50 meV[4-6]. These experimental values are probably the most accurately known in the literature; note that for instance the line-up of the most extensively studied GaAs-$Ga_{1-x}Al_xAs$ system is still controversial[7]. Hydrostatic pressure has a strong effect on the energies of the bands in these semiconductors. The principal energy gap, E_g, increases 10 meV/kBar and 14 meV/kBar for InAs and GaSb respectively[8]. In particular at easily attainable pressures (10 kBar), the band gap variation is comparable to the energy overlap between the valence and the conduction bands, hence interesting effects on the line-up are to be expected.

The main features of the electronic band structure of the investigated superlattice (consisting of many layers of alternate 12 nm InAs and 8 nm GaSb, grown on a GaSb ⟨100⟩ substrate) are illustrated in fig.1. This superlattice shows an electron-like level (E_1, at a higher energy than the InAs bulk CB edge due to confinement in the InAs layer) and a hole-like level (H_1, at a lower level than the GaSb VB edge due to confinement in the GaSb layer). An extensive review of the electronic properties of this kind of superlattices can be found in ref.6. In a simplified manner, appropriate to the understanding of the present experiments, the energy difference between the E_1 and the H_1 subband edge at zero wave vector is given by the InAs-CB GaSb-VB discontinuity Δ minus the confinement energy for the electrons (the shift of the subband with respect to the InAs band edge) minus the hole confinement energy. Therefore a measurement of E_1-H_1 as a function of pressure provides direct information about the pressure dependence of the band line-up Δ. Previous measurements[4,5] on the same sample by use of far-infrared magnetotransmission at zero pressure have determined E_1 to be

40meV lower than H_1, and subsequent theoretical calculations[9] have shown that these experiments can be explained with band-structure calculations using a value of 150 meV for Δ. Here we report on results of the same experiment, i.e., measurements of E_1-H_1 by use of far-infrared absorption in

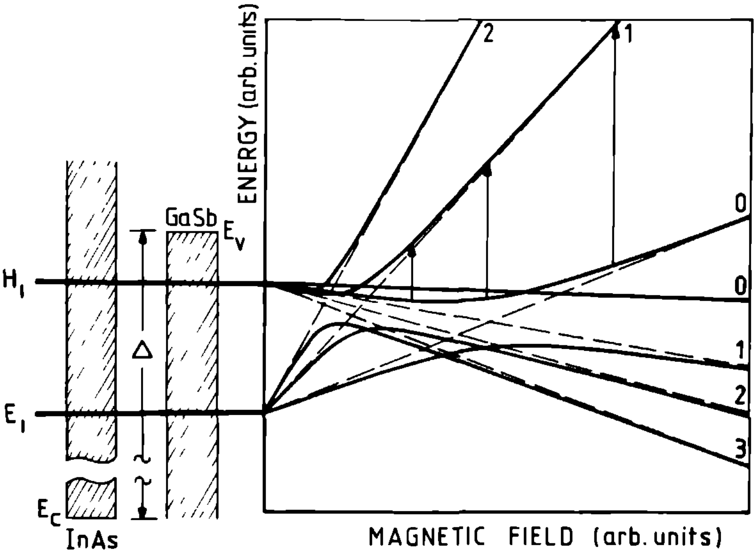

Fig.1. One period of an InAs-GaSb superlattice showing the band line-up of the InAs conduction- and the GaSb valence band edges, and the positions of the electron-like subband (E_1) and the hole-like subband (H_1). In the right part of the figure the hole-like (moving downward) and the electron-like (moving upward) Landau levels of these subbands in the absence (dashed lines), and in the presence (solid lines) of coupling between them are shown schematically for a magnetic field perpendicular to the layers of the superlattice. The arrows indicate transitions as have been observed experimentally. The mixing between inter- and intraband transitions as discussed in the text is clearly evident in the vicinity of the anticrossing of the levels.

a magnetic field, for different hydrostatic pressures up to 12 kBar. The experimental principle can be seen in fig.1, in which the hole-like and the electron-like Landau levels are plotted as a function of a magnetic field perpendicular to the layers. As usual, the continuum of states for motion in the plane of the layers is split into a set of equidistant linearly field dependent levels, with hole levels moving downward and electron levels moving upward in energy. However, a small interaction between the hole-like and the electron-like Landau levels leads to an anticrossing between the two as indicated in the figure. Transitions which can be observed in the present experiment are also shown. The experiments were done at T=4.2K in a commercial Cu-Be liquid pressure cell, with a mineral oil as the pressure transferring medium (see ref.8, p.184). An optically pumped cw molecular gas laser was used to generate the far-infrared radiation.

III. RESULTS AND DISCUSSION

Measurements have been done at 1.7, 6.6, and 10.7 kBar and compared with existing results for zero pressure. Representative transmission curves at different radiation energies as function of the magnetic field at a fixed pressure and a plot of the observed transmission minima as a function of the radiation energy are shown in fig.2. If, in a qualitative way, one assumes unperturbed, equidistant, linearly field dependent Landau levels (no anticrossing), a linear extrapolation to zero field (the dashed lines) leads to a negative energy gap, i.e. E_1-H_1. In this way the applied magnetic field is used to obtain the zero-field properties of the sample. Figure 3 shows the pressure dependence of the last high field transition of fig.2 (labeled 1) with increasing pressure. This transition moves to lower magnetic fields, while at the same time the slope of the energy-versus field dependence tends to decrease. These results are a direct consequence of the pressure dependence of the line-up at the interface: If the energy difference between the GaSb VB and the InAs CB decreases, the energy separation between the E_1 and the H_1 subbands will also decrease. If we assume no interaction between the hole- and the electron-like Landau levels (i.e. simple interband Landau-level transitions obeying the selection rule $\Delta N=0$, no anticrossing), the data can be analysed by drawing straight lines through the transitions as shown in fig.2, and evaluation of the intercept with the energy scale at zero field yields E_1-H_1 at a given pressure. In this way, one finds that this quantity decreases linearly with pressure at roughly 4 meV/kBar.

Obviously such a simplified analysis disregards the coupling between the energy levels and does not explain the tendency of the slope to decrease with pressure as mentioned before. As can be seen from fig.1, inclusion of the coupling between the levels has two effects. First, as E_1-H_1 decreases with increasing pressure, the transitions at a fixed energy (i.e. $0\rightarrow1$, as indicated in the figure) move to a lower field, and second, the field at which anticrossing occurs decreases. This latter effect results in a gradual change in character of this particular transition, i.e. a changeover from a more interband-like transi-

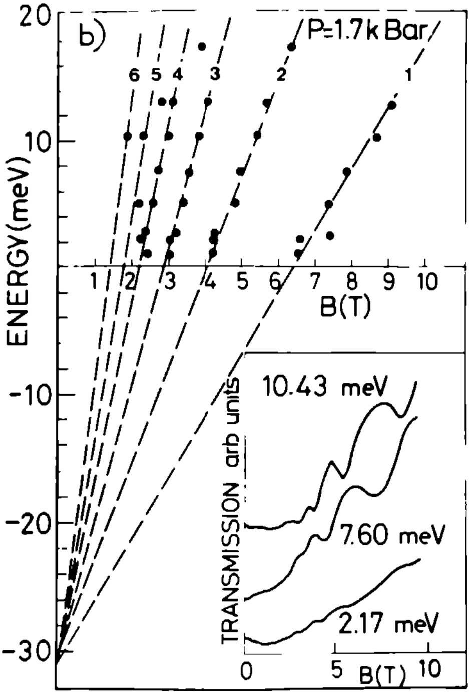

Fig.2. Observed transition energies between the subbands of the InAs-GaSb superlattice as a function of the magnetic field at a pressure of 1.7 kBar. The inset shows the experimental spectra. The dashed lines show the linear extrapolation (i.e. with the assumption of pure interband transitions), indicating a material with a negative energy gap E_1-H_1. The transitions are labeled according to the noninteracting model in which the quantum number is that of the two participating Landau states.

tion with a steeper slope to a more intraband-like transition (cyclotron resonance) with a lesser slope.

To analyse this subtle bandstructure behaviour in more detail, we have calculated the pressure dependence of the bandstructure within the framework of a six-band **k**·**p** model as described elsewhere[9]. In the calculation, the full VB-CB coupling is taken into account, both within each material and between the adjacent unstrained materials, by use of proper boundary conditions for the wave functions at the interface. Standard values for the band parameters are used and the only adjustable parameter is Δ which is assumed to be linearly pressure dependent. The results are shown in fig.3 as the drawn lines. The best agreement with the experiments is obtained using a decrease of Δ of 5.8 meV/kBar. This slightly stronger pressure dependence is obviously a consequence of the inclusion of all other effects of the band structure neglected in the more simple analysis. (nonparabolicity, subband coupling, effects of this coupling on the confinement energies, etc). The calculation also shows the tendency of the slope to decrease with pressure as experimentally suggested. The essential experimental result therefore is that the offset between the InAs CB and the GaSb VB reduces at a rate of $\simeq$5 meV/kBar. Note that because of a slight lattice mismatch between InAs and GaSb, the band offset one measures in superlattice experiments will be affected by strain[10-12]. However, since the compressibilities of InAs and GaSb are nearly equal[8], no additional strain is induced by the pressure, and hence the pressure dependence of the offset is not seriously affected. As the InAs and the GaSb energy gaps increase by 10 and 14 meV/kBar respectively, it is therefore clear that that our experimental results imply that if the pressure is increased, neither the valence bands (which would lead to an decrease of 10 meV/kBar) nor the conduction bands (which similarly would give 14 meV/kBar) in both materials remain constant.

It is evident that if the criterion which determines the band offset is the line-up of a specific reference level, this level will have the same origin for all pressures. The position of the energy bands with respect to that level, however, will in general be pressure dependent. Band line-up models should be able to explain consistently this pressure dependence of the bands and the band offsets. In this connection we will briefly discuss different theoretical approaches of band line-up. The most recent suggestion, proposed by Langer and Heinrich[13], derives the valence band offsets by use of transition-metal impurity levels as the common energy. To be consistent with our experimental results the position of these deep-level impurities must show a pressure dependence with respect to both the VB and the CB. For GaAs this is indeed so (the Cr level increases by 4.8 meV/kBar with respect to the VB[14]. Unfortunately, in InAs and GaSb deep level impurity levels have not been studied in sufficient detail to make a more quantitative statement concerning the pressure dependence. If, as recently postulated[15,16], the charge neutrality level is used as the reference energy (midgap energy), the pressure dependence can be estimated crudely from the work of Tersoff[16] by the assumption that the relative position of this level in the energy gap is not pressure dependent. This estimate yields 2 meV/kBar for Δ, which is considerably close to the experimental results. It should be noted that the pioneering Harrison[17] atomic orbital theory (HLCAO), which measures the position of the valence bands relative to the average atomic potential in the semiconductor,

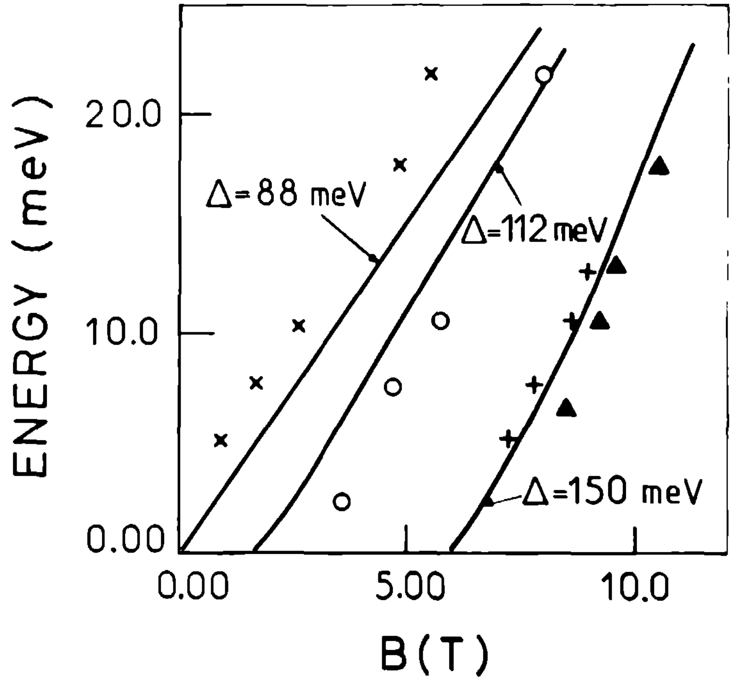

Fig.3. Pressure dependence of the high-field transition (labeled 1 in fig.2) for 0 (▲), 1.7 (+), 6.6 (○), and 10.7 kBar (x). The lines are theoretical calculations of these transitions with the assumption of a linear pressure dependence of the band line-up parameter Δ.

would predict that Δ varies as the InAs gap (the relative positions of the valence bands being almost pressure independent), which is not in agreement with the experiment.This theory however, predicts very nicely zero pressure band discontinuities for our system as well as for many other interfaces. from other methods, such as the electron affinity rule[18], the theory by Frensley and Kroemer[19], and *ab initio* calculations[20], it is rather difficult to extract predictions about the pressure dependence of the band line-up.

IV. CONCLUSION

In summary, we have measured the pressure dependence of the InAs-GaSb band line-up. Our data show that the offset between the GaSb VB and the InAS CB decreases by 5.8 meV/kBar. This value cannot be explained by the pressure dependence of the energy gaps in the bulk materials alone. In addition, the experiments suggest a pressure dependent gradual change from interband to intraband transitions, effects which can be explained by taking into account the full band structure of the system. We believe that the study of the pressure dependence of the band offset may be a useful tool for the test of heterojunction line-up theories, the main point being that since the band structure of each material at the interface is strongly pressure dependent, the comparison of the band offsets with and without pressure is in some sense equivalent to a comparison of different samples of which the differences between them are accurately known.

Acknowledgement.
It is a pleasure to acknowledge many useful discussions about this work with G.Martinez.

References.

1. H.Kroemer, Surf.Sci.132, 543 (1983).
2. H.Kroemer, J.Vac.Sci.Technol. B2, 433 (1984).
3. G.A.Sai-Halasz, L.L.Chang, J.M.Welter, C.A.Chang and L.Esaki, Solid State Commun. 27, 935 (1978).
4. Y.Guldner, J.P.Vieren, P.Voisin, M.Voos, L.L.Chang and L.Esaki, Phys.Rev.Lett. 45, 1719 (1980).
5. J.C.Maan, Y.Guldner, J.P.Vieren, P.Voisin, M.Voos, L.L.Chang and L.Esaki, Solid State Commun. 39, 683 (1981).
6. L.L.Chang, J.Phys.Soc.Jpn. 49, Suppl.A, 997 (1980).
7. G.Duggan, J.Vac.Sci.Technol. B3, 1224 (1985).
8. G.Martinez, in *Optical Properties of Solids*, ed. by M.Balkanski, Handbook on Semiconductors Vol.2 (North Holland, Amsterdam, 1980) p.194.
9. A.Fasolino and M.Altarelli, Surf.Sci. 142, 322 (1984).
10. Y.Guldner, G.Bastard, J.P.Vieren, M.Voos, J.P.Faurie and A.Million, Phys.Rev.Lett. 51, 907 (1983).
11. S.P.Kowalczyk, J.T.Cheung, E.A.Kraut and R.W.Grant, Phys.Rev.Lett. 56, 1605 (1986).
12. G.Y.Wu and T.C.McGill, Appl.Phys.Lett. 47, 634 (1985).
13. J.M.Langer and H.Heinrich, Phys.Lett. 55, 1414 (1985).
14. A.M.Hennel and G.Martinez, Phys.Rev.B 25, 1039 (1982).
15. F.Flores and C.Tejedor, J.Phys.C 12, 731 (1979).
16. J.Tersoff, Phys.Rev. B 30, 4874 (1984).
17. W.A.Harrison, J.Vac.Sci.Technol. 14, 1016 (1977).
18. R.L.Anderson, Solid State Electron. 5, 341 (1962).
19. W.R.Frensley and H.Kroemer, Phys.Rev. B 16, 2642 (1977).
20. M.L.Cohen, Adv.Electron Phys. 51, 1 (1980).

CHAPTER 3

Investigations of the band line-up in a semimetallic InAs-GaSb superlattice under hydrostatic pressure

I. GENERAL INTRODUCTION TO SUPERLATTICES.

A superlattice (SL) is a structure made of alternating thin layers of two different materials, often semiconductors, grown on top of each other. The idea is to impose a new periodicity upon the existing lattice period in the growth direction, i.e. perpendicular to the layers. Layer thicknesses depend on the materials chosen, but range roughly between 1 and 10 nm, which is of the order of the de Broglie wavelength of the electrons. These thicknesses are chosen as such, because now electrons coming from for instance material A can move more or less freely into and across layer B by means of tunneling, due to an overlap of the wave functions of material A that are evanescent in B. This gives the SL a real three-dimensional character.

To grow a neat superlattice one needs techniques able to deposit very pure materials having an abrupt chemical change-over from material A to material B. At present near perfect interfaces can be made using e.g. MBE techniques[1-3]. Furthermore, to avoid internal stresses the materials A and B should preferably be lattice matched[3] i.e. having nearly the same lattice constant. However, there exist SL deliberately made of mismatched materials (strained superlattices) in which the by strain induced uniaxial and bi-axial stresses can lift some band degeneracies and open up the ability to study these phenomena. In this thesis we will only be concerned with near lattice matched SL made of III-V materials.

One of the most studied superlattices is made of GaAs and $Al_xGa_{1-x}As$ layers. On these systems very intensive studies have been made. The GaAs-$Al_xGa_{1-x}As$ system belongs to the socalled type I superlattices[3,4], in which the GaAs energy gap at the Γ-point is totally included in the much wider $Al_xGa_{1-x}As$ gap (which is a function of the Al concentration x), giving rise to a step-like band structure as depicted schematically in fig.1a. In such a system the idea of subband formation can be understood qualitatively in the following way: Electrons in the GaAs conduction band are more or less confined by the potential barrier formed by the $Al_xGa_{1-x}As$ energy gap. Due to the quantum size effect for a particle in a one-dimensional well, discrete flat energy levels are being formed at an energy E_n given by

$$E_n=\frac{(n+1)^2\pi^2\hbar^2}{8ma^2} \tag{1}$$

with n=0 the ground level which determines the confinement energy from the CB bandedge to the first subband. The well width is 2a and m is the effective electron mass. E_n increases with n until E_n exceeds the barrier

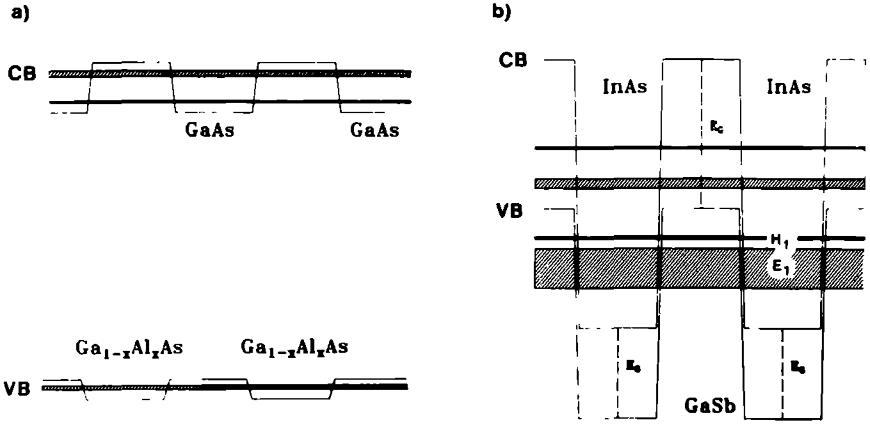

Fig.1. Spatial bandedge variation and subbands in type I (fig.1a), and type II (fig.1b) superlattices at the Γ-point. In fig.1b the two most important subbands are the electron-like band E_1, and the hole-like band H_1.

height defined by the $Al_xGa_{1-x}As$ gap. These subbands have a finite dispersion in the growth direction due to the already mentioned overlap of the evanescent GaAs wave functions in the $Al_xGa_{1-x}As$ gap, yielding tunneling possibilities through these layers. Tunneling across the barriers has been observed in these superlattices[5,6,7] and presents a proof that the system is indeed a real three-dimensional structure. In fact subband broadening is a manifestation of a finite dispersion in the k_z direction which reflects the particle's possibility to actually have some momentum in the growth direction of the SL, and as such being able to move through the layers. Higher subbands have a larger width due to an effective reduction of the barrier height, as can be seen in fig.1a.

In type I superlattices the subband structure can be calculated for the separated CB and VB wave functions using a Kronig-Penney model as discussed in many textbooks. For the electrons this is schematically depicted in

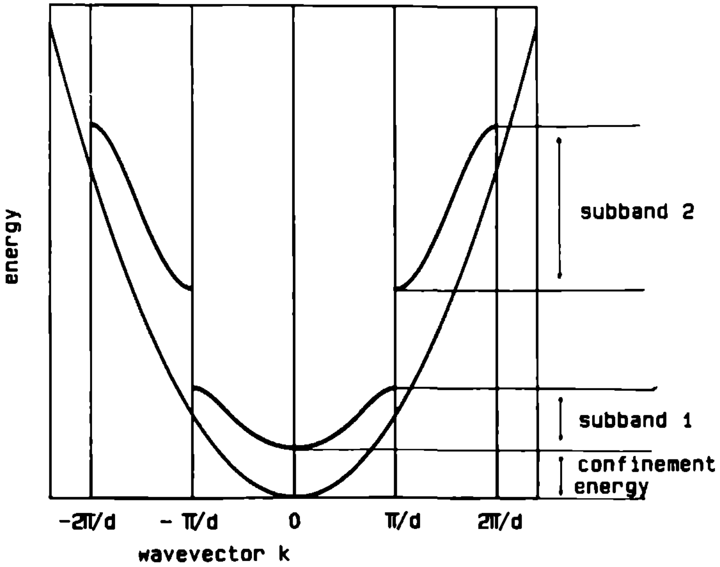

Fig.2. Schematic presentation of subband formation near the CB-bandedge in a type I superlattice, as can be calculated using a Kronig-Penney model. The wavevector k is in the growth direction and the periodicity is d.

fig.2 for a superlattice periodicity d. The new SL Brillouin zones in the growth direction are positioned at $k_z=n\pi/d$. The formation of the minigaps, the subbands, and the confinement are clearly visible, just as the origin of the finite subband width. In this figure it can be seen that going from $k_z=0$ to π/d the effective electron mass in the subband changes sign (i.e. the inflection point). This feature has been the original stimulus to construct a SL because such an effective mass inflection point should open up possibilities for a Bloch oscillator. This could be feasible now because electrons would have to be accelerated up to the inflection point at an energy only slightly higher ($\simeq$ 10 meV) than the bandedge. In bulk materials the inflection point in the conduction band lies of the order of one eV above the bandedge, and due to mostly LO-phonon scattering electrically excited electrons can never reach this energy level. However, such an oscillator has not yet been realised.

Another fascinating superlattice is made of InAs and GaSb, two narrow gap III-V semiconductors. This is a type[3] II SL due to the peculiar "broken gap" line-up at the InAs-GaSb interface at which the InAs CB has a lower

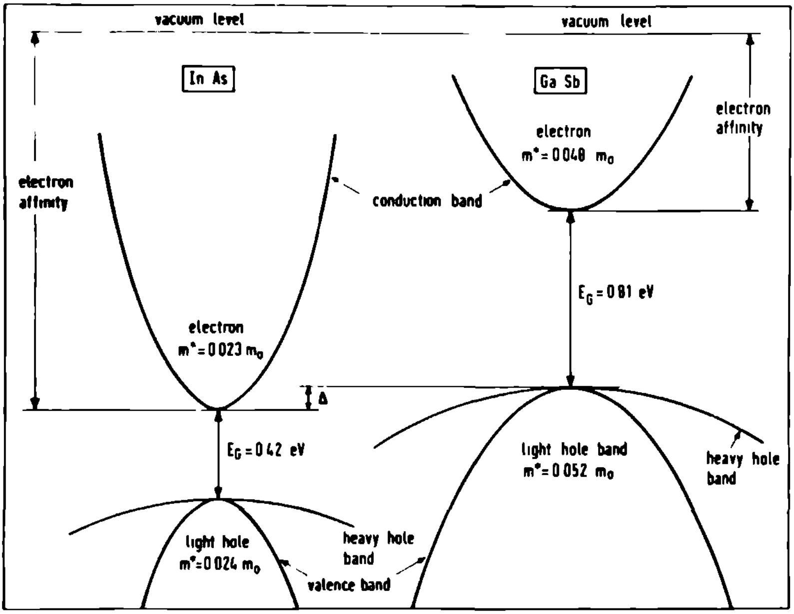

Fig.3. Schematic bandstructure and band line-up of InAs and GaSb at the Γ-point. The vacuum energy levels have been put at an equal energy in this plot. Δ presents the band overlap and amounts to 150±50 meV.

energy than the GaSb VB. .This situation is shown in fig.3 together with the most relevant band parameters. In this picture the line-up is attained by putting the vacuum energy levels at an equal energy. The overlap Δ is 150±50 meV as determined experimentally[6,8]. The spatial bandedge variation in such a SL is shown in fig.1b. The difference with type I superlattices is clearly visible. Now the electrons from the InAs CB are confined between the valence bands of the adjacent GaSb layers, while the holes from the GaSb VB are in a similar way confined between the conduction bands of the adjacent InAs layers. Therefore, the confinement of electrons and holes takes principally place in different layers of the SL, which has important consequences for optical experiments involving transitions between the lowest hole and electron subbands.

Broadening of these lowest subbands occurs in these SL by overlapping of e.g. the electron wave functions from the InAs CB in the valence band states of the GaSb layer in between. In this sense possible transport from InAs electrons through the GaSb occurs in a totally different fashion as in type I superlattices, in which the transport process happens by tunneling through a forbidden energy region. Therefore the simple Kronig Penney model as used for type I superlattices breaks down because the use of plane wave functions and matching them and their derivatives at the interfaces with proper boundary conditions[9] as normally done neglects totally the orthogonality between the cell periodic parts (Bloch) of the conduction band wave functions (s-like) and valence band wave functions (p-like). This orthogonality is assumed to exist also between wave functions in different materials. To solve the problem properly[4,9] one has to use the full Bloch wave functions of the different materials including the orthogonality, and match them and their derivatives at the interface. The wave functions and the bandstructure can best be calculated in the envelope wave function approximation[14,15] in which the boundary conditions at the interface must be chosen in a proper way, reflecting the differences in effective masses in the involved materials.

Due to the aforementioned orthogonality between the Bloch functions of the valence and the conduction band wave functions, the electron CB wave function is in principle evanescent in the GaSb VB and therefore only for very thin GaSb layers a real subband should be present. However, due to a very narrow gap, there exists a strong non-parabolicity in the InAs CB caused by a mixing of the CB and the VB wave functions at nonzero wavevector. The non-parabolicity can be adequately described by a two-band k.p model[10], as will be explained in section IV. Because of this mixing the electron wave function will exhibit both s-like and p-like symmetry and as such forms a resonant state with the GaSb VB. This is the mechanism in type II superlattices responsible for the formation of an electron subband with a large width. A calculation of the subbands in a InAs-GaSb SL is presented in fig.1b. The hatched areas present electron-like subbands of which the lowest one (E_1) has a considerable width. Going to higher energy the subband width decreases according to this figure. This is because these subbands are entering the GaSb energy gap, and as such do not form resonant states anymore. A finite dispersion in the growth direction is now simply established by tunneling, just as in type I superlattices, and therefore these bands are much narrower. This is a phenomenon just contrary to that encountered in type I superlattices in which subband widths increase with energy. Note that for hole levels this simple reasoning leads to erroneous results because of the complexity of the degenerated light and heavy hole bands at the Γ-point.

From now on we will concentrate on the two lowest subbands, E_1 coming from the InAs CB, and H_1 coming from the GaSb VB. The energy positions of these bands relative to the bandedges (confinement) can be near quantitatively explained using eq.1, thus thin layers will tend to push up E_1

and to push down H_1. The energy separation E_1-H_1 can be seen as the effective superlattice gap at the Γ-point. By increasing the SL period this band gap decreases and for periods in excess of ≃19 nm E_1 sinks through H_1 which means the appearance of a "negative" gap in which we have an electron-like level below a hole-like level. This suggest the presence of holes and electrons at the same energy at the same point in k-space, which gives the SL a semimetallic character. However, the semimetallic nature of these systems has been criticised on theoretical grounds concerning anticrossing and the formation of additional energy gaps[12] as will be discussed in the following sections.

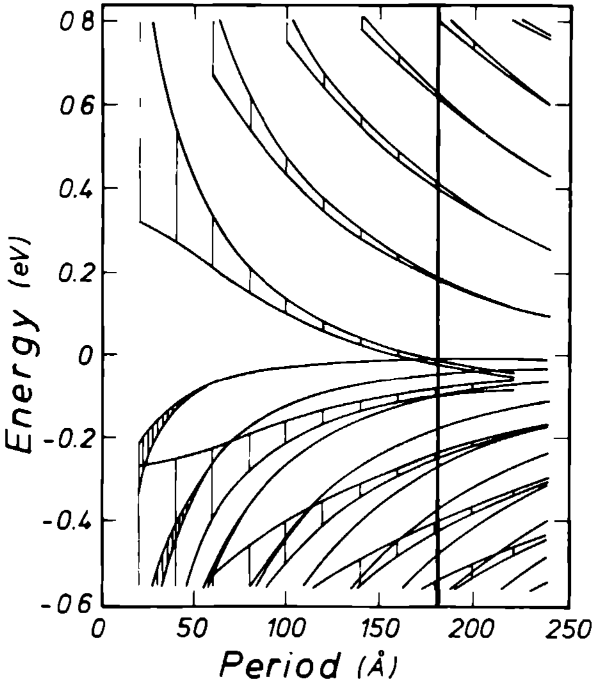

Fig.4. The subband structure of InAs-GaSb superlattices with equal layer thicknesses as a function of the periodicity d. Zero energy on the ordinate scale presents the GaSb valence bandedge at the Γ-point. The hole subbands have an increasing energy with periodicity, whereas the electron subbands decrease in energy as discussed in the text. The vertical bar denotes the difference between semi-metallic (right side), and semiconducting (leftside) superlattices.

The evolution of the subbands and their widths as a function of the superlattice period are presented in fig.4, based on a calculation using a linear combination of atomic orbitals (LCAO method) described elsewhere[13] which yields results very close to the envelope wave function approximation[4,15,16]. In the calculation Δ is taken to be 150 meV. In fig.4. on the left side of the vertical bar the SL will be semiconducting, while on the other side of this bar a semimetallic nature is suggested due to the crossing of E_1 and H_1. Fig.4 also reflects the much more complicated structure of the hole bands due to the degenerate GaSb VB which is discussed in Ref.4.

Due to the band overlap in which the filled hole band is above the empty electron band (for intrinsic materials) charge transfer will occur giving rise to band bending due to the static potential built up by the transferred charge in the depletion regions at both sides of the interface. This band bending will be discussed more fully in chapter 4. It can be shown[4] however that for SL having small periodicities bandbending can be neglected to ±10 meV and the SL can in first order be described in the flat band approximation. For large periods (≃100 nm) flat band conditions do not prevail anymore and the bands are distorted in such a way that the charge carriers tend to be trapped in semi-triangular wells at both sides of the interface. Hence such a system[4] is more a set of single InAs-GaSb heterojunctions than a superlattice in the sense as discussed above.

In the following a study will be made of an InAs-GaSb superlattice made of layers of 12 nm InAs and 8 nm GaSb grown on a ⟨100⟩ GaSb substrate. This SL has the lowest electron subband E_1 well below (≃40 meV) the highest hole subband H_1 hence being semimetallic. From the determined subband separation E_1-H_1 as a function of hydrostatic pressure, the pressure dependence of the band offset Δ will be determined by means of the calculated confinement energies which link Δ with E_1-H_1.

II. INTRODUCTION

A. Measuring principle

The InAs-GaSb interface in an InAs-GaSb SL forms a very interesting and one of the most suited systems to measure band line-ups due to the already discussed broken gap[13,17] line-up in which the InAs CB is at a lower energy than the GaSb VB. The value of this band offset Δ being ≃150 meV. This system has been described comprehensively in Refs.4,12,17-20.

In the most simplified view necessary to understand the experimental data[20], which is the determination of the subband separation E_1-H_1 and the band offset Δ magneto-optically, the coupling between the different subbands due to non-parabolicity can be neglected for the moment. Then in a magnetic field perpendicular to the layers the subbands E_1 and H_1 evolve in a set of equidistantly spaced Landau levels at an energy E_N given by

$$E_N=(N+\tfrac{1}{2})\frac{\hbar eB}{m_{e,h}} \tag{2}$$

with N the Landau index and $m_{e,h}$ respectively the electron and the (negative) hole effective mass. Applying the selection rule[21] $\Delta N=0$ for interband transitions, absorption of a photon with energy $\hbar\omega$ is given by the condition

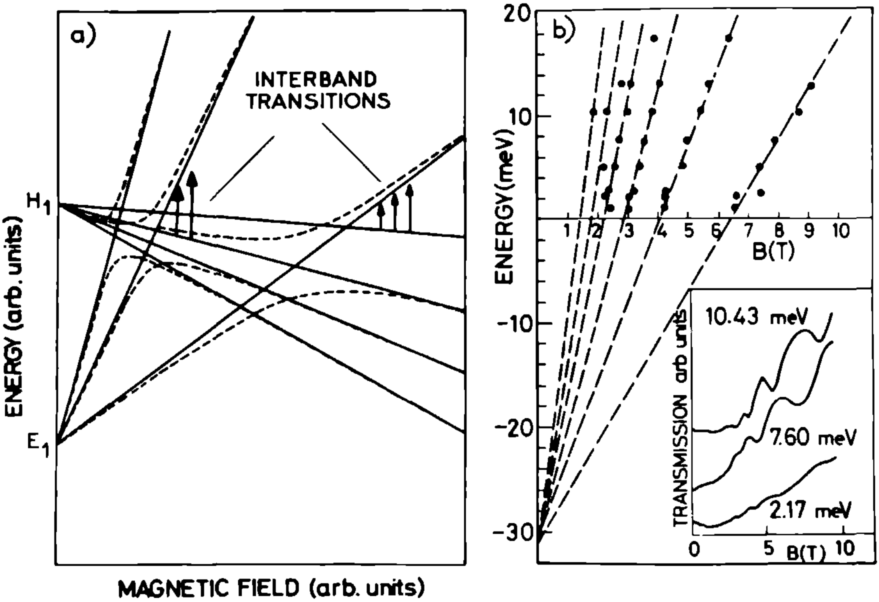

Fig.5. a) Landau level structure of the electron (E_1), and the hole (H_1) subbands. The dashed lines suggest a more realistic level structure in the presence of intersubband coupling. The arrows indicate observable transitions.

b) Measured transition energies between Landau levels at p=1.8 kBar. The dashed lines form a linear fit according to eq.3, and show the idea of linear extrapolation to zero magnetic field to obtain the subband energy separation. The inset shows some experimental spectra.

$$\hbar\omega = E_1 - H_1 + (N+\tfrac{1}{2})\hbar eB\left[\frac{1}{m_e} - \frac{1}{m_h}\right] \qquad (3)$$

in which transitions from the hole- to the electron-like subband have a linear field versus energy dependence that extrapolates at zero magnetic field to the negative energy E_1-H_1. In this way one measures with the use of a magnetic field the zero field subband separation. Subsequently a value for the band offset Δ can be calculated from the known confinement energies. In fig.5a. the evolution of the subbands with magnetic field plus observable transitions are presented. The dotted lines suggest a more realistic model influenced by coupling effects between the subbands.

The measurements are performed by observing the far-infrared (FIR) transmission of the SL for a fixed photon energy as a function of the magnetic field. In fig.5b (insert) some experimental curves have been plotted and their minima which correspond to interband transitions are plotted against the magnetic field. The lines are fitted using eq.3, and the idea of a linear extrapolation to determine the negative energy gap is clearly visible.

B. The need for a magnetic field

Considering the main purpose of the experiment e.g. the determination of the subband separation E_1-H_1 as a function of pressure, one can argue why it is preferred to apply a magnetic field to measure the subband separation in a rather indirect way. Intuitively it should be feasible to induce direct transitions from $E_1$to H_1 at the Γ-point at B=0 T.

From experimental point of view what one should do is to measure the absorption as a function of incident photon energy for different pressures, or use photoluminescence techniques in order to establish directly the energy separation E_1-H_1.

Fundamentally such a direct measurement will be difficult because at zero magnetic field the two-dimensional density of states D(E) in the subbands will be

$$D(E) = \frac{m_{e,h}}{\pi\hbar^2} \qquad (4)$$

in which $m_{e,h}$ refers to either the effective electron mass, or the effective hole mass. For the electron subband E_1, D(E) will be non-zero and given by eq.4 for $E \geq E_1$. For the hole subband H_1, D(E) will consequently be non-zero and given by eq.4 for $E \leq H_1$. As in a semimetallic SL $H_1 > E_1$, it is obvious that no real energy gap will be present between E_1 and H_1, and as such a direct measurement can yield whatever transition energy. However, due to intersubband coupling an anticrossing behaviour is expected, leading to the opening of a small hybridisation gap in the density of states between H_1 and E_1 (as depicted in fig.13). Around this gap the density of states will be increased, which means that a direct measurement risks to measure rather this hybridisation gap than the subband separation.

In a magnetic field both subbands split up in discrete energy (Landau) levels from which transitions can be induced. This allows the identification of the various transmission minima, from which E_1-H_1 can be obtained.

Moreover, at B=0 T transitions at $k_{\parallel}=0$, which could give a value for the subband energy separation E_1-H_1, have a small transition rate. This is because at zero wave vector in the plane of the layers the valence and conduction bands as well as the subband wave functions will be totally decoupled and orthogonal, as will be explained in section IV (see eqs.10, and 17). This means that at $k_{\parallel}=0$ the electron-like wave functions forming E_1 will be strongly localised in the InAs layers, and likewise those forming H_1 in the GaSb layers which leads to a spatial separation of electrons and holes diminishing strongly the transition probability between the subbands E_1 and H_1, even in semiconducting SL in which $E_1>H_1$. It has been suggested[22] that such a separation of electrons and holes could lead to photovoltaic effects. Recently[23] this effect has been observed in InAs-GaSb SL demonstrating this spatial separation.

C. The influence of pressure

Applying hydrostatic pressure to this superlattice changes the band offset Δ. In principle the effect of hydrostatic pressure on semiconductors is accurately[24] known and is mainly an increase of the energy gap at the Γ-point linearly with pressure. Experimentally, the energy gaps of bulk InAs and GaSb increase with a rate of 10 and 14 meV/kBar respectively[22]. Therefore applying hydrostatic pressure to an InAs-GaSb SL will directly affect the broken gap line-up given by Δ. This is suggested in fig.6. in which the relevant bands, subbands, and energy separations have been plotted. From this picture it is evident that although both the energy gaps change with pressure in a known way, there is no unique solution for the way the band offset Δ changes with pressure. Considering experimentally accesible pressures of over 10 kBar, the changes in the energy gaps are of the same order as the zero pressure offset Δ which means that in principle pressure could be capable to remove totally the band overlap hence changing the nature of the superlattice completely. Less stringent, it could be possible to move E_1 above H_1 and as such have a pressure induced semimetallic-semiconducting transition in the SL. These speculations show the fascinating possibilities opened up by applying hydrostatic pressure to this superlattice.

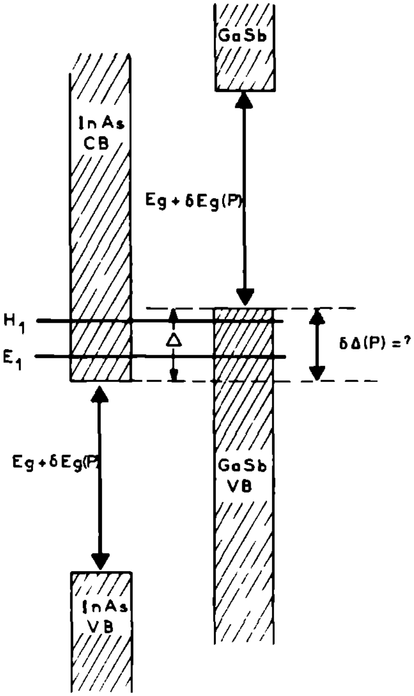

Fig.6. One period of the InAs-GaSb superlattice showing the relative positions of both conduction bands (CB) and valence bands (VB), as well as the bandoverlap Δ. The increase of the energy gaps with pressure is indicated by $\delta E_g(p)$, (10 meV/kBar for InAs and 14 meV/kBar for GaSb) resulting in an unknown change in the bandoffset Δ. The involved subbands E_1 and H_1 are also drawn (not to scale).

III. EXPERIMENTAL SET-UP

The experiments were all done at a temperature between T=1.8K and T=4.2K with a magnetic field perpendicular to the layers in the Faraday configuration, in which the wavevector of the randomly polarised FIR radiation is parallel to the magnetic field. The radiation was supplied by a molecular gas laser optically pumped by a CW CO_2 gasdischarge laser. Using different pumping lines and gasses the spectral range from λ=56 μm to 1223 μm could be covered. DC magnetic fields up to B=22T were generated by the

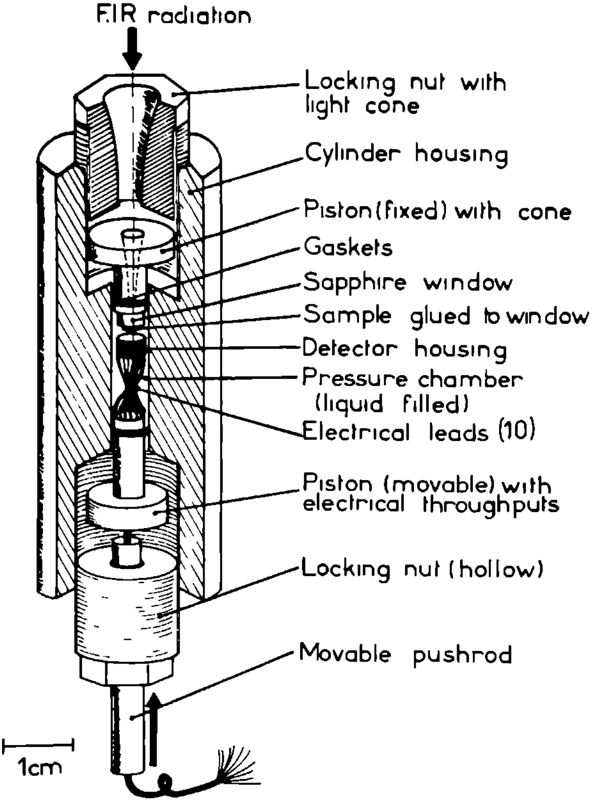

Fig.7. The Cu-Be liquid pressure cell suited for far-infrared experiments up to a hydrostatic pressure of 14 kBar. See the text for details.

polyhelix magnet of the Grenoble high-field facility.

In the experiment the transmission of the sample was measured at a fixed photon energy as a function of a swept magnetic field. As a detector a bolometer made of a 470Ω Allen and Bradley carbon resistor mounted directly behind the sample (in the pressure cell) was used. For normalisation purposes and to correct for laser power fluctuations, a second bolometer was mounted just above the sample. Standard techniques for phase-sensitive detection and normalisation of the signals were used.

To induce pressure on the sample a commercially available Cu-Be liquid

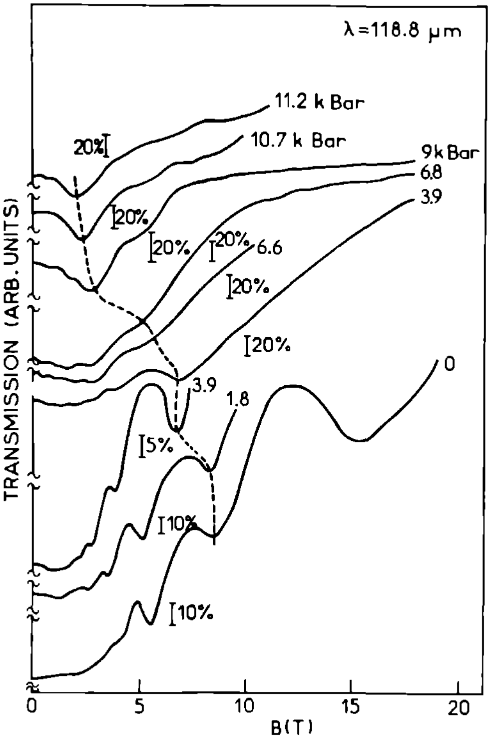

Fig.8. Sample transmission for λ=118.8 μm FIR radiation for different pressures. The vertical bars denote relative transmission changes. The zero- and 1.8 kBar traces were recorded at T=4.2 K, the others at T=1.8 K. Further details are given in the text.

pressure cell, obtained from Unipress, Warsaw, was used. This cell[24] is shown in fig.7. It consists mainly of a rigid Cu-Be cylinder with two pistons that are used to reduce the volume of the pressure chamber by means of a hydraulic press. As the pressure transferring medium a mineral oil is used. One of the pistons contains electrical throughputs while the other contains a light cone and a rigid sapphire window to allow the FIR radiation to enter the pressure chamber. After pressurising the locknuts are tightened and the cell can be transported and mounted in a cryostat. The pressure is measured with a pressure gauge made of a heavily n-doped InSb crystal of which the resistance as a function of both temperature and pressure is accurately known. In this way the pressure can be measured to ±0.1 kBar. The FIR bol-

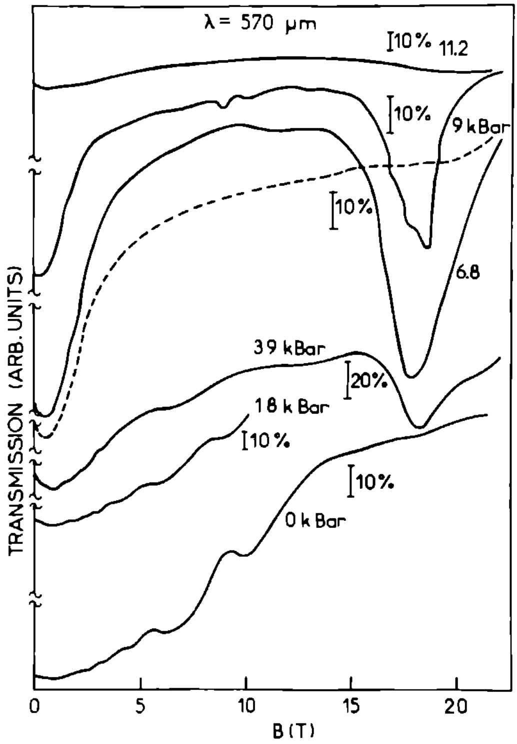

Fig.9. Sample transmission for λ=570 μm radiation. Comments are the same as for fig.8. The dotted line presents a 6.8 kBar spectrum, also measured at T=4.2 K. See the text for details.

ometer is also mounted in the pressure cell just behind the sample which is glued with silverpaint to the sapphire window. Care has been taken not to strain the sample and to minimise leakage radiation around the sample. By cooling down this system to LHe temperatures the mineral oil freezes out which can give rise to pressure inhomogeneities in the cell causing uniaxial and biaxial strain on the sample. However, by cooling down very slowly the liquid freezes out in a very homogeneous fashion and it is generally believed[24-26] that deviations from hydrostatic pressure are less than 1%. With this pressure technique pressures up to 14 kBar can be easily reached at ambient temperature, which correspond to roughly 12 kBar at LHe temperatures. In this way measurements have been done at zero, 1.8, 3.9, 6.6, 6.8, 9, 10.7, and 11.2 kBar.

Some transmission results for various pressures are presented in figures 8 and 9 for FIR wavelengths of 118.8 and 570.6 μm respectively. In these plots, which have different ordinate scales, the relative transmission changes are indicated by a vertical bar. The dotted line in fig.8 follows the 1→1 transition according to eq.3 with pressure. To allow better comparison between low and high pressure spectra, the 3.9 kBar trace has been plotted in two different transmission scales. The very pronounced high field structure as seen in fig.9 has a very strong temperature dependence which is demonstrated by the dotted spectrum at 6.8 kBar that has been measured at a slightly higher temperature. This phenomenon will be discussed later.

IV. ANALYSIS OF THE EXPERIMENTAL RESULTS

A. non-interacting, non-parabolic bands without pressure

Due to the interaction between the conduction and the valence bands in narrow-gap semiconductors such as InAs, the dispersion relation for the conduction band will not be quadratic, but will suffer from non-parabolicity. Even if one neglects interaction between the subbands in the SL it is not allowed to ignore totally the non-parabolicity and therefore eqs.2 and 3 present a strong oversimplification, although they are qualitatively correct. In the case of the InAs CB the non-parabolicity can be reasonably well accounted for by a two-band k·p model[4,10,20,21,27,28]. Following this model, the bulk wave functions for band j are described by the Schrödinger equation

$$\left[\frac{p^2}{2m} + V(r)\right]\Psi_{j,k}(r) = E_j\Psi_{j,k}(r) \tag{5}$$

in which V(r) is the periodic lattice potential and the Bloch functions are

$$\Psi_{j,k}(r) = u_{j,k}(r)e^{ikr} \tag{6}$$

Substitution and calculation lead for the cell periodic part $u_{j,k}(r)$ to

$$\left[\frac{p^2}{2m} + \frac{\hbar}{m}k\cdot p + \frac{\hbar^2k^2}{2m} + V(r)\right]u_{j,k}(r) = E_j u_{j,k}(r) \tag{7}$$

As the bandedge functions (k=0) $u_{j,0}(r)$ form a complete orthogonal set, we expand $u_{j,k}(r)$ in

$$u_{j,k}(r)=\sum_{i} A_{i,j} u_{i,0}(r) \tag{8}$$

where the summation is over all bands. The Hamiltonian can now be written in the matrix form

$$\langle u_{j,0}|H|u_{i,0}\rangle=E_i(0)\delta_{ij}+\frac{\hbar^2k^2}{2m}\delta_{ij}+\langle u_{j,0}|\frac{\hbar}{m}\mathbf{k}\cdot\mathbf{p}|u_{i,0}\rangle \tag{9}$$

which in the case of a two-band model reduces to

$$H=\begin{pmatrix} E_{gap}+\frac{\hbar^2k^2}{2m} & \frac{\hbar}{m}\mathbf{k}\cdot\mathbf{p} \\ \frac{\hbar}{m}\mathbf{k}\cdot\mathbf{p} & \frac{\hbar^2k^2}{2m} \end{pmatrix} \tag{10}$$

in which the complete set used as a base is $u_{1,0}=u_c$ and $u_{2,0}=u_v$, respectively the CB and VB bandedge functions. m is the free electron mass, and **p** is Kane's momentum matrix element[12,28] given by $\langle u_{c,0}(r)|\mathbf{p}|u_{v,0}(r)\rangle$. The zero of energy is chosen at the VB bandedge. Note that the off-diagonal elements in (10) present the k·p CB-VB coupling which is totally absent at k=0. This means that at zero wave vector the CB and VB wave functions are orthogonal and decoupled. Diagonalisation of the Hamiltonian (10) yields the wave functions of the interacting CB and VB and the eigenvalues of (10) give the non-parabolic energy versus wave vector dispersion relation as

$$\frac{\hbar^2k^2}{2m_o^*}=E(1+\frac{E}{E_g}) \tag{11}$$

in which k presents the 3D wave vector, m_o^* the effective electron mass at the CB bandedge, E the energy from the bandedge and E_g the energy gap at the Γ-point. From eq.11 the non-parabolic effective electron mass m^* at an energy E above the bandedge is given by

$$m^*=m_o^*(1+\frac{2E}{E_g}) \tag{12}$$

In a SL with $\hat{z}$ the growth direction, it can be assumed that the dispersion in the $\hat{x},\hat{y}$ plane (i.e. in the plane of the layers) remains unmodified by the structure of the sample. Therefore the total dispersion relation in the plane of the layers will according to eq.11 be given by

$$\frac{\hbar^2 k^2}{2m_o^*}=E(1+\frac{E}{E_g})-E_1(1+\frac{E_s}{E_g}) \tag{13}$$

in which k is the wavevector in the plane of the layers and $E_s=E_s(k_z)$, the energy in the subband due to a finite dispersion in the growth direction. If $k_z=0$, then $E_s=E_1$, which equals the confinement energy. For a magnetic field in the growth direction the kinetic energy can be replaced[4,29,30] according to eq.2 by

$$\frac{\hbar^2 k^2}{2m_o^*}\rightarrow(N+\tfrac{1}{2})\frac{\hbar eB}{m_o^*} \tag{14}$$

Now by replacing E by E_N in eq.13, a modified expression for the interband transition energies (see eq.3) corrected for non-parabolicity can be obtained

$$\hbar\omega=-\frac{E_g}{2}+\frac{E_g}{2}\left[1+\frac{4\hbar eB}{m_o^* E_g}(N+\tfrac{1}{2})+\frac{4E_s}{E_g}(1+\frac{E_s}{E_g})\right]^{1/2}-H_1-(N+\tfrac{1}{2})\frac{\hbar eB}{m_h} \tag{15}$$

where $E_s=E_1+E(k_z)$, as given by the SL dispersion relation. The hole band dispersion relation in GaSb has been assumed parabolic with m_h the heavy hole mass. In principle the hole subband has a small confinement energy due to a heavy hole mass in the growth direction. These holes however, should be partially light in the plane of the layers due to the symmetry of the p-wave functions. Therefore it is not obvious which hole mass one should take in eqs.3 and 15. However, it has been established experimentally[4,20,31] that taking $m_h=-0.33\ m_e$ (i.e. roughly the heavy hole mass) yields a reasonable agreement between experiment and theory. It must be noted here that these kind of experiments are not very sensitive to the exact value of the heavy hole mass, which can in fact not be determined as being one single scalar mass.

The main difference between eq.3 and eq.15 is that in the latter the energy positions of the Landau levels are corrected for an effective electron mass increase in the band due to non-parabolicity as given in eq.12, and hence the Landau levels do not form straight lines anymore. For the analysis of the experimental results eq.15 is used in which the only free parameter is the subband separation E_1-H_1.

B. Effects of pressure

As can be seen from fig.6 the main influence of hydrostatic pressure on the SL is an increase of the energy gaps resulting in a change of the band overlap Δ, and consequently also in a change of E_1-H_1. Another effect of the pressure that cannot be neglected is an increase of the effective electron mass at the CB bandedge. As the electron mass has a strong influence on the confinement and as such on the positions of the subbands (as qualitatively given by eq.1), its pressure dependence must be included in the analysis. Moreover, the slope of the observed transitions will also change with pressure due to these effective mass changes.

The real effect of the hydrostatic pressure on the electron mass enters mainly through the change in the energy gaps and can be calculated[32,33] according to

$$\frac{m}{m_e^*} = 1 + \frac{2P^2}{3}\left(\frac{2}{E_g} + \frac{1}{E_g+\Delta_{so}}\right) \tag{16}$$

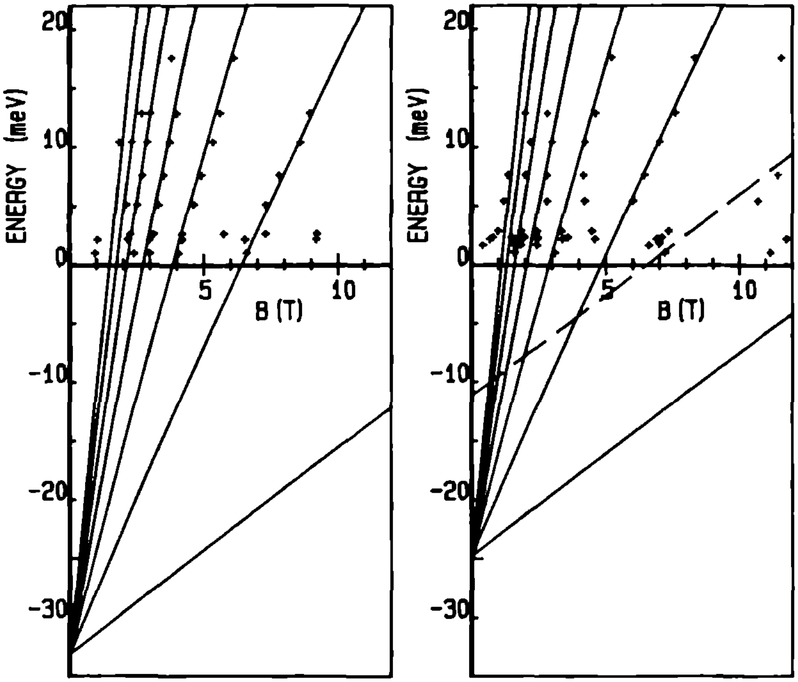

Fig.10. Experimentally observed transition energies as a function of the magnetic field. a) 1.8 kBar, b) 3.9 kBar. The lines present interband transitions as calculated by eq.15 for N=0 to 7. The dotted line in fig b) suggests an N=0 zone-boundary transition as will be discussed in section IV.B.

which relates the effective electron mass at the bandedge to the bandgap[21].

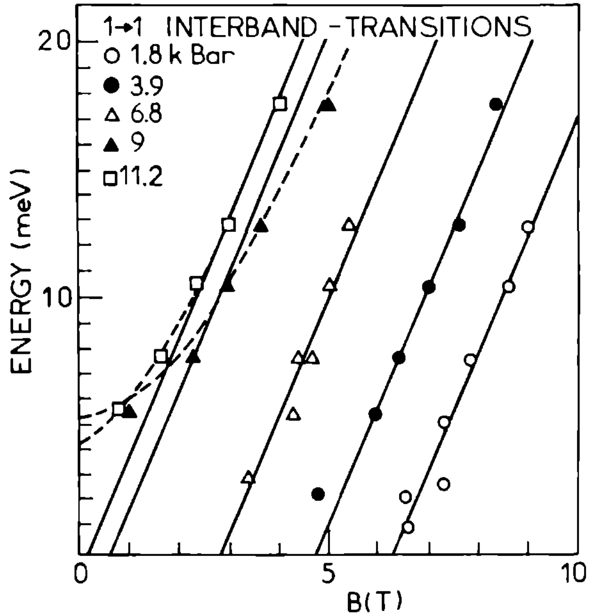

Fig.11. The experimental N=1 interband transitions for various pressures. the drawn lines are calculated as explained in the text. The dotted lines present a calculation including line-broadening due to collision damping.

All quantities are given in atomic units, and m presents the free electron mass, E_g the bandgap at the Γ-point between the CB (Γ_6) and the VB (Γ_8) bandedges, and Δ_{so} the energy gap between the Γ_8 valence band and the split off valence band Γ_7. P is a matrix element[21] determining the CB-VB interaction. P and Δ_{so} can be assumed to have a very small[24] pressure dependence compared to E_g. Including the change in E_g with pressure (which is 10 meV/kBar for InAs), predicts an increase in the bandedge mass of 20% if going from zero to 10 kBar. Therefore in order to fit properly the experimental data, E_g and m_0^* were for every experimental pressure adjusted according to eq.16 and substituted in eq.15 with the subband energy separation as the fitting parameter.

The experimentally observed transition energies are plotted as a function of the magnetic field in fig.10 together with a theoretical fit conform eqs.15 and 16 for two different pressures. As discussed before, the extrapolated intercept of the interband transitions with the ordinate present the "negative" gap E_1-H_1. For the highest field interband transitions (N=1) the experimental

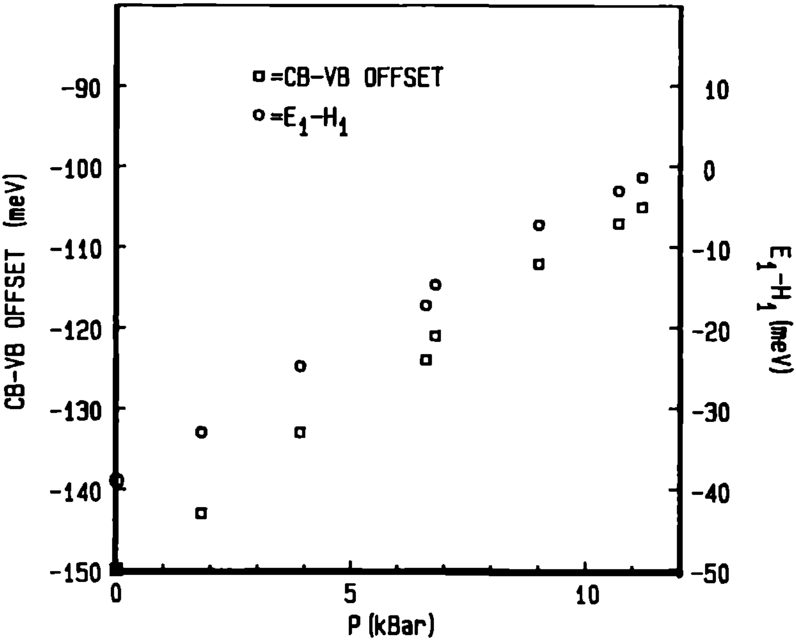

Fig.12. Experimentally obtained results for the subband separation E_1-H_1, and the from this value deduced band overlap Δ.

points and the best fit to the experiment are plotted in a single picture in fig.11 for several pressures. The dotted lines present a theoretical fit for the two highest pressures in which Landau level broadening due to collision damping[34] has been taken into account. The influence of this kind of damping can be expected to be more pronounced at high pressures due to possible distortions in the lattice. The in this manner obtained dependence of E_1-H_1 on pressure is depicted in fig.12 for all pressures by the open circles. From this figure it can be concluded that E_1-H_1 decreases linearly with pressure with a rate of 3.4 meV/kBar. According to this picture the previously suggested crossover of E_1 and H_1, i.e. the semimetal-semiconductor transition appears not to occur at experimentally attainable pressures.

As can be seen in figs.1 and 6, E_1-H_1 is given by the band offset Δ minus the hole confinement energy minus the electron confinement energy. Therefore in zeroth order approximation the rate of change of Δ with pressure should be equal to the rate of change in E_1-H_1. However, the pressure changes both the bandedge masses (eq.16) and the non-parabolicity due to a change in E_g. These two effects change the confinement energies considerably, hence the relation between Δ and E_1-H_1 becomes more complicated. On grounds of eq.16 it is expected that the confinement decreases with pressure which means that the rate of change with pressure of Δ will be a little more than the observed rate of change in E_1-H_1. In reality the total pressure effect is rather complicated because although the bandedge mass increases with pressure, the non-parabolicity decreases because of a larger energy gap, two effects which tend to compensate each other more or less as far as the subband confinement is concerned. It is interesting to note that the final effect of the pressure on the effective electron mass near the Fermi level (pinned just below H_1, as will be discussed later) is almost negligible. The correct way to proceed is to calculate in the envelope wave function approximation selfconsistently directly the transition energies as a function of both pressure and Δ. This is however a very tedious and time consuming work. An approximated not selfconsistent analysis of a limited amount of experimental data was made in this way[20,32] and has been presented in chapter 2. This calculation showed Δ to decrease with 5.8 meV/kBar which is indeed more than the observed rate of change of E_1-H_1. However, as can be seen in the literature[4,12,19], there is still a fair amount of uncertainty in the exact value of the overlap Δ which depends strongly on the way of analysing the experimental data, even at zero pressure. Moreover, even some results obtained in a similar approximated way as presented by eq.15 (see references 4 and 6) seem to reflect more precisely the experimental facts than more fundamental calculations[12,19]. Therefore in view of the limited accuracy both experimentally as well as theoretically, we can follow a rather simple approach to obtain Δ from E_1-H_1 as a function of pressure without deterioration of the essential results and conclusions.

Using the envelope wave function approximation to calculate the SL band structure at zero wave vector and zero magnetic field, the confinement energies of E_1 and H_1 have been calculated as a function of pressure using an initial (not very relevant) assumption[32] on the dependence of Δ on pressure. From these calculations, as presented in reference 32, together with the obtained E_1-H_1 values from fig.11, a value for the band offset Δ as a function of pressure has been derived and also plotted in fig.11 as the squares. From this plot a rate of change in Δ of $\simeq$4.2 meV/kBar can be deduced, which is indeed higher than in E_1-H_1 ($\simeq$3.5 meV/kBar).

We like to note that the absence of selfconsistency in the calculations linking Δ with the subband separation E_1-H_1 also introduces some errors. The main effect is that due to a charge transfer from the filled GaSb-VB to the empty InAs-CB a band bending occurs, as will be discussed more fully in chapter 4. Due to this band bending the bandedges (as sketched in fig.1b and fig.6) will be curved; the InAs CB bandedge will be pushed up in the middle of the InAs layer, while the GaSb VB bandedge will be pushed down in the middle of the layer[4]. This causes a slightly more complicated relation between Δ and E_1-H_1 due to an inhomogeneous confinement energy across the layer. By increasing the pressure, charge transfer and accordingly band bending decreases which presents an additional pressure effect that can blur the proportionality between Δ and E_1-H_1. However, as stated before, in the investigated SL due to a rather small periodicity the total band bending will be small ($\simeq$ 10 meV) which introduces over the whole pressure range a correction to the relation between Δ and E_1-H_1 which falls below the experimentally attainable accuracy, and therefore can be neglected.

As already shortly discussed in chapter 2 and in the beginning of this chapter, the InAs-GaSb SL forms no perfectly lattice-matched system, but has a slight mismatch in which the InAs lattice constant is about 0.6% smaller than the GaSb lattice constant[4,35]. This means that the SL will be strained. Due to the geometry of the sample, grown on a GaSb substrate, the lattice mismatch will be compensated for by a stretching of the InAs layers. Therefore the deviations in the bandstructure will be mainly incorporated in the InAs. The most important changes due to this strain will be a minor change in the energy gap at the Γ-point due to a hydrostatic component induced by the strain, and a possible lifting of the degeneracies at k=0 of the light and heavy hole valence bands at Γ. The latter change stems from the fact that non-isotropic deviations in the lattice constant, as caused by strain, will affect mainly the non-isotropic p-like wave functions of which the valence bands are constituted. However, as can be seen in fig.6, the InAs VB is not of major importance to the band offset problem presented here. As far as pressure is concerned, due to nearly equal compressibilities[35] of InAs and GaSb no additional strain will be induced. Therefore the pressure dependence of the band offsets is assumed to be not affected by strain, although this might be the case for the absolute values of the offsets.

C. Effects of intersubband coupling

In the foregoing sections the effects of mixing of the originally orthogonal VB and CB wave functions have been discussed in the framework of a two-band k·p model, in order to calculate non-parabolic electron masses in the CB. It was argued that such a mixing also existed between the wave functions of InAs and GaSb, and that therefore a resonant state could exist in the GaSb VB leading to a very wide electron subband. However, for the calculations of the Landau levels coming from the subbands E_1 and H_1 as suggested in eqs.4 and 15, any possible mixing between these subbands similar to the CB-VB interaction has been totally neglected. This has resulted in non-interacting crossing Landau levels leading to rather straightforward simple transitions as calculated and presented in figs.10 and 11. Although these calculations describe very well the experiment, and suggest a semimetallic behaviour due to the crossing of electron and hole levels, its validity has been criticised strongly[12,19] on theoretical grounds suggesting an interaction between the different subbands. This interaction will lead to an anticrossing behaviour and to the formation of small but finite hybridisation gaps between hole and electron states at $k \neq 0$, with k the wave vector in the plane of the layers. Due to this anticrossing the Landau levels will display strong deviations from linearity as a function of field.

Instead of using a many band envelope wave function approximation to obtain the SL band structure as presented in the literature[18,19,36], we will approach the problem using a two-band k·p model with the assumption that the subband interaction has the same nature as the CB-VB interaction in a single bulk. Following this assumption, the subband dispersion at $k_z=0$ can be calculated in a similar two-band k·p model as presented for the non-parabolicity. As a basis for the Hamiltonian as given in expression 10, the CB and VB wave functions which diagonalise this Hamiltonian are chosen. These functions have, if corrected for confinement energy, for small $k_\parallel$ the same dispersion in the plane of the layers as the subband wavefunctions in the absence of intersubband coupling. The subband interaction is now introduced in the Hamiltonian in an analogous way as in expression 10, giving

$$H=\begin{pmatrix} H_1+\frac{\hbar^2k^2}{2m_h} & Q\cdot k \\ Q\cdot k & E_1+\frac{\hbar^2k^2}{2m_e} \end{pmatrix} \tag{17}$$

with m_e and m_h respectively the electron and the (negative) hole effective masses, as derived from eqs.10-12. Q is a matrix element similar to Kane's momentum matrix element presenting the intersubband coupling.

The subband dispersion relations for k in the plane of the layers, as obtained by diagonalisation of Hamiltonian (17) are presented in fig.13 for the case of the discussed InAs-GaSb SL. The matrix element Q has been chosen to comply with other calculations[12]. The dotted line presents the parabolic dispersion in the absence of intersubband coupling. The Fermi level in this case lies at the crossing. As can be seen, due to the interaction a small hybridisation gap opens up at the Fermi level. For n-doped materials the Fermi energy increases and a small pocket filled with electrons can be formed near the crossing. This effect is thought to be responsible for observed semimetallic behaviour in these systems.[12,36].

For the case of a magnetic field perpendicular to the plane of the layers (the $\hat{z}$-direction), the usual transformation[19,21] $p \rightarrow p+eA$ with **A** the vector potential defined by $A=-r \times B$ has to be made. This leads to

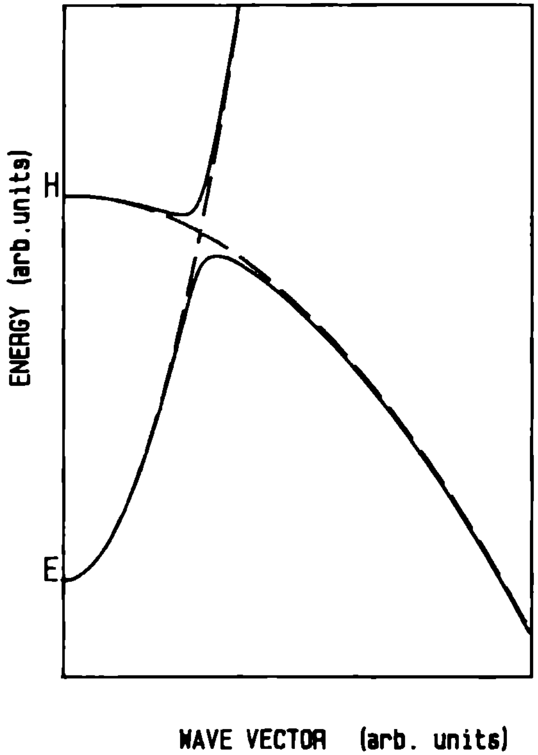

Fig.13. Subband dispersion for the wave vector k in the plane of the layers, according to a two-band k·p model. The dotted line presents the parabolic dispersion in the absence of intersubband coupling.

$$\hbar k=(\hbar k_x,\hbar k_y,\hbar k_z)\rightarrow(\hbar k_x,\hbar k_y+eBx,\ \hbar k_z) \tag{18}$$

in which r=(x,0,z) and B=(0,0,B). The momentum operator is now defined as $p_x=\hbar k_x$ and $p_y=\hbar k_y+eBx$, and the lowering and raising operators $a^{\pm}$ according to

$$a^{\pm}=\frac{1}{\sqrt{2eB\hbar}}(p_x\pm ip_y) \tag{19}$$

which satisfy the commutation relations

$$[a^-,a^+]=1 \quad a^+a^-+\tfrac{1}{2}=\frac{p^2}{2eB\hbar} \tag{20}$$

Now the Hamiltonian (17) can be rewritten according to the second quantisation rules of the operands $a^\pm$ on the base of harmonic Landau functions (ψ_n,ψ_{n-1}) for n=1,2,3,... and $(\psi_0,0)$ as

$$H=\begin{pmatrix} H_1-(n+\frac{1}{2})\hbar\omega_{ch} & \frac{\hbar}{\ell}\sqrt{2}Q\sqrt{n} \\ \frac{\hbar}{\ell}\sqrt{2}Q\sqrt{n} & E_1+(n-\frac{1}{2})\hbar\omega_{ce} \end{pmatrix} \tag{21}$$

in which the cyclotron frequencies ω_{ch} for the holes, ω_{ce} for the electrons, and the magnetic length ℓ are defined as

$$\hbar\omega_{ch,e}=\frac{\hbar eB}{m_{h,e}} \qquad \ell=\sqrt{\frac{\hbar}{eB}} \tag{22}$$

Diagonalisation of (21) yields the wave functions for the Landau levels in the case of intersubband coupling, and the energy versus magnetic field dispersion. The evolution of the Landau levels with magnetic field is plotted according to (21) in fig.14 in the case of $Q\simeq0$ to show (see the circles) where the hybridisation gaps open up. In fig.15 the same calculation is presented for a more realistic[12] value for Q. The indices are the quantum numbers n as in (21), which for hole-like levels are equal to undisturbed Landau indices N as described in eqs.2 and 3, but which for electron-like levels are Landau indices augmented with unity. Transitions according to Hamiltonian 21 obey the selection rule $\Delta n=1$, which corresponds to interband transitions having $\Delta N=0$ as in eq.3. Both figs.14 and 15 are calculated using the parameters for the measured SL at a pressure of 1.8 kBar.

To illustrate the mixing of interband transitions (having a slope of $(N+\frac{1}{2})\hbar\omega_c$) and intraband (cyclotron resonance) transitions (having a slope of $\hbar\omega_c$), as mentioned in chapter 2, some allowed transitions are suggested by arrows in fig.15: (a) and (c) present interband-like transitions, and (b) is an intraband-like transition. Finally (d) presents again an "across the gap" interband transition. In other words; following a transition from level n=2 to n=3 in fig.15 from low to high energy, one has first an interband-like transition (a), similar to an interband transition having N=2 as calculated by eq.3 in the

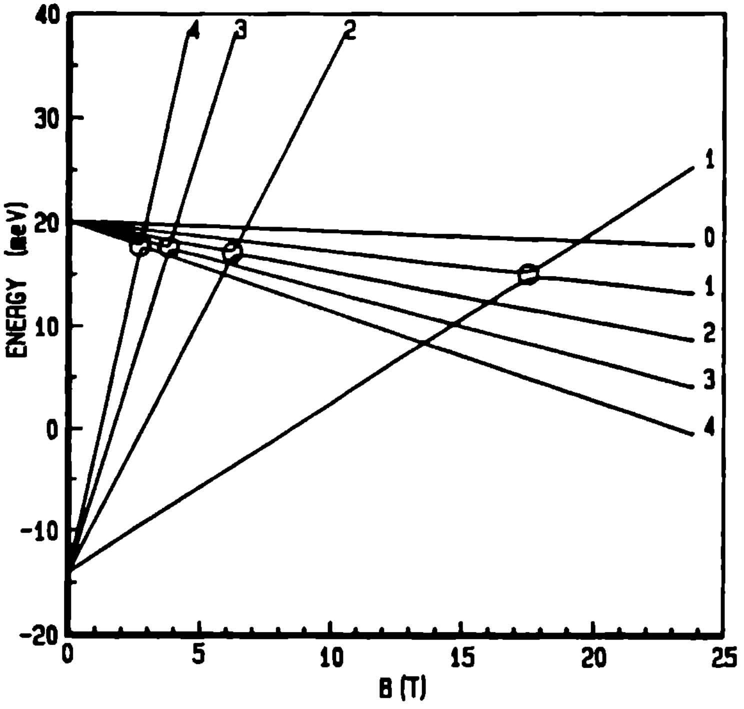

Fig.14. Evolution of electron and hole Landau levels with magnetic field in the presence of a small intersubband coupling, leading to an anticrossing as indicated by the circles. The indices are according to eq.21.

simple model. With higher energy it becomes intraband-like (b), corresponding to an N=2 cyclotron resonance. Subsequently, with still higher energy it becomes again an interband-like transition (d).

For the situation as presented in fig.15, all allowed transitions have been plotted in fig.16, in which the capitals refer to the transitions of the nature as suggested in fig.15 by the arrows. The main influence of the coupling is evident from fig.16, and consists in a slight overall decrease of the slope of the transitions, especially at very low excitation energies, and a change-over to a more cyclotron-like resonance as discussed before[20] for higher excitation energies. Moreover a forbidden energy region is formed due to the hybridisation gaps, of which however no experimental observation exists.

Although the two-band model as presented above presents a simplification of the real bandstructure, its results are in good agreement with more realistic six-band calculations as presented in references 12 and 19. For zone-

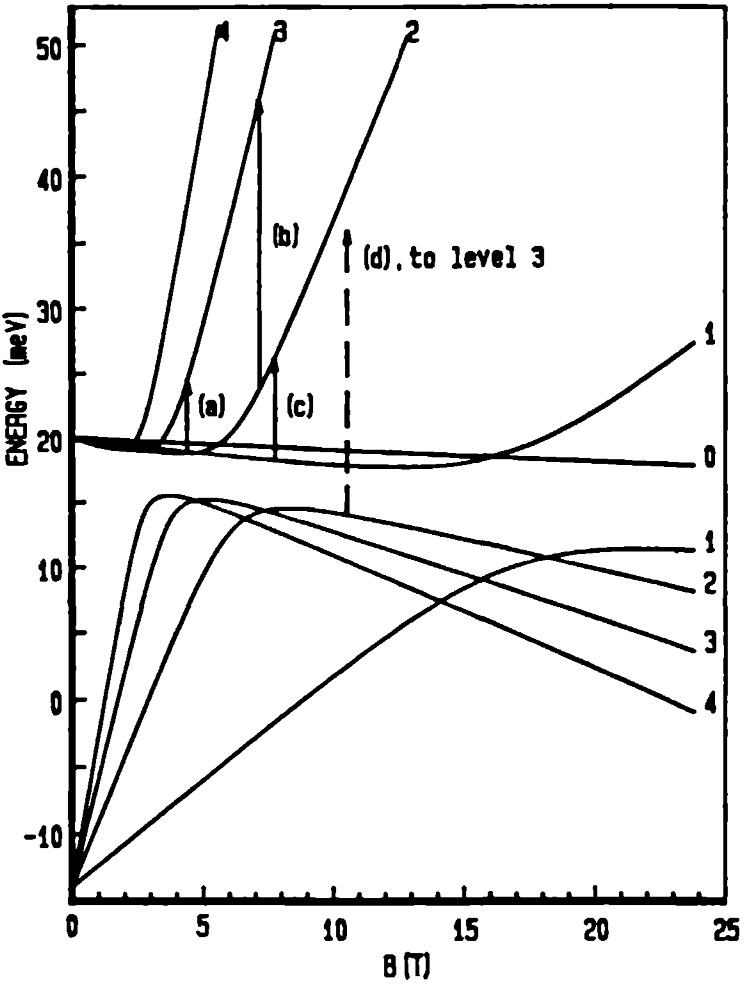

Fig.15. Evolution of the Landau levels in the presence of a realistic intersubband coupling. The arrows (a), (b), (c), and (d) present possible transitions of different character as discussed in the text.

centered (k_z=0) transitions the calculations of ref.19 reveal practically the same results as presented by the more simple method in fig.16, in spite of a far more complicated Landau level structure. The possible existence[4,6] of zone-boundary transitions ($k_z=\pi/d$) will be discussed in this context lateron.

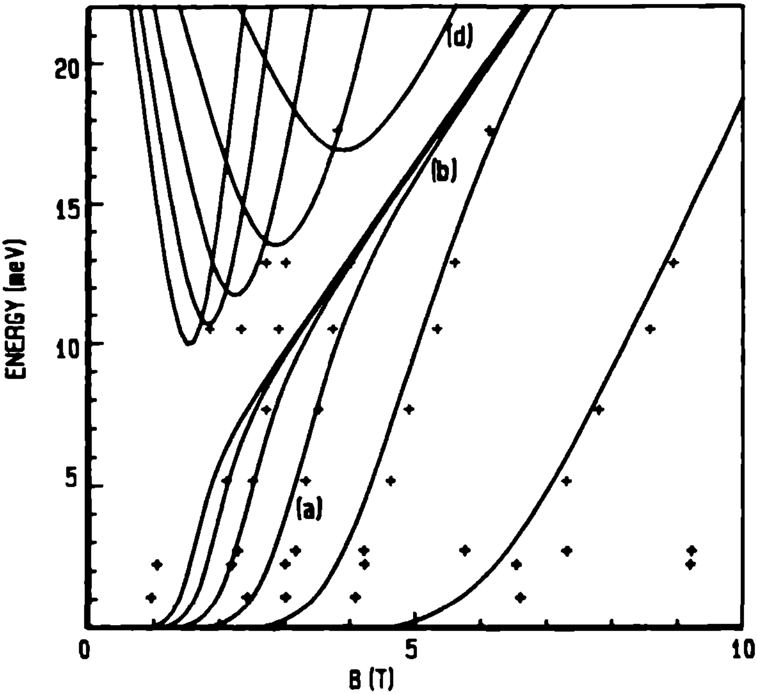

Fig.16. Allowed transitions for the situation as presented in fig.15, together with experimental results obtained at p=1.8 kBar. The capitals refer to transitions as suggested in fig.15.

D. Influence of the Fermi level and of extrinsic charges.

i) Low pressures without coupling

In all previous calculations the position of the Fermi level determining which transitions are allowed on grounds of the occupation of the bands, has been totally ignored. The Fermi level in the InAs-GaSb SL is established by both intrinsic and extrinsic charges. If we assume firstly both materials to be perfectly pure, then the Fermi level E_F will be formed by the spill over of electrons from the filled hole-subband H_1 to the empty electron band E_1. In the case of no intersubband coupling, E_F can be calculated from the equality

$$n=\int_{E_1}^{E_F}\frac{m_e^*(E)}{\pi\hbar^2}dE=\int_{E_F}^{H_1}\frac{m_h^*(E)}{\pi\hbar^2}dE \qquad (23)$$

in which the two-dimensional density of states has been used, and the masses are non-parabolic according to eq.12. The principle of eq.23 is that the number of electrons in the subband E_1 is the same as the number of holes in the subband H_1. For a subband separation E_1-H_1=39 meV, the charge transfer n equals 5.5x10^{11}cm^{-2} , which establishes a Fermi level at an energy E_F=36 meV above E_1, compatible with literature values[4,12].

Any extrinsic additional charge will be electrons due to the inherent residual n-doping of the InAs. As reported in the literature[37] n will be of order of 10^{16}cm^{-3}. Therefore in reality the Fermi energy E_F will be raised. However, the density of states above the intrinsic Fermi level is very large due to a heavy hole mass. Hence even for an extrinsic charge of the same order of magnitude as the intrinsic spilled over charge, the Fermi level will stay more or less pinned several meV below the hole subband H_1. In the case of strong intersubband coupling the charge density will strongly increase at the anticrossing, an effect that even enhances the Fermi level pinning on H_1.

In a magnetic field all Landau levels, regardless of intersubband coupling, have a degeneracy β=eB/$\pi\hbar$ (two-fold spin degenerated), for the holes as well as for the electrons. Using β to determine the filling factor of the Landau levels, the exact position of E_F can be found as a function of field. In this procedure one assumes that for intrinsic materials all hole levels will be filled and all electron levels empty at high magnetic fields in which all hole-like Landau levels are below the electron-like levels. (This point is marked by the crossing of the two lowest numbered Landau levels at B$\simeq$19.5 T in fig.14.) For the experimental situation of p=1.8 kBar, the Fermi level has been calculated for intrinsic, as well as for extrinsic materials containing various densities of n-doping and presented in fig.17. For the calculation of E_F all extrinsic charges coming from the InAs layer of 12 nm thickness are assumed to accumulate as a two-dimensional sheet of charge. In this way a residual n-doping of n=10^{17}cm^{-3} causes an additional charge of 1.2x10^{11}cm^{-2}. In fig.17 a small subband interaction is included in order to show the relative position of E_F with respect to possible hybridisation gaps. To keep the picture surveyable only part of the electron-like levels below the anticrossing have been plotted. E_1 should be at -13 meV on the ordinate scale at B=0 T. Vertical arrows indicate possible transitions according to eqs.3 and 15. Their number corresponds to the relevant Landau index N. The horizontal bar shows the range in B in which (for intrinsic material) the transition with Landau index N=2 can be observed, and how it changes in this

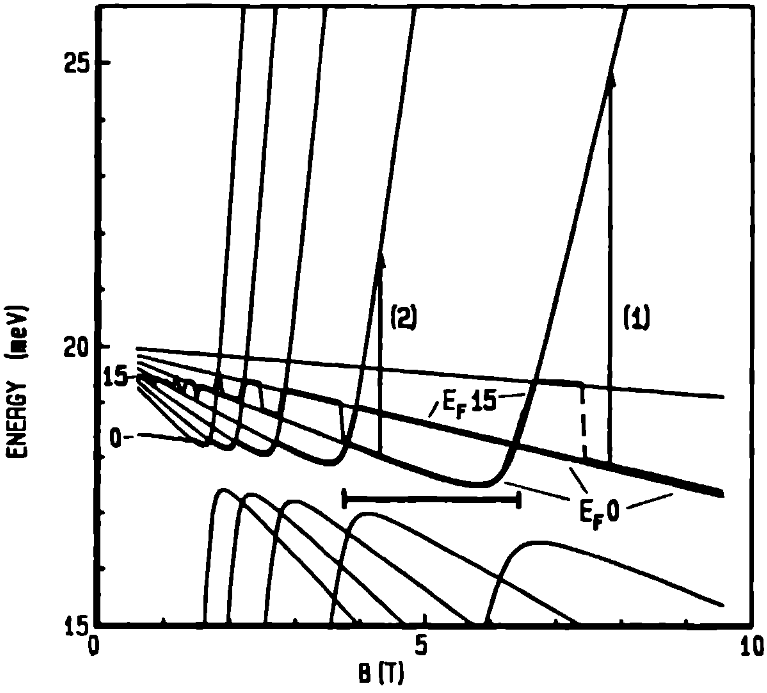

Fig.17. Positions of the Fermi level E_F as a function of magnetic field for intrinsic (E_F0), and for an extrinsic charge density (E_F15) in the InAs layer equal to $15 \times 10^{16} cm^{-3}$. A small intersubband coupling is included in this calculation for p=1.8 kBar. The horizontal bar indicates the range in B over which the transition having Landau index N=2 can be followed. Details are given in the text.

region from interband-like to intraband-like with magnetic field. This picture suggest that interband transitions for low N are not very strongly affected by a high additional n-doping as the Fermi level stays roughly at the same place. In fig.18, allowed transitions have been plotted for a highly doped SL. A calculation for an intrinsic sample shows more or less the same results, and complies well with the experiment.

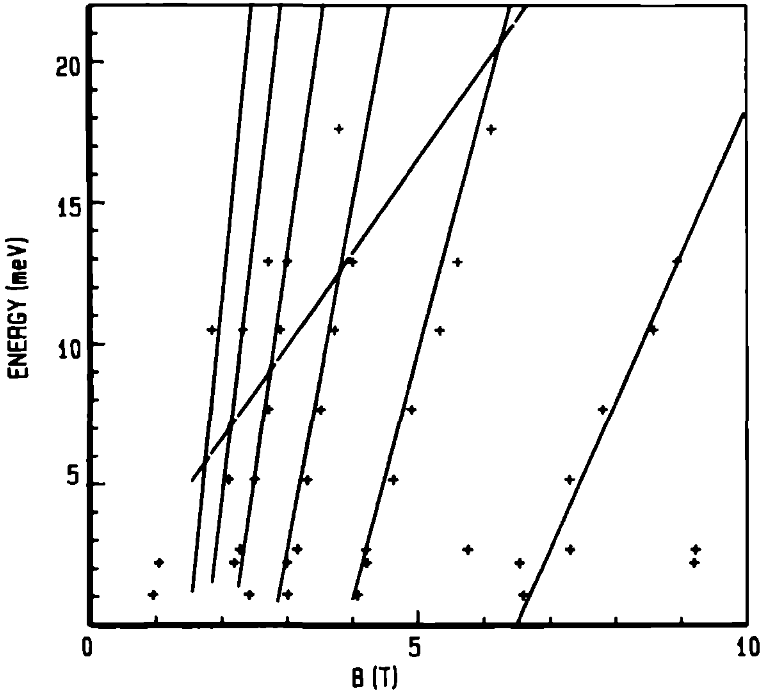

Fig.18. Calculated transitions together with experimental points for p=1.8 kBar, and an extrinsic InAs charge density of $10^{17}cm^{-3}$. No intersubband coupling has been included.

ii) Low pressures with coupling

In fig.19 the same calculations have been made in the presence of an intersubband coupling thought to be realistic according to the literature. Comments are the same as for fig.17, and allowed transitions are plotted against field in fig.20. The results as plotted in fig.20 are also only slightly doping dependent. The large forbidden region and the absence of transitions at medium to high energies is very clear and can be qualitatively understood from fig.19. In this plot the horizontal bar as discussed above has considerably shortened with respect to the situation in fig.18 (no coupling). This shortening is due to a strong anticrossing behaviour and limits the possible transitions from this level. It is interesting to compare directly fig.20 with

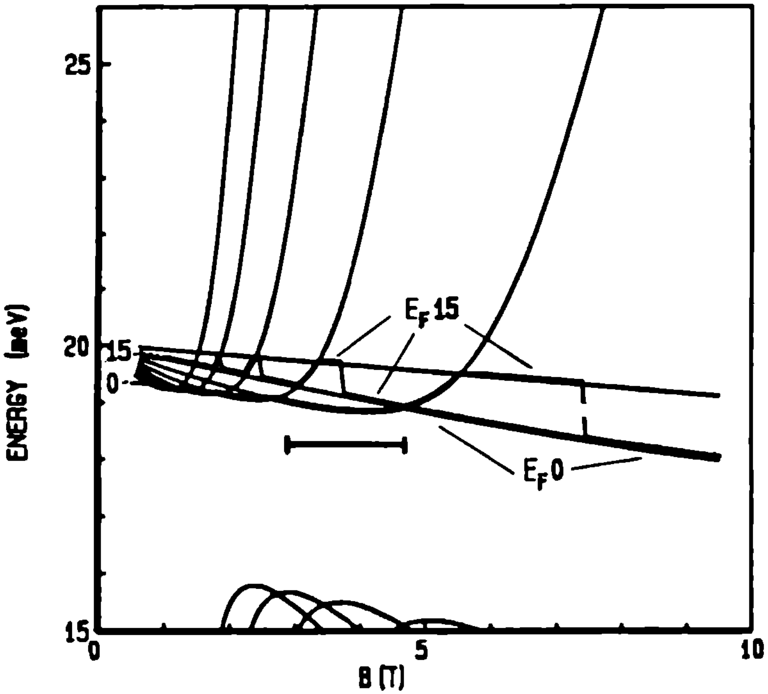

Fig.19. Positions of the Fermi levels just as in fig.17 but for a realistic value of the intersubband coupling as according to the literature.

fig.16, as the difference between them is solely caused by taking into account the position of the Fermi level. The situation as presented in figs.19 and 20, present a strong qualitative evidence *against* the presence of intersubband coupling.

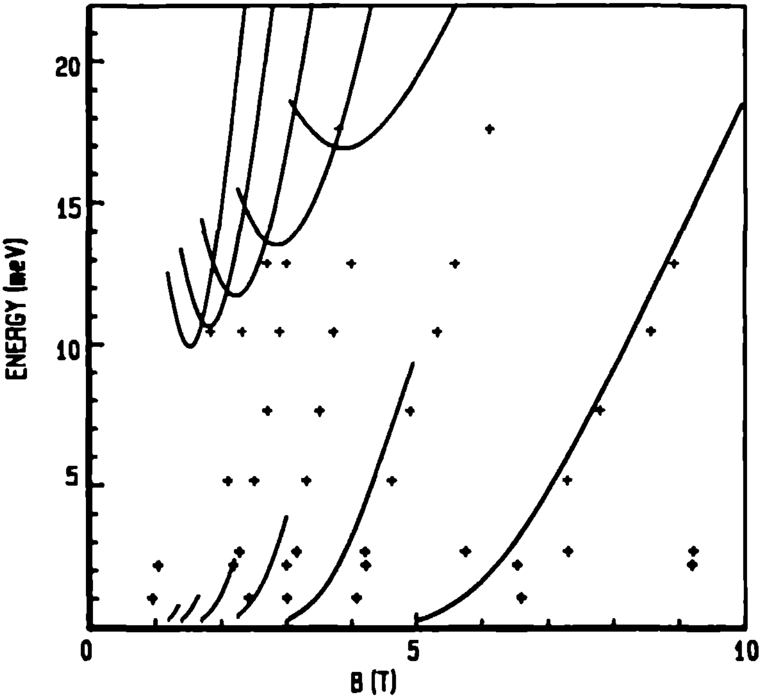

Fig.20. Calculated transitions for the situation as presented in fig.19. the extrinsic charge density of the InAs amounts to 10^{17}cm^{-3}.

iii) High pressures

With increasing pressure the subbands grow closer together, which means according to eq.18 a reduction of the amount of transferred charge from H_1 to E_1. Therefore any residual n-doping will become relatively more important with pressure as there will be less high density hole states left to accommodate the extrinsic electrons. In this way pressure will tend to decrease the Fermi level pinning to the hole band. In fig.21 this effect is shown for a pressure of 9 kBar. Fig.21 should be compared with fig.17 and it is immediately obvious that for a residual doping of for instance $n=10^{17}$ cm^{-3} (which is not unlikely), the low-field high-energy transitions will turn cyclotron-like (intraband) in nature. This is illustrated by the arrows marking interband transitions; (a) remains interband-like up to high extrinsic charge densities, whereas (b) disappears already at medium additional electron densities and turns up higher in this plot as a cyclotron resonance. This explains

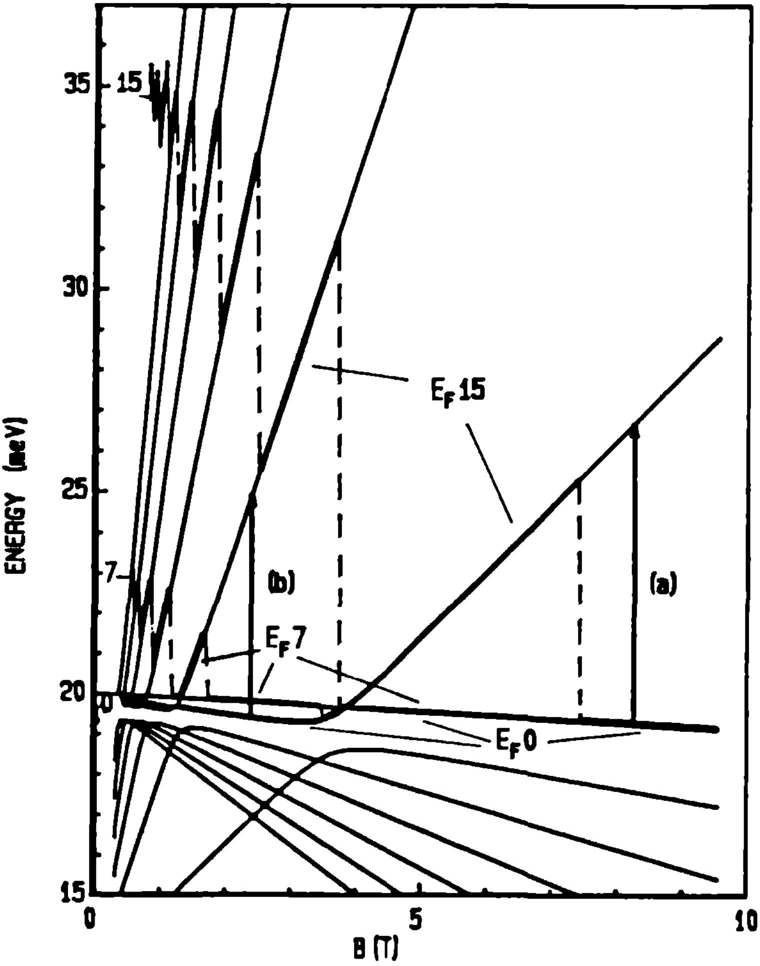

Fig.21. Positions of the Fermi level as a function of extrinsic charges for a pressure equal to 9 kBar. Further comments are as for fig.17. Arrows (a) and (b) indicate interband transitions sensitive to extrinsic effects as discussed in the text.

the change-over of the resonance line-shape and slope from inter- to intraband as discussed before, and as is visible in fig.8 at higher pressures. Therefore, all experimental results at very high pressures are more sensitive to extrinsic doping effects and as such less suited for a determination of the subband separation E_1-H_1. To show explicitly the mixing of different types

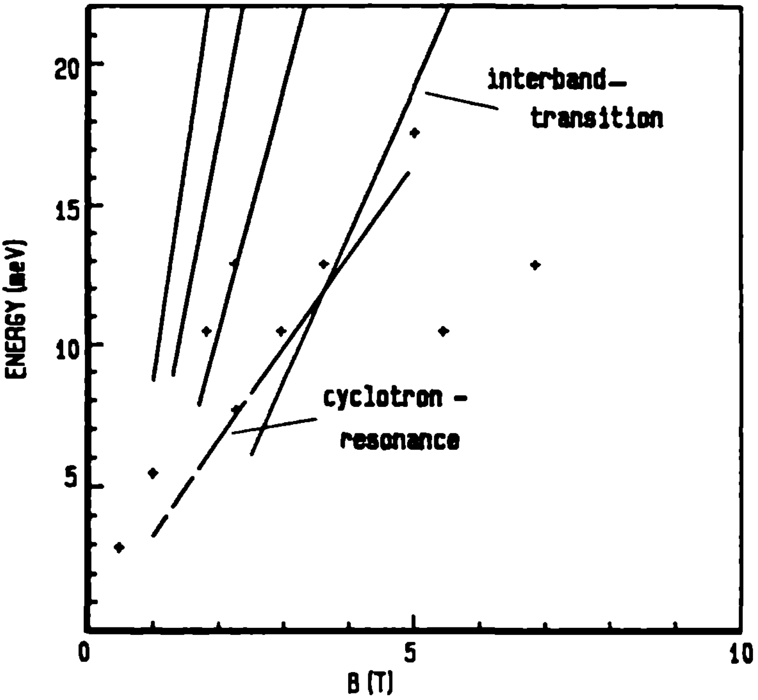

Fig.22. Calculated transitions for the situation of fig.21, but without intersubband coupling and an extrinsic charge density equal to 10^{17}cm^{-3}.

of resonances, we have plotted in fig.22 the strongest observed transitions at p=9 kBar together with a theoretical fit assuming no intersubband coupling, and an external charge density $n=10^{17}$ cm^{-3}. This figure illustrates the difficulty at these pressures to distinguish between cyclotron resonance and interband transitions.

A comparison of figs.17, 19, and 21 reveals that the "active energy region" which determines the nature of the transitions is situated between the (anti)-crossing and H_1. As can be seen in fig.21 this region gets very narrow at high pressures, even in the absence of hybridisation gaps. Therefore it is suggested that at high pressures a strong intersubband coupling will not change drastically the allowed transitions, a situation that can easily be verified in a calculation. This is a tendency just contrary of what was assumed in previous work[20,32] (see chapter 2), in which it was argued that at high pressures the intersubband coupling would increase due to the subbands growing closer together.

iv) Conclusion

The analysis given above shows that for low pressures extrinsic doping effects do not have a large influence on the optical properties of the SL as far as our experiment is concerned. However, at high pressures these extrinsic effects become relatively more important, and the best agreement with the experiments is obtained by assuming an n-doping of 10^{17} electrons per cm^3 in the InAs layers.

V. DISCUSSION

A. Results and validity

The essential results of the experiment, i.e. the pressure dependence of the band offset Δ and of the subband separation E_1-H_1 are presented in fig.12. The main topic to be discussed now is the validity of these results. Fig.12 has been obtained using rather straightforward methods, that are from theoretical point of view strongly oversimplified. However, the experiment can be very well described by them as is shown in figs.10 and 11. It has been shown that introducing an intersubband coupling by a two-band model leads to results that become increasingly worse with increasing interaction between the subbands, especially if the position of the Fermi level is taken into account. Therefore no coupling has been included in the final analysis as presented in fig.12. An analysis as correct as presently possible using Landau levels calculated with a full six-band model in the envelope wave function approximation[12,19,32] (see chapter 2) show a result deviating only little from fig.12, however having overall a slightly worse agreement with the experiment over the whole pressure range than as presented in figs.10 and 11.

It must be stressed that although totally unjustified on theoretical grounds, the zero pressure experimental data on the same sample[4] can be perfectly explained by the non-interacting model of eq.15, whereas the full six-band calculations as presented in ref.19 show less agreement but can be extremely accurately reproduced by the two-band model as discussed in this chapter. Therefore as far as the scope of this thesis is concerned fig.12 suffices, and the outcome is a dependence on pressure of the overlap Δ given by

$$\frac{d\Delta}{dp} = -(4.5 \pm 1.0) \text{ meV kBar}^{-1} \qquad (24)$$

As discussed throughout this text, the exact value for the rate of change of Δ with pressure is dependent on the way of analysing the experimental results. The error displayed in eq.24 is therefore chosen as such to incorporate the upper and lower limits in the rate of change of Δ with pressure as determined by the different methods discussed above. Moreover, one has to realise that even at zero pressure there is a certain (pressure independent) uncertainty in the exact value of Δ.

As mentioned before, for the highest pressures the obtained results are less accurate, but still according to fig.12 the electron and hole subbands do not cross at the highest attainable pressures, and as such no semimetal-semiconductor transition is induced.

B. zone-boundary transitions

Until now only transitions having $k_z=0$ (i.e. zone-centered transitions having no wave vector component perpendicular to the layers) have been discussed. However due to a finite subband width, the dispersion relation in the $\hat{z}$-direction also favours transitions at the zone-boundary, i.e. at $k_z=\pi/d$. In the simple non-interacting picture transitions at the zone-boundary should be similar interband transitions as given by eqs.4 and 15, only with E_1 increased by the subband width ΔE. This can be understood if we assume the hole band H_1 to have an infinitely small width, then the effective electron subband energy at $k_{\parallel}=0$ and $k_z=\pi/d$ will be $E_1+\Delta E$. Therefore transitions are similar however with effectively a smaller subband separation (decreased by ΔE). At zero pressure a transition has been observed[4] and identified as a N=0 interband transition coming from the subbandedge, from which a subband width $\Delta E=23$ meV has been derived, a value compatible with theoretical[12] predictions. Higher order transitions from the zone-boundary are however not reported in the literature.

In our experiment the only weak evidence of the presence of zone-boundary transitions has been seen at a pressure of 3.9 kBar and is suggested by the dotted line in fig.10b, which could be a N=0 transition assuming a subband width of roughly 14 meV. This width is considerably less than reported[4] at zero pressure, and it can be argued that with pressure the subband width decreases because the electron-like band E_1 near the zone-boundary could be pushed down by the approaching hole-like band H_1 due to some intersubband coupling which leads to an anticrossing behaviour. However, Altarelli[12] has shown that due to symmetry reasons bandcrossings are allowed at $k_z\neq0$, which suggests the subband width ΔE not to depend too much on pressure. Therefore in view of the very weak experimental evidence for zone-boundary transitions at non-zero pressure, no credit can be given to the observed decrease of the subband width. Moreover, it can be argued that zone-boundary transitions become less strong at higher pressures due to the position of the Fermi level which favours more interband transitions at zero wave vector k_z.

C. Low energy high field anomalous transmission results

As shown in fig.9, there is a very strong transition at high magnetic fields and low excitation energies which has not been discussed yet. This transition manifests itself in a very deep resonance line, at some pressures accompanied by usually two weak satellite resonances. This resonance extrapolates to zero energy at zero magnetic field and as such resembles a cyclotron resonance with an effective mass very close to the free electron mass. Further experimental facts are that at the lowest excitation energy (1.01 meV) no such resonance was observed. Furthermore a strong temperature dependence was observed making the resonance only visible at temperatures below 2 Kelvin at pressures above 4 kBar. It was verified that both at zero pressure and at the highest attainable pressure (11.2 kBar), no significant resonance was seen at any temperature. Finally, the position of the resonance seemed to be almost pressure independent.

This phenomenon was thought to originate in a heavy hole cyclotron-like transition at the zone-boundary $k_z=\pi/d$. However, neither the two-band model nor the six-band model were able to produce a similar transition, even not if pressure effects were correctly incorporated in the latter model[38].

Recently, it has come to our attention that Rikken[39] has observed almost similar anomalous transmission minima in a far-infrared magneto-optical experiment on the two-dimensional electron gas in a GaAs-$Al_xGa_{1-x}As$ heterojunction. These minima were only seen if sample and detector were cooled down very rapidly. Considering the similarities in both experiments, it is now argued that the observed resonances are caused by a strained Allen and Bradley carbon resistor which was used in both experiments as a detector. The strain could have been induced by either rapid cooling or by pressure. Investigations on the (now suspected) reliability of these detectors under similar conditions are currently planned.

References

1. H. Kroemer, Surf.Sci. 132, 543 (1983).
2. H. Kroemer, J.Vac.Sci.Technol. B2, 433 (1984).
3. L. Esaki, IEEE J.Quantum Electron. QE-22, 1611 (1986).
4. J.C. Maan, "Infrared and Millimeter Waves", ed. by K.J. Button Ac.Press, N.Y, 8 387 (1982).
5. J.C. Maan, Superlattices and Microstructures, 2, 557 (1986).
6. G. Belle, J.C. Maan, and G. Weimann, Solid State Commun. 56, 65 (1985).
7. T. Duffield, R. Bhat, M. Koza, F. de Rosa, D.M. Hwang, P. Grabbe, and S.J. Allan, Phys.Rev.Lett. 56, 2724 (1986).
8. G.A. Sai-Halasz, L.L. Chang, J.-M. Welter, C.-A. Chang, and L. Esaki, Solid State Commun. 27, 935 (1978).
9. G.A. Sai-Halasz, R. Tsu, and L. Esaki, Appl.Phys.Lett. 30, 651 (1977).
10. E.O. Kane, J.Phys.Chem.Solids 1, 249 (1957).
11. G. Bastard, Phys.Rev. B 24, 5693 (1981).
12. M. Altarelli, Phys.Rev. B 28, 842 (1983).
13. G.A. Sai-Halasz, L. Esaki, and W.A. Harrison, Phys.Rev. B 18, 2812 (1978).
14. G. Bastard, Phys.Rev. B 25, 7584 (1982).
15. M. Altarelli, in *Heterojunctions and semiconductor superlattices*, proc. of the winterschool Les Houches, march 12-21 ,1985, Ed. by G.Allan, G. Bastard, N. Boccara, M. Lannoo, and M. Voos, p12.
16. L.L. Chang, ref.15 p.152.
17. H. Sakaki, L.L. Chang, G.A. Sai-Halasz, C.-A. Chang, and L. Esaki, Solid State Commun. 26, 589 (1978).
18. L.L. Chang, and L. Esaki, Surface Sci. 98, 70 (1980).
19. A. Fasolino, and M. Altarelli, Surface Sci. 142, 322 (1984).
20. L.M. Claessen, J.C. Maan, M. Altarelli, and P. Wyder. Superlattices and Microstructures, 2, 551 (1986).
21. C.R. Pidgeon, in *Optical Properties of Solids* ed. M. Balkanski, Handbook on Semiconductors Vol.2, (North Holland, Amsterdam, 1980) p.223.
22. J.A. Brum, P. Voisin, and G. Bastard, Phys.Rev. B 33, 1063 (1986).
23. J.Bleuse, P. Voisin, M. Voos, L.L. Chang, and L. Esaki, "Proceedings of the Third International Conference on Modulated Semiconductor Structures", Montpellier 1987, to be published.
24. G. Martinez, ref.21 Vol.2, p181.
25. G. Martinez, private communication.
26. J.C. Portal, private communication.

27. J.C. Maan, Thesis university of Nijmegen, 1979, unpublished.
28. E.O. Kane, in *Semiconductors and Semimetals*, ed. by R.K. Willardson, and A.C. Beer, Vol.1 (Ac. Press New York 1966), p.75.
29. H.J.A. Bluyssen, J.C. Maan, P. Wyder, L.L. Chang, and L. Esaki, Phys.Rev. B **25**, 5364 (1982).
30. M. Zawadski, J.Phys.C. **16**, 229 (1983).
31. Y. Guldner, J.P. Vieren, P. Voisin, M. Voos, J.C. Maan, L.L. Chang, and L. Esaki. Solid State Commun. **41**, 755 (1982).
32. J.C. Maan, in *Optical Properties of Narrow-gap Low-dimensional Structures*, ed. by C.M. Sotomayor Torres, J.C. Portal, J.C. Maan, and R. Stradling, (Plenum Press New York 1986), p.325.
33. L.M. Roth, ref 21 Vol.1, p474.
34. K.H. Seeger: Semiconductor Physics, ed. by M Cardona, P. Fulde, H.-J. Queisser, (Springer Verlag New York 1982), p.358.
35. Landolt-Bornstein: Numerical Data and Functional Relationships in Science and Technology, ed. by D. Bimberg (Springer Verlag New York 1982) vol.17.
36. M. Altarelli, J.of Luminescence, **30**, 472 (1985).
37. L.L. Chang, N. Kawai, G.A. Sai-Halasz, R. Ludeke, and L. Esaki, Appl.Phys.Lett. **35**, 939 (1979).
38. A. Fasolino, private communication.
39. G.L.J.A. Rikken, private communication.

CHAPTER 4

Theoretical and experimental band line-ups in semiconductors

I. INTRODUCTION TO BAND LINE-UPS

The *Leitmotiv* of part IV of this thesis is the pressure dependence of the band offset in an InAs-GaSb SL. In this chapter therefore, we would like to discuss more fully the general concept of band line-ups in semiconductors. Afterwards the obtained experimental results will be compared with predictions on the pressure dependences based on several theories.

The band discontinuity or rather band line-up problem appears generally at every interface between to different media. In the literature the two most important ones are;

i) at the metal-semiconductor interface,

ii) at the interface between two semiconductors.

At the first kind of interfaces, normally a Schottky barrier[1] is formed. These interfaces will not be discussed in this chapter. The second kind forms the group of heterojunctions which will be treated here. Per definition the band offset can be seen as the way in which the energy positions of two equivalent bands in two adjacent semiconductors in contact exhibit a discontinuity at the interface. The solution to this problem is given by the experimental determination of either ΔE_c or ΔE_v, i.e. the differences in energy of respectively the conduction bands E_c, or the valence bands E_v at the interface.

However, the influence of an interface between two semiconductors A and B is more than just the energy jump at the interface (i.e. the discontinuity), therefore a better definition is given by the band line-up with which we can name the whole region around the interface between A and B in which, due to this interface, the material properties deviate from the pure bulk A and B properties. According to this definition, the band line-up at the hetero-interface must be divided in two parts:

i) The short-range band discontinuity (or the band offset). This discontinuity consists of an abrupt change in energy of the bands at the interface over a distance a fraction of the lattice constant, which is caused by a difference in the periodical lattice potentials in the two materials.

ii) The long-range band bending, which is due to an electrostatic potential built up by a redistribution of charge carriers across the interface. This is a macroscopic effect over a range of order of the screening length of the conduction electrons ($\simeq$ 100 nm).

The short-range band discontinuity as mentioned under i) presents the main topic of this chapter. Without referring to any theory, its origin can be understood by considering a very simple model of a solid in which the periodic lattice potential is established by a linear combination of overlapping[2,3] atomic-like potentials of the individual atoms. Very close to the atom this potential will resemble the free-atom potential, but at the interstitial places it will be considerably different. From the periodic potential, the bandstructure can be calculated. As such, the positions of all the bands are known relative to the atomic-like potentials. Deeply lying valence bands are in this picture coming from the potential close to the atom, and reflect the energy of strongly bound electrons in the inner atomic shells. The upper valence band (VB), and the conduction band (CB) are coming from places further away of the atom, reflecting weakly bound valence electrons in the outer shells.

At the interface atomic-like potentials from the different atomic species overlap. From this overlap the periodic potential across the interface can be calculated. The band line-up is now correctly described, and can in principle be calculated. The only considerable problem resides in the calculational[3] method to be followed. This situation is visualised in fig.1. In this figure the

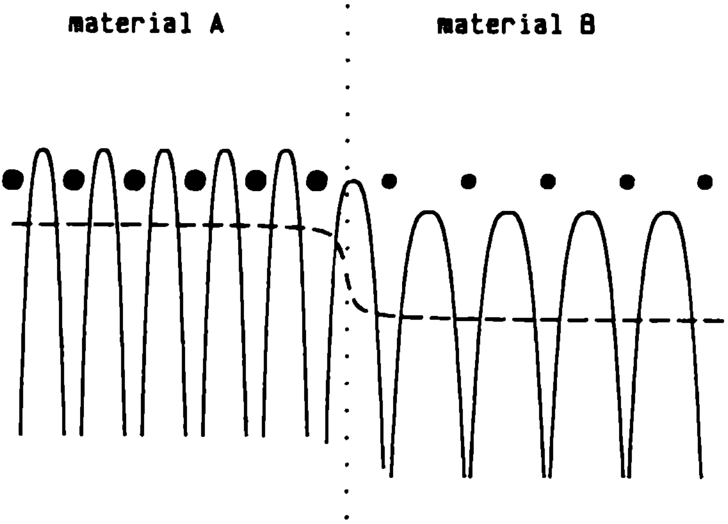

Fig.1. A qualitative representation of the periodic lattice potential derived from free atomic-like potentials, and the position of an energy band, calculated relative to this potential (dashed line), at the interface between A and B. The dots present the positions of the atoms.

atomic positions are presented by the dots, and the atomic-like periodic potential is plotted relative to the atomic sites. The dashed line presents the energy of a deep lying valence band, calculated relative to the periodic potential. The formation of the "discontinuity" across the interface is obvious. Due to the drop in energy of this band, going from A to B, electrons are drawn from A towards B, until the electric field established by this charge redistribution, can compensate for the potential difference formed by the band discontinuity. Due to a very high density of states of the strongly bound electrons, all the charges needed to establish this compensating potential can be concentrated very close to the interface, by deplacing all individual electrons in the inner shells only a very small amount. Therefore the "discontinuity" as depicted in fig.1, can be compensated in a distance small compared to the lattice constants. Another way to see this is that the strongly bound inner valence electrons feel more or less only the host atom, and therefore dislocations, deep impurities, or interface effects are only felt if they are very near, which means that there is a very effective screening.

As the relative positions of all the energy bands are uniquely related to the deep valence bands, the band discontinuities of all bands at the interface are now determined by the discontinuity as presented in fig.1.

The situation as sketched above leads to an interface as depicted in fig.2. In this figure the several effects which establish the total band line-up are displayed according to a rough calculation for an InAs-GaSb interface, and can be regarded as being qualitatively correct. In fig.2a, the band discontinuity Δ at the interface between slightly p-doped GaSb and n-doped InAs is shown. These dopings are the normally present residual dopings in these two materials. If there were no charge redistribution this would be the total band line-up, resulting from the situation presented in fig.1. The line-up has a step in the Fermi level, which is in the case of electrodynamical equilibrium however not allowed. Therefore charge carriers will be transferred from the filled GaSb valence band to the partly occupied InAs conduction band, in order to re-establish an equilibrium situation at the Fermi level. Qualitatively what happens can be understood[1] by realising that due to the charge transfer a depletion region is formed by the positive impurities in the GaSb, and the negative ones in the InAs. This gives rise to a compensating electric field as indicated in fig.2b. The electric field in the depletion region established by the charge redistribution gives rise to a built in potential V_B which can be calculated from the Poisson equation in letting a positive charge move from far away in the GaSb across the interface to far in the InAs, and assuming some spatial charge distribution. V_B has to be added to the energy bands (i.e. the GaSb VB and the InAs CB from fig.2a) in order to obtain the real band line-up as presented in fig.2c. It must be realised that the sign of V_B must be inverted prior to the addition because the band diagrams in fig.2 are plotted for a negative electron charge. This situation in

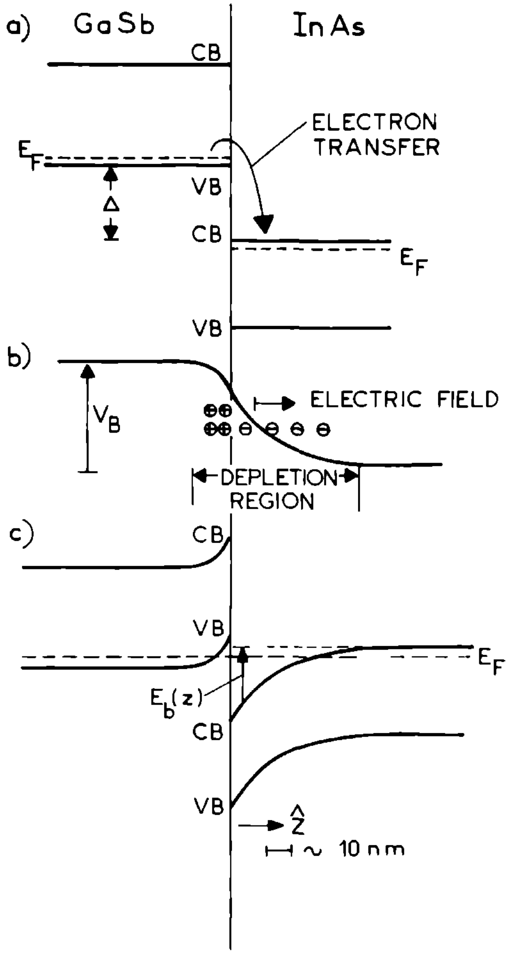

Fig.2. Schematic view of the different aspects that lead to the total band offset at the interface of an InAs-GaSb heterojunction. a) The discontinuity in the absence of charge transfer. b) The static potential built up by the transfer of charge across the interface. c). The total line-up including band bending as resulting from the effects of figs. a and b.

which charge transfer establishes a compensating potential is principally the same as discussed in sec.I for the case of strongly bound electrons screening out the band discontinuity (see fig.1). The only difference is that, due to a low density of states of the charge carriers, more space is needed to accumulate enough charges in order to establish (see fig.2b) an adequate compensating potential V_B. In other words, the screening is effectively much weaker for these electrons, and therefore the interface effects have a macroscopic range.

A slightly more sophisticated but still approximate way to obtain the real band bending at this heterojunction as presented in fig.2c is given in references 4 and 5. Here the band bending potential $E_b(z)$ (see fig.2c.) is calculated according to the Poisson equation, in which the charge $\rho(z)$ is given as a function of the distance z from the interface. $\rho(z)$ is further determined by the three-dimensional density of states in the InAs CB, filled from the bandedge to $E_b(z)$ with electrons. This condition suffices to find an expression for the potential $E_b(z)$. However, as the semi-triangular well below E_F as depicted in fig.2c gives rise to the formation of discrete subbands, the actual calculation is more complicated, and the interested reader is referred to the cited literature as this falls beyond the scope of this chapter.

II. DEFINITION OF THE PROBLEM

Now we would like to discuss more fully the band discontinuity at the interface as depicted in fig.2a. There exists a wide body[2,3,6-28] of experimental and theoretical work and discussions about validities of several natures of band line-ups. The aim of this section is not to be complete, nor to ferret out one theory or experimental method as being the most valid. Rather a concise description of what goes on among the most known approaches to the problem will be presented. An outstanding resume to which will be referred often is presented by Kroemer (ref.2 and references therein).

Before diving into the several theories or philosophies about band offsets, the general problem of what is actually a band offset has to be defined more precisely. In the literature this band discontinuity is "freely" defined as the jump in e.g the valence band energies at the interface. However, the concept of energy bands in a semiconductor is essentially a bulk feature. In bandstructure calculations, a zero energy is arbitrary defined as a reference, often the highest valence bandedge at the Γ-point. All energies in *one* bulk can be described relative to this energy level. However, the assessment of some absolute value to any energy level in a bulk calls explicitly a reference level outside this bulk, in fact at infinity. This presents a structural problem as now a surface (i.e. a bulk boundary) is needed which was assumed to be not there in the calculations leading to the bandstructure. A famous example being the metal workfunction or the electron affinity in a semiconductor (which will be discussed shortly, in the context of a band line-up theory based on vacuum energy levels). The electron affinity (EA) relates bandedges to a zero energy at which an electron at infinite distance from the bulk resides. The EA is defined experimentally as the energy needed to remove an electron from a specific bandedge to a site at infinity, which is per definition at zero energy. Both theoretical and experimental ways of transferring the electron to this reference site are not uniquely defined, but in attaining this site at infinity, the electron must leave the bulk by crossing a surface. At this surface the band energies cannot be defined in the same way as in the bulk, and by pulling the electron out, image charges and charge redistribution will affect the energy needed to remove this electron. This makes the assessment of an absolute energy to a band at an interface a less trivial work than often realised. Moreover, the bandgaps as depicted in figs.2a and 2c at the interface do not exist in the same way as in the bulk. In the bulk the bandgap originates in the periodicity of the atomic potentials establishing the bandstructure for an infinite solid. The wave functions stretching to infinity are totally imaginary in the gap, hence this is a forbidden energy region. At e.g. a semiconductor-vacuum interface, the continuity of the wavefunctions is violated and consequently they become partially real leading to the formation of surface states in the gap. This situation as explained heuristically above leads to a strong band bending and subband forming at the interface. In fact the band bending reflects the additional energy the electron has to acquire in order to reach the interface. In doing so, it passes through an area having a different potential with respect to the bulk due to a charge redistribution, as depicted in fig.2b.

Once agreed upon the energy relation between bulk bands and the bands near the interface, we can extend our definition in a similar way to a heterointerface. Supposing a heterojunction formed by A and B, we can now see the band energies in each material near the interface as the energy the electron has to gain or loose to reach the interface, by coming either from deep in A to this interface or from deep in B. The effective band discontinuity i.e. the energy jump at the A/B interface must now be seen as the energy needed to move in experiment an electron in the band at the interface an "infinitely" small distance across this interface, hereby transporting it from A to B or vice versa. The experimental energy needed for this process determines the band offset at the interface and thereby the total line-up.

It will be clear now that to obtain the band offsets at an interface, it is surely not obvious to take just the electron affinity or a related energy of the two materials involved and take the difference in those energies as the band offset. Having pointed out that defining and determining a band offset presents a tedious task, we would like to discuss in the following some existing theories concerning this problem.

III. SOME THEORIES

Conceptually the band offset problem[26] can be divided in two parts as already mentioned in chapter 2:

i) Which energy level must be lined-up at the interface in order to obtain the band offsets.

ii) Where does such a possible level lay with respect to the bandedges in the bulk materials.

Or formulated in a slightly different way[2] as;

a) the problem of the line-up of the energy bands in a semiconductor relative to the periodic potential in the same semiconductor and

b) the problem of the alignment of the two periodic potentials relative to eachother.

a) is a bulk problem, therefore the real band offset is formulated in b). As presented in a) and b), the band offset problem is formulated in a very correct way, and has in this form already been discussed in sec.I (see fig.1). However, the formidable calculational task to be performed, and the way how charge redistributions at the interface have to be taken into account, makes the practical use of this formalism very doubtful.

In general, band line-up theories can be divided in two classes which will be discussed in sections A and B.

A. Absolute theories

The "absolute" theories, often called "linear" theories, assume that there is a specific absolute energy associated with the bandedges of a semiconductor. Therefore line-ups should simply be formed by the differences in these absolute energies. This family of theories takes point i) of the last section for granted as the only remaining task is to calculate or measure a specific absolute bulk energy independent on interfaces surface effects, impurities etc. The second group (to be discussed in section B) takes into account the interface effects and/or impurity effects which means that principally the line-up is not solely determined by intrinsic bulk parameters.

Without discussing the origin of absolute theories it is still obvious that they should display transitivity. This means that given the band offsets of two semiconductor pairs A/B and B/C the line-up of the third possible pair A/C should follow from the simple addition property[2]

$$\Delta\epsilon_b(A/B)+\Delta\epsilon_b(B/C)+\Delta\epsilon_b(C/A)\equiv 0 \qquad (1)$$

with ϵ_b the energy of e.g. the valence bandedge. Transitivity seems to hold for some triplets[2]for instance Ge, GaAs, and ZnSe. For this triplet there exist experimental band line-up data which yield when substituted in eq.1 a non-zero term of only 30 meV. However, the material choice made here is both experimentally as well as theoretically very poor. Experimentally there exists namely a very large variety in the band offsets in e.g. Ge on GaAs, which makes every value suspect. Theoretically these materials are not well chosen due to either the growth of monatomic materials on a compound semiconductor[2], or the growth of two highly lattice mismatched materials on top of eachother. The first situation will lead to possible charge transfer along the different bonds, whereas the latter will cause strain and/or dislocations. These two effects will cause the material properties to deviate strongly from bulk properties at the interface, which makes the line-up far from ideal to use as an example for absolute theories. Still, transitivity remains an important feature to be verified experimentally, as its experimental existence could rule out classes of theories on grounds of simple experimental facts.

Most of the absolute theories yield socalled natural line-ups. These are line-ups that directly correlate the band offset to the valence bands or the conduction bands[7]. The two most widely acknowledged and relatively reliable methods to yield natural line-ups are the Harrison[2,7,8,10] atomic orbital (HAO) method, historically preceded by the electron affinity[2,18,26] rule (EAR).

i) The electron affinity rule

The EAR asserts that the conduction band offsets are equal to the difference in electron affinities (EA) of the two semiconductors involved. With EA the energy is meant needed to free an electron at the Fermi level near the surface from the bulk material. This definition stems from metal physics in which this energy is called the work function, which can be rather accurately measured[26] using photo-electric threshold techniques, or the Kelvin contact-potential capacitor method. The work function or EA establishes a sort of vacuum level at which the electron taken from the material resides an infinite distance away from the surface. Therefore it is intuitively appealing to put equal the vacuum energies of the two semiconductors as being the band offset determining level. The drawbacks of this method have been thoroughly discussed in the preceding sections.

Experimentally, the EAR suffers the great disadvantage that electron affinities are of the order of 5 to 10 eV, which calls upon very accurate measuring techniques to yield results to better than a few hundred meV. For example all kind of image forces as exerted by an applied electric field (Schottky effect, see ref.1) lowers the potential barrier and affect seriously the obtained results. Furthermore all kind of surface effects such as freed electrons residing on the surface influence the experimental EA. For semiconductors a bycoming problem is still the exact determination of the point from which the EA has to be counted as this is obviously not the chemical potential, but for e.g. n-type material more near the CB bandedge. An excellent review on the EAR is given in ref.26, in which it is also mentioned that due to surface states semiconductors can exhibit strong band bending which makes the experimental EA indeed strongly surface dependent. Moreover, the EAR is based[18] on electron affinities characteristic for semiconductor-vacuum interfaces, which exhibit an extremely large material discontinuity, and therefore a fundamentally different situation than at a semiconductor-semiconductor interface, at which only relatively small changes are present. Therefore obtained EA results for two vacuum interfaces cannot be trivially extended to heterointerfaces.

However, once agreed upon the theoretical validity of the EAR, the only remaining task is to obtain experimental values for the EA. In spite of all the arguments against the EAR, it works surprisingly well, yielding[26] for InAs-GaSb a band overlap Δ of 140 meV, which is correct within experimental error, and which ranks among the best theoretical predictions for Δ.

ii) The Harrisons atomic orbital theory

As already mentioned another very convenient absolute theory is the Harrison atomic orbital (HAO) method[2,7,8,10], based on establishing absolute energies for the valence bandedges in bulk materials and taking the differences in the thus obtained E_v as the valence band offsets. Therefore this is a natural line-up method. Although this method suffers similar drawbacks as other absolute theories as discussed in the previous sections its amazing capability to predict band offsets[10] justifies its recognition as being one of the most reliable theories. Actually however, no one understands completely why it works so well in spite of its simplicity.

The HAO is based on an elementary LCAO theory of bandstructure calculations (linear combination of atomic orbitals). In this approach, which is a tight binding model, the one-electron states as a function of wave number (i.e. the energy bands in the solid) are approximated by a linear combination of local atom-like states. Dependent on the approach, real atomic wave functions or modified functions are used. For a thorough review on LCAO we refer to ref.6.

It can be shown that for many solids rather accurate tight binding bandstructure calculations can be made by only including the s- and the p-like atomic states and their mutual interaction, and to use the free-atom values for their energies. However this simple "s-p" approach, although yielding very good HAO results, has been criticised recently[19,20]. For some specific hetero line-ups much better results seem to be attainable by including the d-orbitals of the cations of the compound in the HAO.

The free-atom energies of the s- and p-states, respectively $-\epsilon_s$ and $-\epsilon_p$, denote more or less the energy required to remove[6] the electron from the free atom and as such are atomic equivalents of the electron affinity. As comprehensively discussed in ref.6, bonding and antibonding levels of s- and p- orbitals form respectively conduction and valence bands in the solid. Heuristically this can be understood as follows: In free atoms the s-states have a lower energy than the p-states. However, p-states have orbitals reaching further away from the atom, which means that due to nearest-neighbour overlap between two p-states in a crystal, the bonding state drops considerably in energy. Therefore the band having p-symmetry (valence band) is lower in energy than the conduction band which has s-symmetry. Generally, the more or less absolute VB bandedge energy of a tetrahedral binary semiconductor[6,7,10] is in this context given by a suitable combination of the p-state free-atom energy values ϵ_p^c and ϵ_p^a for respectively the cation and the anion according to

$$E_v = \frac{\epsilon_p^c + \epsilon_p^a}{2} - \left[\left(\frac{\epsilon_p^c - \epsilon_p^a}{2} \right)^2 + V^2 \right]^{1/2} \tag{2}$$

The term V^2 presents the discussed overlap of the p-orbitals and is given by[7]

$$V = \eta_{ll'm} \frac{\hbar^2}{md^2} \tag{3}$$

with l, l,′ and m the usual quantum numbers of angular momentum of the two involved orbitals and d the internuclear distance.

Eq.2 presents a remarkably simple way to obtain an absolute value for E_v. Conceptually, it is just an average of the two free atom p-state energies minus a correction term consisting of an overlap matrix element, and a correction due to the difference in p-energies of the two atoms of which the semiconductor is constituted. η (eq.3) can be exactly calculated for atomic wave functions, but to obtain reasonable band parameters from the HAO slightly different[7,10] values for η seem to be better.

The power and validity of the HAO method stands with finding accurate values for the p-state energies to substitute in eq.2 and with finding a suitable value for η. As can be seen in the cited references, there is a rather large spread in available data for the energies ϵ_p and for η. At present it seems that the Herman-Skillman values for the neutral atom energies ϵ_p as given by Kraut[10], in combination with $\eta=2.16$ yield the best results as far as HAO band line-ups are concerned. For the InAs-GaSb heterointerface the bandoverlap Δ is in such a way determined as $\Delta=92$ meV, which is not far of the experimentally accepted value of 150 ± 50 meV. Although taking ϵ_p values from other sources will shift E_v considerably, the effect on the band line-up stays within several tens of meV the same, provided[10] the same source is used for all atomic species involved.

iii) The common anion rule

Partly supported by the HAO method is the common[2,22] anion rule which states that if the anion species on both sides of the interface are the same, the valence band offsets should be much smaller than the conduction band offsets. This rule of which the validity has been accepted but is now strongly disputed[19,20,21], stems from the fact[6] that in polar semiconductors the valence band wave functions originate largely from the anion atomic wave functions. This can be already expected by looking at values for ϵ_p which are more negative for the anion species. In eq.2 therefore, anion values for ϵ_p will tend to be more decisive for the value for E_v. However, being much stronger in its statements than the HAO method, there exist several convincing examples against the common anion rule. One of the most recent examples being the HgTe-CdTe interface[22,23,24] of which by optical measurements on a SL of these materials a VB offset of $\simeq$40 meV was deduced, in agreement with the common anion rule. However using very direct measuring techniques[20,21] the VB discontinuity on a single heterointerface of HgTe-CdTe is currently believed to be about 350 meV.

iv) The pseudopotential theory

The last absolute theory to be discussed now is the Frensley-Kroemer[2,3] pseudopotential (FKP) theory. The basic idea of this method is to calculate the bandstructure of the bulk materials relative to some effective interstitial potential V_i. V_i is some kind of an average atomic-like potential at interatomic sites in the lattice. It can be shown on grounds of symmetry that V_i matches closely the idea of an effective zero potential at infinity. Therefore lining up the interstitial potentials to obtain the band offset is a method closely related to the EAR method, the difference being the calculational procedure to obtain the V_i values with respect to the bands.

An extension of the FKP with respect to the EAR is the inclusion of a dipole potential V_d at the interface. Due to different electronegativities of the different atomic species on opposite sides of the interface, a charge transfer along the bonds connecting them occurs which gives rise to a dipole potential V_d. This potential can be more or less[3] exactly calculated for every heterointerface from the geometrical crystal structure at the junction. Note that the charge transfer leading to V_d should not be confused with charge transfer from a full band to an empty one giving rise to band bending, nor is it the same as the charge redistribution discussed in sec.I in the framework of strongly bound charges that are slightly displaced in order to compensate for the potential difference at the interface due to the band discontinuity. The charge transfer along the bonds leading to V_d is caused by differences in electronegativities, and *not* by an existing band discontinuity. Contrary, the potential V_d *causes* in the refined FKP model a jump in the interstitial potentials V_i at the interface.

By its principle of calculation to find the band offset out of the alignment of the interstitial potentials, the FKP method is a linear transitive theory. The introduction of the dipole potential V_d blurs the absolute nature of the FKP because now the effects of an interface are taken into account. However, calculations show V_d to posses full transitivity, a somewhat surprising result that makes the FKP a fully transitive method. Just for terminology, the FKP is not a natural line-up theory as the line-up is not directly correlated to some bandedges.

Although not as consistently successful as the HAO in predicting band offsets, the FKP works very well. The main doubt around the FKP is that for some heterojunctions, among which InAs-GaSb, omission of the dipole potential term V_d and lining up directly the V_i potentials yields better results than including this potential, which according to the theory should be necessary. For InAs-GaSb a band overlap Δ=130 meV is found by lining-up the interstitial potentials as calculated by the FKP directly, whereas including the dipole potential V_d the InAs CB is found 10 meV above the GaSb VB which means a disappearance of the broken-gap line-up and a disagreement with experiment of 160 meV. We like to stress that in the particular case of InAs-GaSb this is relatively far of the mark, however for most heterointerfaces a deviation between theory and experiment of hundred meV is still considered as quite small.

B. Relative theories

i) The charge neutrality level concept

An approach conceptually different from the EAR, HAO, and the FKP methods was proposed by Flores and Tejedor[27], and elaborated by Tersoff[12,13]. Here, the influence of interface dipoles is supposed to have the strongest influence on the exact value of the band offsets.

Due to a discontinuity at an interface, surface states appear in the normally forbidden energy gap, called gap-states. Such a state is a mixture of valence and conduction band states. Whether the gap-state has more a valence- or conduction band character depends on its position relative to those bands (i.e. its spectral distribution of valence- and conduction band wave functions). Therefore a gap-state close to the VB bandedge will be valence-like, and if occupied will correspond only to a slight excess in charge. Leaving this state empty will result in a charge deficit of almost one electron at the interface. Consequently a gap-state close to the CB will cause an excess charge of almost one electron if filled. Generally[12], an occupied gap-state will lead to a net charge at the interface proportional to its conduction band character. At a heterointerface, filling of these gap-states occurs because bulk CB or VB states in one semiconductor fall at the junction energetically in the gap of the adjacent material in which they can tunnel several angstroms and occupy or empty a gap-state. The occupation of the gap-states introduces a strong interface dipole due to the excess or the deficit of charge at the interface. A strong interface potential is therefore built up which tends to rearrange the band line-up in such a way as to minimise the interface dipole. The problem therefore resides in finding a line-up suffering very little or not at all from interface dipoles.

Gap-states that are valence-like can be denoted as bonding states, because they have to be occupied in order not to introduce a charge deficit. Likewise, conduction-like gap-states are called antibonding because if left empty they do not cause a charge excess that could lead to an interface dipole. Now, there must exist a certain energy level at which the gap-states are nonbonding in character. At this energy, which we will call the midgap[12,13,16] energy (E_b), the states are on the average neutral in character. Ideally, local charge neutrality at the interface is achieved by filling up all gap-states up to E_b and leaving them empty above. Therefore E_b plays the role of a sort of "Fermi level" for the gap-states, and can be seen as a charge neutrality level. If as just argued, in both materials gap-states have to be filled up to this charge neutrality level, it seems reasonable to put these levels E_b at an equal energy position at the heterointerface to minimise the interface dipole. For any details on the calculational methods to obtain this level the reader is referred to the cited literature.

The best results for the band overlap Δ at an InAs-GaSb interface using this charge neutrality concept[13] yields a value Δ=141 meV, which is in perfect agreement with the experiments.

ii) The dielectric midgap energy

A somewhat related method is presented by Cardona and Christensen[16]. They calculate for bulk semiconductors a dielectric midgap energy (DME). The idea is that potentials acting on energy bands have in general to be screened by the dielectric constant. If lattice perturbations are caused not by an external potential, but by deformations due to e.g. strain, the deformation potentials which act on the bands have to be screened in a different way in each band, and it is not anymore correct to use the same dielectric constant for this screening. The DME is calculated as the (virtual) energy level at which the screening is simply given by division through the dielectric constant $\epsilon(k)$, just as would be the case for an external potential acting on all the bands in the same way. This DME can be shown to be related closely to the midgap energy and charge neutrality level as discussed above.

In their concept, Cardona and Christensen interpret VB offsets as the difference in absolute VB bandedge energies in the same sense as using the HAO method, but corrected for the thus resulting differences in DME at the interface using an effective "interface" dielectric constant. In principle their theory can account for effects on the band offsets introduced by strain and hydrostatic pressure. The results using the DME concept on the InAs-GaSb interface yield a band overlap $\Delta \simeq$ 130 meV, which is also very close to the experimental value.

iii) The matching of hybrids

In the context of the DME model that uses the model of screening of an interface potential due to the differences in the line-up of two bulk potentials, we should also mention the matching of hybrids method as proposed by Harrison[7] in order to improve the already discussed HAO method. On grounds of screening arguments involving potential steps at the interface between two adjacent ϵ_s and ϵ_p levels, (respectively the atomic-like s- and p-energy states), an average hybrid energy ϵ_h can be defined as

$$\langle\epsilon_h\rangle_{av}=\tfrac{1}{4}(\epsilon_s+3\epsilon_p) \tag{4}$$

in which the averaging is over the two atom species of the compound. $\langle\epsilon_h\rangle$ presents a level, which if aligned at the interface, calls for the least potential step to be screened. In some sense (based on a very simple argument, see ref.7) this level is strongly related to the DME and to Tejedors charge neutrality level. It is proposed therefore to take the average hybrid energy as the reference level to be lined up. Keeping the VB bandedge relative to the atomic levels according to eq.2 yields consequently the VB offset. For InAs-GaSb this gives however a staggered line-up in which no overlap is present.

iv) Transition metal deep impurity levels

Another very recent but rather heuristic method to predict band line-ups is what we will call the Transition Metal method (TMM), as proposed by Langer and Heinrich[7,9,15]. The TMM asserts that particular deep levels of transition metal impurities such as Fe, Cr, and Ni may be taken as universal energy levels which have the same absolute value in all semiconductors, and therefore should determine the band offset at the interface. This idea has evolved principally out of experimental observations, and as far as experimental data are available seems to hold within some hundred meV.

Why the TMM method works can be understood by considering that transition metals (TM) form strongly localised deep impurity states in semiconductors due to their unfilled d- or f-shells which couple very strongly to the atomic-states of the host-lattice atoms. To produce however the highly localised wave functions which localise the 3d-electrons of the impurity, many (plane-wave-like) band states[14] are necessary. Therefore the TM levels should not depend to much on a specific bandedge energy, but be more or less related to an absolute energy. This seems to hold in practice but still is is strange that an electron from such an impurity can almost totally neglect the surrounding host lattice, and determine its energy position relative to the vacuum. This problem has been tackled by Hasegawa[14] who has calculated an universal energy level (Hasegawa-Ohno's hybrid orbital energy) which is a similar average energy level as presented in eq.4, but corrected for electron-

electron interaction, and at which TM impurities tend to reside. As the TM levels are experimentally not known for InAs and GaSb, we will not go into further detail concerning the TMM.

IV. EXPERIMENTAL RESULTS AND THEORETICAL PREDICTIONS.

A. Theoretical predictions on the band offset under pressure

In chapter 3, eq.24 we have seen that the overlap Δ between the InAs-CB and the GaSb-VB decreases with pressure with a rate of ca. 4.5 meV/kBar. This is slightly less than concluded before (5.8 meV/kBar, see for instance ref.25). According to fig.6, chapter 3, this means that the Γ_8 VB offsets increase with 5.5±1 meV/kBar. As already argued, possible effects of strain on the band offset[28] are supposed to be pressure independent.

We now like to compare these results with possible theoretical predictions using theories discussed in the foregoing sections.

i) The EAR method

First of all the EAR method is not very suited to predict pressure dependent band offsets because this method has effectively no mathematical background. All EAR band offsets stem from experimental data which are on the average already suspect at ambient pressures, and to our knowledge not even available at high pressures.

ii) The FKP method

From the FKP[3] it should principally be feasible to extract predictions on pressure dependence of band offsets, if one assumes the atomic-like states to have a pressure independent energy. The calculations using the FKP however lie outside the scope of this work, and have not yet been performed.

iii) The HAO method

The aforementioned assumption that the atomic-like states (e.g. the s- and p-states with energies respectively ϵ_s and ϵ_p) have no pressure dependence, make the HAO method the first to predict pressure dependences in band offsets in a simple way. According to eq.2, the only pressure dependence in the absolute energy position of the VB bandedge E_v comes from the compressibility of the lattice and can be easily substituted in this equation. Although the results of the HAO strongly depend on the data source which is used, it can be shown that the dependence of ΔE_v on pressure is rather independent on this choice. Depending on the choice of the nearest neighbour coupling matrix element η (see eq.3), the HAO predicts a lowering in energy of the VB bandedges ranging from 1.5 to 3 meV/kBar for both InAs and GaSb. Using the values for η yielding the best zero pressure band offset ΔE_v gives a decrease with pressure of this offset of 0.2 meV/kBar. This means that virtually the VB offsets should be pressure independent in the InAs-GaSb system. This is however in strong disagreement with the experimental results.

Together with the general theoretical trend that the HAO model, (although surprisingly effective), presents a strong oversimplification of the problem, the pressure dependence of ΔE_v as established experimentally presents additional evidence against the HAO method.

iv) The matching of hybrids

Another approach closely related to the HAO method, is to take the average hybrid energy from eq.4 as a reference level. In the pressure version of the HAO this level should have no pressure dependence, and the way to proceed is to calculate at every pressure the positions of the VB bandedges relative to this energy according to eq.2, and to line-up these hybrid energies at the interface in order to obtain the VB offsets. Although as discussed before, the matched hybrid method yields a staggered line-up at the InAs-GaSb interface, it is interesting to investigate the rate of change of this staggered line-up with pressure according to this approach. (The absolute errors in the band offset prediction can be due to a wrong data source to which the HAO is very sensitive.) Dependent on the choice of η in eq.3, it is subsequently found that the staggered line-up in which the InAs-CB is above the GaSb-VB, increases with 1.8 to 2.8 meV/kBar. This means that allowing for an absolute shift in the line-up, the tendency is to reduce a possible overlap Δ with 1.8 to 2.9 meV/kBar, of which the latter value is quite close to the experimental results. Converted to Γ_8 VB offsets, this leads to respectively 9.2 and 7.1 meV/kBar increase, compared to an experimental value of 5.5±1 meV/kBar.

v) The charge neutrality level concept

In the context of Tejedors charge neutrality level, the pressure effect can be crudely incorporated by keeping the relative positions of the midgap energy E_b with respect to the bandedges the same. This is a sort of "elastic" model, in which the whole structure including valence-, conduction-, and midgap energy bands are elastically stretched by the pressure. The real incorporation of pressure in the calculations however is not trivial and has not yet been attempted, but the approach described above is thought[29] to be not irrational. In the calculations, values for the energy gap E_g and for the split-off valence band Δ_{so} are taken from Laewatz[30] and an effective energy gap is defined according to

$$E_{geff}=E_g+\tfrac{1}{3}\Delta_{so} \qquad (5)$$

in order to take into account the splitting of the Γ_8-Γ_7 valence bands. Pressure dependences for E_g and Δ_{so} are according to Martinez[31]. Zero pressure midgap energy values are those from ref.13. In this way a linear decrease of the overlap Δ with pressure is obtained at a rate of 1.4 meV/kBar. Omitting any pressure dependence of the split off gap Δ_{so}, as done in ref.25, yields a rate of 1.75 meV/kBar. These rates are compatible with the matched-hybrid method as discussed before and yield Γ_8 VB offsets which increase with pressure at a rate of 8.6 and 8.25 meV/kBar.

vi) The DME formalism

Using the concept of the DME and the deformation potential formalism, Cardona and Christensen[16] have calculated a value for the pressure dependence of the Γ_8-VB offset at the InAs-GaSb interface. They conclude that the VB offset should increase with a rate of 1.5 meV/kBar, which would lead to a decrease of the overlap Δ with 8.5 meV/kBar. This value is however rather far from the experimentally obtained result. A probable cause could be the accuracy to which the deformation potentials are known. According to the authors of ref.16, this is indeed a problem of experimental nature.

vii) TM deep impurity levels

It should be of considerable interest to know the positions and pressure dependences of deep TM levels in the InAs-GaSb system. However to our knowledge no such data are available. The only report known to the authors concerning pressure effects on TM levels is the experiment by Hennel and Martinez[32], in which the pressure dependence of the Cr^{1+} level with respect to the GaAs-VB bandedge is measured, and found to shift with a rate of 4.8 meV/kBar. This would mean that the GaAs VB drops in absolute energy with this rate when applying pressure to the GaAs. Such a similar measurement would be of extreme value if done in both InAs and GaSb. However the cited experiment concerns a measurement of the Cr^{1+} level which is situated in the GaAs CB, and which is not equal to the Cr^{2+} groundstate assumed by the TMM to reside at an universal reference energy. As it is not obvious that the $Cr^{1+} \rightarrow Cr^{2+}$ energy separation has no pressure dependence, the rate of change of the Cr^{1+} level to the VB cannot be directly related to a pressure dependent line-up as was previously[25] assumed.

B. Other experimental work on InAs-GaSb

Beerens[33,34] et al. have reported magnetotransport measurements on an InAs quantum well sandwiched between GaSb layers under pressure. From an observed reduction of hole-states at the InAs-GaSb interfaces with pressure, the band overlap Δ has been found to decrease indeed with pressure, at a rate of 7 meV/kBar. However, their results might possibly be influenced by a strong band bending in the outer GaSb layer, leading to an increase in the number of electrons due to an effective rise of the Fermi level in the well. This situation could lead to an erroneous interpretation of the experimental results as a function of pressure. The presence of such a band bending causing a rise of the Fermi level in these structures has recently been calculated and experimentally verified by Altarelli and Maan[35].

V. CONCLUDING REMARKS

A. General conclusion

As far as the experimentally observed pressure dependence of the overlap Δ is concerned, no theory exists yet which yields a theoretical prediction in total agreement with the experiment. However, most available theories ranging from simple linear ones to very complicate interface theories all come up with the same trend as observed in experiment.

Finally, we like to note that a band offset in a SL might be fundamentally different than at a single heterointerface. Although not very likely in the case of InAs-GaSb, it is suspected that for a HgTe-CdTe SL an actual difference in the VB discontinuities exists between the SL[22,23,24] ($\simeq$40 meV as deduced from optical experiments), and the heterojunction[20,21] ($\simeq$ 350 meV as measured by UPS and XPS techniques).

B. Future work

To conclude, we want to mention that it would be extremely useful to measure directly the band offsets at a single InAs-GaSb interface using the now widely accepted method of UPS and XPS (ultraviolet or x-ray emission spectroscopy) as described in ref.21 and references therein. This method measures directly some core-level binding energies from which the actual VB offset can be relatively easy deduced very accurately. Especially for the case of HgTe-CdTe this method has lead to some controversial yet partially understood results, as well in experiment[21,23,24], as in theory[20,22]. However such measurements which are now believed to form the best experimental method to measure band offsets at a *single* heterojunction, have not yet been performed on InAs-GaSb, and certainly not under pressure.

References.

1. See for instance; S.M. Sze: Physics of Semiconductor Devices, 2nd Edition. (John Wiley & Sons, New York 1981).
2. H. Kroemer, J.Vac. Sci. Technol. **B2**, 433 (1984).
3. W.R. Frensley, and H. Kroemer, Phys.Rev. B **16**, 2642 (1977).
4. J.C. Maan,"Infrared and Millimeter Waves", ed. by K.J. Button, Ac.Press, N.Y., **8**, 387 (1982).
5. Y. Guldner, J.P. Vieren, P. Voisin, M. Voos, J.C. Maan, L.L. Chang, and L. Esaki. Solid State Commun. **41**, 755 (1982).
6. W.A, Harrison: Electronic Structure and the Properties of Solids. (W.H. Freeman and Co. San Francisco, 1980).
7. W.A. Harrison in *Two-Dimensional Systems: Physics and New Devices*, proc. of the Winterschool Mautendorf, February 24-28, 1986, ed. by G. Bauer, F. Kucher, and H. Heinrich, p.62.
8. T.W. Hickmott, *ibid.*, p.72.
9. H. Heinrich, and J.M. Langer, *ibid.*, p.83.
10. E.A. Kraut, J.Vac.Sci.Technol. **B2**, 486 (1984).
11. C.G. Van de Walle, and R.M. Martin, Phys.Rev. B **34**, 5621 (1986).
12. J. Tersoff, Phys.Rev. B **30**, 4874 (1984).
13. J. Tersoff, Phys.Rev.Lett. **52**, 465 (1984).
14. H. Hasegawa, Solid State Commun. **58**, 157 (1986).
15. J.M. Langer, and H. Heinrich, Phys.Rev.Lett. **55**, 1414 (1985).
16. M. Cardona, and N.E. Christensen, to be published in Phys.Rev.B. See also N.E. Christensen in "Proceedings of the 7th General Conference of the Condensed Matter Division of the E.P.S, Italy 7-10 april 1987".
17. G. Duggan, J.Vac.Sci.Technol. **B3**, 1224 (1985).
18. J.L. Shay, S. Wagner, and J.C. Phillips, Appl. Phys.Lett. **28**, 31 (1976).
19. S.-H Wei, and A. Zunger, Phys.Rev.Lett. **59**, 144 (1987).
20. C.K. Shih, and W.E. Spicer. Phys.Rev.Lett. **58**, 2594 (1987).
21. S.P. Kowalczyk, J.T. Cheung, E.A. Kraut, and W. Grant, Phys.Rev.Lett. **56**, 1605 (1986).
22. G.Y. Wu, and T.C. McGill, J.Appl.Phys. **58**, 3914 (1985).
23. Y. Guldner, G. Bastard, J.P. Vieren, M. Voos, J.P. Faurie, and A. Million, Phys.Rev.Lett. **51**, 907 (1983).
24. J.M. Berrior, Y. Guldner, J.P. Vieren, M. Voos, and J.P. Faurie, Phys.Rev. B **34**, 891 (1986).
25. L.M. Claessen, J.C. Maan, M. Altarelli, P. Wyder, L.L. Chang, and L.Esaki, Phys.Rev.Lett. **57**, 2556 (1986).
26. G.W. Gobeli, and F.G. Allan, in *Semiconductors and Semimetals*, ed. by R.K. Willardson, and A.C. Beer, vol.2 (Ac.Press New York 1960), p.263.
27. F. Flores, and C. Tejedor, J.Phys. C **12**, 731 (1979).

28. G.Y. Wu, and T.C. McGill, Appl.Phys.Lett 47, 634 (1985).
29. C. Tejedor. Private Communication.
30. P. Lawaetz, Phys.Rev. B 4, 3460 (1971).
31. G. Martinez, in *Optical Properties of solids*, ed. by M. Balkanski, Handbook on Semiconductors Vol.2 (North Holland, Amsterdam, 1980), p.181.
32. A.M. Hennel, and G. Martinez, Phys.Rev. B 25, 1039 (1982).
33. J. Beerens, G. Grégoris, S. Ben Amor, J.C. Portal, E.E. Mendez, L.L. Chang, and L. Esaki, Phys.Rev. B 35, 3039 (1987).
34. G. Grégoris, J. Beerens, L. Dmowski, S. Ben Amor, and J.C. Portal, in *Optical Properties of Narrow-gap Low-dimensional Structures*, ed. by C.M. Sotomayor Torres, J.C. Portal, J.C. Maan, and R. Stradling, (Plenum Press New York 1982), p.337.
35. M. Altarelli, J.C. Maan, L.L. Chang, and L. Esaki, Phys.Rev. B 35, 9867 (1987).

SUMMARY

This thesis deals with four independent far-infrared investigations on various solid state systems, and is therefore divided in four separated parts.

In part I an experiment is presented concerning the optical responses of thin bismuth films as a function of both wavelength of the incident radiation and film thickness. Films with thicknesses between 50 and 830 nm are irradiated with far-infrared radiation, and the absorption and transmission is measured. The frequency range covering the theoretical electron plasma frequency in Bi is continuously scanned. Strong resonances are observed around this frequency for films thicker than ca. 200 nm. These results are firstly intuitively explained in terms of virtual modes excited in the films, and the disappearance of the resonance below a critical film thickness is visualised using a simple energy-loss concept for radiative excitations in thin dielectric slabs. After having understood qualitatively what happens, the results are analysed with a model in which the optical transmission and absorption are fitted to a dielectric function of the thin films on a quartz substrate. This analysis reveals the presence of ionised-impurity scattering, and two-phonon excitations in the thin films.

In the last section the influence of the optical dielectric constant on the character of the observed optical properties for obliquely incident s- and p-polarised light is discussed. It is shown that strong absorption peaks around the plasma frequency seen in the transmission of p-polarised radiation in thin films made of alkali-metals, often explained as coming from the excitation of real longitudinal plasmons, are in reality induced by transversal electron oscillations derived from a simple Drude-model.

Part II deals with electron paramagnetic resonances (EPR) in dilute magnetic semiconductors (DMS). The experiments are done on CdTe crystals in which part of the Cd^{2+} ions are replaced by paramagnetic Mn^{2+} ions. The magnetic excitations at far-infrared energies are investigated as a function of manganese concentrations. If more than 20% of the Cd^{2+} are replaced by Mn^{2+}, magnons are formed in the crystal due to nearest neighbour antiferromagnetic interactions. The magnon resonance energy has been followed as a function of the magnetic field. It is observed that these magnons posses a finite resonance energy at zero magnetic field, and evolve with field according to a g-factor equal to two. This has enabled us to identify previous experimental resonances as coming from the same magnon mode. Due to the determination of the g-factor, it can be concluded now that only single magnon excitations are involved, and not, as previously assumed, two-magnon excitations.

Part III describes an experiment dealing with the dynamics of electron-shallow donor recombination in pure InP. The photoconductivity of very pure InP has been measured on a nanosecond time scale. The sample is irradiated with pulsed far-infrared radiation (pulse-duration ca. 70 nsec.), and the rise and decay of the photoconductive signals are studied both as a function of incident laser power and DC bias voltage across the sample.

Strong tails lasting microseconds after the initial pulse are observed for applied bias voltages exceeding a few volts per cm. These tails appear to be rather random, and develop more or less superlinearly with laser power. A four level model including the impurity ground state, the ionised state, and two excited impurity states is developed with impact re-excitation between all levels. The two excited states are found to act as bottlenecks that trap the electrons for several microseconds.

At low bias voltages the photoconductive response is proportional to both the intensity and the duration of the incident laser puls. The decay time which determines the speed of the InP if used as a detector, is found to be about 60 nanoseconds.

The last part of this thesis describes an experiment on a superlattice made of thin alternating layers of InAs and GaSb. At the interface of an InAs-GaSb heterojunction, there exists a very peculiar band line-up in which the InAs conduction band has a lower energy than the GaSb valence band. Due to this peculiar overlap, the actual line-up of the bands at the interface can in a well chosen system, such as a superlattice, be determined with an accuracy unattainable in any other heterostructure.

The aim of this experiment is to investigate this band overlap at the InAs-GaSb interface as a function of hydrostatic pressure. As pressure changes in a known way the band gaps of both InAs and GaSb, changes in the overlap between the InAs conduction band and the GaSb valence band are also expected. It is however not known how the band overlap will change exactly with pressure due to these changes in the band gaps. Any existing band line-up theory that predicts accurately the zero pressure band overlap, is expected to be able to predict the observed pressure dependence of the band overlap in a correct way provided the pressure effects are incorporated in this theory. Therefore this experiment constitutes a severe test for theoretical models concerning band line-ups.

In the experiment the band line-up is determined by measuring magneto-optically the energy separation between the two lowest electron- and hole subbands in the superlattice. These subbands are strongly correlated with respectively the InAs conduction band and the GaSb valence band, and consequently they reflect the actual overlap between these bands.

The conclusion of the experiment is that this band overlap decreases with pressure as can be qualitatively explained by some band line-up theories. However, no theory has up to the present been found that predicts the experimental rate of change correctly.

SAMENVATTING

Dit proefschrift behandelt vier onafhankelijke ver-infrarood experimenten aan verschillende vaste stoffen, en bestaat daarom uit vier afzonderlijke delen.

In deel I wordt een experiment beschreven betreffende de absorptie en transmissie van dunne bismuth-films bestraald met ver-infrarood licht. Het spektrale gebied van het ingestraalde licht bestrijkt de elektron-plasmafrekwentie van bismuth.

Zowel in absorptie als in transmissie van films die dikker zijn dan 200 nm, is een sterke resonantie waargenomen rond deze plasma frekwentie. Deze resultaten worden eerst kwalitatief verklaard in termen van zogenaamde virtuele trillings-modi in de films, en het verdwijnen van de resonantie in dunne films wordt verklaard met behulp van een eenvoudige theorie voor stralende excitaties in dunne dielektrische lagen. Vervolgens zijn de experimentele resultaten geanalyseerd met behulp van een model dat de optische eigenschappen van de films vertaald naar een dielectrische funktie van dunne lagen op een kwartssubstraat. Deze analyse toont duidelijk aan dat in de films zowel de strooiing van elektronen aan geladen verontreinigingen, als de simultane excitatie van twee fononen een belangrijke rol spelen bij het bepalen van de ver-infrarode eigenschappen.

Als laatste wordt ingegaan op de invloed van de optische dielektrische konstante op de transmissie en absorptie van schuin invallend s- en p-gepolariseerd licht. Het blijkt dat de sterke resonanties rond de plasmafrekwentie, zoals waargenomen in de transmissie van p-gepolariseerd licht door dunne films gemaakt van alkali-metalen, niet te wijten zijn aan de excitatie van longitudinale plasmonen, maar veroorzaakt worden door een sterke transversale oscillatie van de elektronen, die met een simpel Drude-model verklaard kan worden.

Deel II gaat over paramagnetische resonanties aan elektronen (EPR) in verdunde magnetische halfgeleiders. De metingen zijn gedaan aan CdTe kristallen, waarin een deel van de Cd^{2+} ionen vervangen zijn door paramagnetische Mn^{2+} ionen. De magnetische excitaties zijn onderzocht bij ver-infrarood energiën als funktie van de mangaan koncentratie.

Wanneer meer dan 20 % van de Cd^{2+} vervangen is door Mn^{2+}, worden er magnonen gevormd in het kristal vanwege antiferromagnetische wisselwerking van naast elkaar gelegen mangaan-ionen. Een dergelijk magnon bestaat uit een keten van gekoppelde spins die zich in het kristal uitstrekt. Het blijkt dat de magnonen zelfs zonder een extern magneetveld al een eindige resonantie-energie bezitten. Onder invloed van een extern magneetveld vermeerdert deze energie in overeenstemming met een magnetische resonantie die een g-factor gelijk aan twee heeft. Deze meting heeft ons in staat gesteld eerder waargenomen resonanties te identificeren als komende van hetzelfde magnon. Uit het feit dat nu eenduidig bepaald is dat de g-factor gelijk aan twee is, kan men konkluderen dat alleen één-magnon excitaties aanwezig zijn, en dat er geen processen met twee magnonen bij betrokken zijn zoals vroeger werd aangenomen.

Deel III beschrijft een experiment betreffende de dynamika van de rekombinatie van elektronen aan ondiepe verontreinigingen in InP. De fotogeleiding in zuiver InP wordt gemeten op de tijdschaal van een nanoseconde. Het materiaal wordt hiertoe bestraald met ver-infrarood laserpulsen met een tijdsduur van ca. 70 ns, en het verloop in de tijd van het geinduceerde fotosignaal wordt onderzocht als funktie van zowel het ingestraalde laserlicht, als van de aangelegde voorspanning over het preparaat.

Bij een voorspanning met een elektrisch veld groter dan enkele volts per cm, blijkt er zich een zeer sterke fotogeleidende staart te vormen die microseconden lang stand kan houden. Deze staart reproduceert niet perfect van puls tot puls, en is sterk afhankelijk van het ingestraalde laservermogen. Een model met vier nivo's wordt gepresenteerd, waarin de grond-toestand van de verontreiniging, de geioniseerde toestand, en twee aangeslagen toestanden een rol spelen, met botsings-reëxcitatie tussen alle nivo's. De twee aangeslagen toestanden blijken als reservoirs te fungeren waarin de elektronen gedurende microseconden opgeslagen kunnen worden.

Bij zeer lage voorspanningen over het preparaat is de fotogeleiding evenredig met de invallende lichtpuls, zowel in intensiteit als in tijdsduur. De typische vervaltijd is ongeveer 60 ns, hetgeen de snelheid van de detektie voorstelt van het InP, indien gebruikt als snelle detektor in het verre-infrarood.

In het laatste deel van dit proefschrift worden metingen gepresenteerd, gedaan aan een superrooster, gemaakt van dunne lagen InAs en GaSb. Aan het scheidingsvlak in een heterojunktie van deze twee materialen bestaat een zeer zeldzame band-diskontinuiteit, waarin de InAs geleidingsband een lagere energie heeft dan de GaSb valentieband. Vanwege deze speciale overlapping van de banden kan de preciese waarde van de band-diskontinuiteit aan een InAs-GaSb scheidingsvlak nauwkeuriger bepaald worden dan in strukturen gemaakt van andere materialen.

Het doel van dit experiment is het onderzoek van deze band-diskontinuiteit als funktie van hydrostatische druk. Aangezien hydrostatische druk de relatieve posities van de energiebanden in de bulk materialen InAs en GaSb op een nauwkeurig bekende wijze verandert, is het te verwachten dat de band-diskontinuiteit aan het scheidingsvlak tussen deze twee materialen ook verandert. Het is alleen niet bekend op wèlke wijze deze diskontinuiteit van de druk afhangt. Iedere theorie die deze diskontinuiteit korrekt voorspelt bij normale druk, moet konceptueel in staat zijn de drukafhankelijkheid ook te voorspellen, vooropgesteld dat de effecten van de druk op een juiste manier in deze theorie gesubstitueerd worden. Daarom is dit experiment een strenge test voor theoretische modellen die proberen band-diskontinuiteiten te voorspellen.

In het experiment wordt de diskontinuiteit bepaald door middel van het meten (met behulp van magneto-optische technieken) van het energieverschil tussen de laagste elektronen-subband en de hoogste gaten-subband in het superrooster. Deze subbanden zijn sterk gekorreleerd aan respektievelijk de InAs geleidingsband en de GaSb valentieband, en daarom kan uit een meting van de onderlinge energiepositie van deze subbanden, de verlangde overlapping betrekkelijk eenvoudig afgeleid worden.

De konclusie van het experiment is dat deze overlapping vermindert met druk, zoals kwalitatief voorspeld is door verschillende theorien. Tot nu toe is er echter nog geen theorie ontwikkelt die de waargenomen drukafhankelijkheden kwantitatief beschrijft.

CURRICULUM VITAE

L.M. Claessen

geboren 18 februari 1960 te Eindhoven

1972-1978 : V.W.O opleiding aan het Dominicus college te Nijmegen, afgesloten met een Atheneum B diploma

1978-1983 : Studie natuurkunde aan de Katholieke Universiteit Nijmegen, met als afstudeer richting experimentele vaste stoffysica, en als bijvak astrofysica, onder leiding van Prof. dr. P. Wyder

10 november 1983 : doctoraal examen natuurkunde (cum laude)

16 november 1983 : in dienst van de Universiteit van Nijmegen, promotie onderzoek o.l.v. prof.dr. P. Wyder

1 april 1985 : detachering aan het Max Planck Institut für Festkörperforschung, Hochfeld Magnetlabor, Grenoble, Frankrijk

STELLINGEN

behorende bij het proefschrift

"Bandstructure and Electron Dynamics in
Semimetallic and Semiconducting
Systems"

van L.M. Claessen

I

Het door J.M. Irvine gesuggereerde behoud van magnetische flux tijdens de gravitationele inkrimping van een ster tot een neutronenster is twijfelachtig vanwege sterke dissipatie van de magneetveld-opwekkende stromen in het binnenste van de ster tijdens deze inkrimping. Het hierop gebaseerde model dat de extreem hoge magneetvelden op het neutronensteroppervlak ($B \propto 10^8 T$) verklaart met behulp van superfluide stromen is daarom niet aannemelijk.

J.M. Irvine; "Neutron stars", Claredon Oxford 1978.

II

De bewering van Sichel et al. dat de twee-punts weerstand van een twee-dimensionaal elektronen gas tussen twee metallische kontakten altijd groter moet zijn dan de Hall weerstand van het elektronen gas is niet korrekt.

E.K. Sichel, M.L. Knowles en H.H. Sample, J. Phys. C 19, 5695 (1986).

III

De afsnijfrekwentie (Ft) van een bipolaire transistor is evenals het begrip intelligentiequotient (IQ) sterk afhankelijk van de manier waarop deze gemeten wordt.

IV

Bij het opstellen van een theorie over kwantum-oscillaties in puntkontakten gaan Bogachek et al. uit van de veronderstelling dat de magnetische lengte veel kleiner is dan de puntkontakt diameter. Deze aanname is voor gebruikelijke magneetvelden en puntkontakten onjuist.

E.N. Bogachek, I.O. Kulik en R.I. Shekhter, Solid State Commun. 56, 999 (1985).

V

In acht nemend zowel het diffraktie patroon van kommercieel verkrijgbare Schmidt-Cassegrain teleskopen als ook de diameter van konvektie cellen in de onderste lagen van de aardatmosfeer, is het eenvoudig te begrijpen dat het visueel haalbare kontrast in dit soort teleskopen aanzienlijk vergroot kan worden door het aanbrengen van een zo groot mogelijk elliptisch diafragma voor de Schmidt-korrektielens naast de centrale obstruktie.

VI

Het optreden van "anti-level-crossings" in het energiespektrum van een tweedimensionaal elektronengas in een gekanteld magneetveld zou behalve in de optische eigenschappen, ook in magneto-transport zichtbaar moeten zijn.

G.J.L.A. Rikken et al., Phys.Rev.B 34, 5590 (1986).

VII

Het vertrouwen in de naam van een concern is sterk gekorreleerd aan de kwaliteit van de geleverde produkten, en is niet zoals vaak wordt aangenomen omgekeerd evenredig met de prijs die de konsument voor deze produkten betalen moet.

VIII

Uit de voorgaande stelling is het meteen duidelijk dat verlaging van de kwaliteitsnorm omwille van het goedkoper op de markt kunnen brengen van produkten een "eigen ruiten inslaan" praktijk is, en dus volkomen zinloos.

IX

De bewering door Claessen et al. dat intraband-achtige overgangen in GaSb-InAs superroosters een sterkere én een zwakkere magneetveldafhankelijkheid hebben dan interband-achtige overgangen is onzin.

L.M. Claessen, J.C. Maan, M. Altarelli, P. Wyder, L.L. Chang en L. Esaki, Phys. Rev. Lett. 57, 2556 (1986).